UNIVERSITY OF CALIFORNIA, SAN DIEGO

The Role of Vinculin in Cardiac Mechanotransduction

A dissertation submitted in partial satisfaction of the requirements for the degree
Doctor of Philosophy

in

Bioengineering

by

Amy Lee Hsieh

Committee in charge:

Professor Andrew D. McCulloch, Chair
Professor Michael W. Berns
Professor Shu Chien
Professor Mark Ginsberg
Professor Robert S. Ross

2010

The dissertation of Amy Lee Hsieh is approved, and it is acceptable in quality and form for publication on microfilm and electronically:

_____

_____

_____

_____

_____
Chair

University of California, San Diego

2010

DEDICATION

For my family

EPIGRAPH

The secret of life is to have a task, something you devote your entire life to, something you bring everything to every minute of the day for your whole life. And the most important thing is – it must be something you cannot possibly do.

Henry Moore

TABLE OF CONTENTS

LIST OF ABBREVIATIONS

+/- Vcl KO ..... heterozygous vinculin knockout mice

α ..... alpha

αMHC ..... α-myosin heavy chain

AA ..... amino acid

Ad-Cre ..... adenovirus containing Cre

Ad-FAK FRET ..... adenovirus containing FAK FRET reporter

Ad-LacZ ..... adenovirus containing β galactosidase

AHA ..... American Heart Association

Amp ..... ampicillin

Arg ..... arginine

β ..... beta

BDM ..... 2,3-butanedione monoxime

BE ..... Bioengineering or beam expansion system

bp ..... base pair

BP ..... blocked path

BS ..... beam splitter

°C ..... degrees Celsius

c ..... speed of light in free space

$CaCl_2$ ..... calcium chloride

CCD ..... charge-coupled device

cm ..... centimeter

cm^2 ..... centimeter squared

CMC ..... cardiac myocyte

CMV ..... cytomegalovirus

COM ..... serial port cable

Cre- ..... Cre negative

Cre+ ..... Cre positive

del ..... deletion
DM ..... dichroic mirror
DMEM ..... Dulbecco's Modified Eagle Media
DNA ..... deoxyribonucleic acid
DPBS ..... Dulbecco's phosphate-buffered saline
eCFP ..... enhanced cyan fluorescent protein
eYFP ..... enhanced yellow fluorescent protein
E ..... embryonic day
ECFP ..... enhanced cyan fluorescent protein
ECM ..... extracellular matrix
EDTA ..... ethylenediaminetetraacetic acid
ENH ..... Enigma homolog protein
ERK ..... extracellular signal-regulated kinase
ET-1 ..... endothelin-1
f ..... focus position
$F_{viscous}$ ..... viscous force in the Stokes flow equation
FAK ..... focal adhesion kinase
FAK-P ..... phosphorylated focal adhesion kinase
FBS ..... fetal bovine serum
fl/fl ..... floxed alleles
FRET ..... fluorescence resonance energy transfer
fs ..... femtosecond
%FS ..... percent of fractional shortening
FSM ..... fast steering mirror
GAPDH ..... glyceraldehyde 3-phosphate dehydrogenase
GFP ..... green fluorescent protein
HS ..... horse serum
HUVEC ..... human umbilical vein endothelial cells
HWP ..... half wave plate

I . . . . . iris

IACUC . . . . . Institutional Animal Care and Use Committee

IGEPAL . . . . . 2-[2-(4-nonylphenoxy)ethoxy]ethanol

ILK . . . . . integrin-linked kinase

IP . . . . . immunoprecipitation

IR . . . . . infrared

KCl . . . . . potassium chloride

KH_2PO_4 . . . . . potassium dihydrogen phosphate

L . . . . . lens

Leu . . . . . leucine

LVIDd/BW . left ventricular internal dimension in diastole with respect to body weight

LVIDs/BW . . left ventricular internal dimension in systole with respect to body weight

kDa . . . . . kilodalton

KO . . . . . knockout

kPa . . . . . kilopascals

μ . . . . . viscosity of fluid

M . . . . . mirror

Met . . . . . methionine

mg . . . . . milligram

$MgSO_4$-$7H_2O$ . . . . . magnesium sulfate heptahydrate

MHC . . . . . myosin heavy chain

MHz . . . . . megahertz

mL . . . . . milliliter

MLC2v cVcl KO . . . . . cardiac specific floxed vinculin knockout mice

MLP . . . . . muscle LIM protein

mm . . . . . millimeter

MOI . . . . . multiplicity of infection

MP . . . . . multiphoton

ms . . . . . milliseconds

MVcl . . . . . metavinculin

mW . . . . . milliwatt

n . . . . . refractive index of the medium

NA . . . . . numerical aperture

Na-HEPES . . . . . HEPES sodium salt

Na_2HPO_4 . . . . . disodium hydrogen phosphate

NaCl . . . . . sodium chloride

$NaHCO_3$ . . . . . sodium bicarbonate

NIH . . . . . National Institute of Health

nm . . . . . nanometer

NMVMs . . . . . neonatal mouse ventricular cardiac myocytes

NRVMs . . . . . neonatal rat ventricular cardiac myocytes

p . . . . . magnitude of the momentum flux

pfu . . . . . plaque forming unit

PC . . . . . personal computer

PCI . . . . . peripheral component interconnect

PCR . . . . . polymerase chain reaction

pN . . . . . piconewton

PS . . . . . periscope or penicillin-streptomycin

r . . . . . microsphere radius

RNA . . . . . ribonucleic acid

S . . . . . shutter

SDS . . . . . sodium dodecyl sulfate

sec . . . . . seconds

T-cap . . . . . telethonin

T-Control . . . . . tamoxifen injected control

T-KO . . . . . tamoxifen injected knockout

TA . . . . . teaching assistant

Tamo . . . . . tamoxifen

Tamo cVcl KO ... tamoxifen inducible cardiac specific floxed vinculin knockout mice

tau ..... kinetic constant

TCre- ..... tamoxifen inducible Cre negative

TCre+ ..... tamoxifen inducible Cre positive

Ti:sapphire ..... titanium-sapphire

Tom Tamo cVcl KO .... double reporter tamoxifen inducible cardiac specific vinculin knockout mice

Tris-HCl ..... tris(hydroxymethyl)animomethane

Trp ..... tryptophan

Tyr ..... tyrosine

UCSD ..... University of California, San Diego

ug ..... microgram

um ..... micron

uM ..... micromolar

VA ..... Veteran Affairs

vcf ..... velocity of circumferential fiber shortening

Vcl ..... vinculin

Vcl KO ..... vinculin knockout

W ..... watt

WHO ..... World Health Organization

wk ..... weeks

WT ..... wildtype

YPet ..... yellow fluorescent protein derivative

LIST OF FIGURES

ACKNOWLEDGEMENTS

I would like to thank Irwin and Joan Jacobs for supporting my graduate education through the Jacobs School of Engineering Fellowship. I would also like to thank the American Heart Association (AHA) for supporting me through the AHA Pre-doctoral Fellowship, the generous benefactors who supported me through the University of California, San Diego Cardiovascular Science Scholarship, Mr. and Mrs. Siebel and the Siebel Foundation who supported me through the Siebel Scholars award. In total, these fellowships benefited many aspects of my education, providing me the ability to work on a highly interdisciplinary project, to attend conferences to further my understanding of the bioengineering field, and ultimately in enabling me to pursue my interests in translational research.

I would like to acknowledge Dr. Andrew D. McCulloch for his support as a terrific mentor and chair of my committee. With his guidance, he provided me with academic freedom to pursue an interdisciplinary research plan. Through his advice, I pursued new directions in my research, helping me to discover new areas that interfaced with my research to new levels and through his support, I was encouraged to participate in volunteer and outreach activities and to further my professional development skills. Dr. Michael Berns has been a wonderful co-advisor, always encouraging my scientific creativity, asking me to look from different perspectives, to step back and assess not only what the technology does, but what else can it do. Dr. Robert S. Ross has been a great co-advisor. With his guidance, support, and sponsorship I was able to pursue my highly interdisciplinary research plan and was provided valuable advice on my research directions. Dr. Shu Chien and Dr. Mark Ginsberg also provided valuable advice on my research directions and future career. Many other individuals offered additional perspectives and suggestions, including Dr. Elliot Botvinick, Dr. Jeffrey Omens, and Dr. Kirk Knowlton.

Dr. Jaclyn Nascimento, Dr. Bing Shao, Dr. Linda Zhi, and Dr. Qingyuan Zhu have provided valuable advice on experimental approaches. Dr. Alice Zemljic-Harpf

taught me a number of molecular biology and biochemistry techniques and Dr. Hideshi Okada aided me adenovirus design, amplification, and purification. Dr. Yingxiao Wang provided me with valuable advice on FRET imaging and provided me with the FAK FRET reporter necessary to perform these studies. Ruixia Li and Yuan Yang provided technical assistance with adult cardiac myocyte isolations and echocardiograms. I'd like to thank everyone at the Cardiac Mechanics Research Group, Cellular Biophotonics Lab, Ross Lab, and Chien Lab, who have made it fun a working environment and providing valuable feedback and advice. I'd particularly like to thank Joyce Chuang and Barbara Murienne for their help with the cell membrane stretch experiments, and Stuart Campbell for his help with programming and modeling. I would also like to thank the various undergraduates, Monica Kim, Annie Liu, Tiffany Hsu, Ming-Hui Chen, and Samantha Clark who have worked with me and all their help.

Most of all I'd like to thank my family and friends for their continued support and encouragement. Michael and Millie, my parents, encouraged me and helped me to recharge when needed. Allen, my brother, provided his support and technical help with laser optics. Oreo and Keebler, my beloved dogs, provided support and helped me to recharge in difficult times. My friends provided me with laughs and encouragement and Jimmy, who provided me with inspiration, hope, and encouragement to pursue a career in bioengineering.

Chapter 6 is being prepared for publication titled "A Mechanotransduction Response in Cardiac Myocytes Using Optical Tweezers and Multiphoton Fluorescence Resonance Energy Transfer" by Amy L. Hsieh, Tiffany W. Hsu, Qingyuan Zhu, Marcellinus S. Harsono, Yingxiao Wang, Alice Zemljic-Harpf, Robert S. Ross, Andrew D. McCulloch, Michael W. Berns for submission. The dissertation author is the primary investigator of this paper.

Chapter 8 is being prepared for publication titled "Vinculin mediates anisotropic mechanotransduction response of focal adhesion kinase in neonatal murine cardiac ventricular myocytes" by Amy L. Hsieh, Tiffany W. Hsu, Alice Zemljic-Harpf, Robert S. Ross, Michael W. Berns, Andrew D. McCulloch for submission. The dissertation author

is the primary investigator of this paper.

VITA

2010	Doctor of Philosophy in Bioengineering University of California, San Diego
2008	Master of Science in Bioengineering University of California, San Diego
2006	Bachelor of Science in Bioengineering : Pre-medical University of California, San Diego

AWARDS

2010	Siebel Scholar, Class of 2010 - awarded annually for academic excellence and demonstrated leadership to 80 top students from the world's leading graduate schools
2009	Candidate of Philosophy in Bioengineering
2008 - present	American Heart Association Pre-doctoral Fellowship
2008	Master of Science in Bioengineering
2008	TA Excellence Award for BE 110: Continuum Mechanics
2008	UCSD Cardiovascular Science Scholarship
2007	TA Excellence Award for BE 186B: Bioinstrumentation
2006 - present	Jacobs School of Engineering Fellowship
2006	Bachelor of Science in Bioengineering: Pre-medical, Summa Cum Laude
9/2005 - 8/2006	Warren College Honors Student
9/2005	William H. Stout Scholar
6/2005, 6/2006	Academic Excellence Award in Bioengineering at UCSD
9/2004 - 6/2006	Provost's Honors at UCSD
2003 - 2004	Dean's List at De Anza College

RESEARCH EXPERIENCE

Graduate Student Researcher - UCSD, 2006 - present

- Investigated how disruptions of cell-extracellular matrix complexes disrupt structural integrity, electrical, mechanical, and signaling functions in isolated murine cardiomyocytes
- Advisors: Dr. Andrew McCulloch, Dr. Michael Berns, Dr. Robert S. Ross

Research Chemistry Intern - Amylin Pharmaceuticals, 2005, 2006

- Involved in chemical analysis of endogenous fluids and performing compound stability studies

Undergraduate Research Assistant - UCSD, Cardiac Mechanics Research Group, 2004 - 2006

- Investigated the role of biglycan in post-myocardial infarcted hearts

TEACHING EXPERIENCE

Graduate Student Advisor - Bioengineering Senior Design, UCSD 2008 - 2009

- Led students in discussions to design and implement magnetic tweezers used to study cardiac mechanotransduction

Head Teaching Assistant - Bioinstrumentation, UCSD, 2007, 2008

- Led discussion sections in Bioinstrumentation at the undergraduate level

Head Teaching Assistant - Continuum Mechanics, UCSD, 2007

- Led discussion sections and taught lectures in Continuum Mechanics at the undergraduate level

PUBLICATIONS AND ABSTRACTS

Manso, A.M., **Hsieh, A.L.**, Thor, A.K., Perkins, G.A., Zemljic-Harpf, A.E. (2010) Expression of the Tight Junctional Protein Occludin in Cardiac Myocytes Suggests the Presence of a Novel Cardiac Junction. Mol. Biol. Cell 21 (suppl), abstract #2549

Clark, S.A., **Hsieh, A.L.**, Campbell, S.G., McCulloch, A.D. (2009) Modeling the Mechanical Stretch Response of the Individual Cardiomyocyte, Biomedical Engineering Society Annual Meeting, Pittsburgh, PA

Israeli, S., **Hsieh, A.L.**, Patel, H., Roth, D., Ross, R.S. (2009) Integrin-Caveolin Crosstalk in the Cardiac Myocyte. Basic Cardiovascular Sciences Annual Conference 2009-Molecular Mechanisms of Cardiovascular Disease

Hsieh, A.L., Wang, Y., Ross, R.S., Berns, M.W., McCulloch, A.D. (2009) Mechanotransduction in Single Cardiac Myocyte Studied Using Laser Tweezers and FRET. 2009 Biophysical Society Meeting Abstracts. Biophysical Journal, Supplement, B458, Abstract, 1614-Pos

Taylor, S., Sun, C., **Hsieh, A.L.**, Andon, N., Ghosh, S. (2008). A Sulfated, Phosphorylated 7 kDa Secreted Peptide Characterized by Direct Analysis of Cell Culture Media. Journal of Proteome Research, 7(2), 795-802

ABSTRACT OF THE DISSERTATION

The Role of Vinculin in Cardiac Mechanotransduction

by

Amy Lee Hsieh

Doctor of Philosophy in Bioengineering

University of California, San Diego, 2010

Professor Andrew D. McCulloch, Chair

Cardiac mechanotransduction is the process by which mechanical signals are transduced into biochemical signals in cardiac myocytes. It is important for moderation of changes in sarcomeric protein assembly, hypertrophic markers, and cell survival. Within a single cardiac myocyte, costameres are complex multi-protein structures which have been shown to be the site where forces generated by cardiac myocytes are transmitted to the external extracellular matrix (ECM) as well as the site where forces externally applied by the ECM are transmitted into the cardiac myocyte. Defects in vinculin and its isoforms, metavinculin, have been implicated in the development of dilated and hypertrophic cardiomyopathy. Due to vinculin's role in contributing to the development of cardiomyopathy and its position in forming a bridge between the ECM and the cytoskeleton, it is hypothesized that vinculin is required for normal mechanotransduction. To study vinculin's role in mechanotransduction, a method using laser tweezers and multifocal multiphoton fluorescence resonance energy transfer (FRET) microscopy was

developed. This method allowed the application of calibrated localized forces to cardiomyocytes and the measurement of the cell's response to the force. Results demonstrated that this system can be used to study cardiac mechanotransduction, and that focal adhesion kinase autophosphorylation (FAK-P) as reported by a FRET biosensor changed locally in the cell, but not distally from the site of force application. Additionally, in wildtype cells, FAK-P responses were dependent on cell geometry. These results reveal that types of load depending on orientation of a cell may trigger regulation of hypertrophy. Lastly, using this system, it was determined that anisotropic responses to mechanotransduction as reported by the FAK FRET biosensor is mediated by vinculin. These results reveal the role of the microanatomy of the costamere in determining mechanotransduction events and alterations in hypertrophic signaling. In conclusion, an optically based novel method for studying cardiac mechanotransduction has been developed and it has been used to determine that abnormal vinculin levels alter the biochemical signaling of FAK in response to directionally applied forces. These alterations may contribute to the development of cardiomyopathy and possibly in the development of heart failure.

Chapter 1

Introduction

Cardiomyopathies were first defined as ”heart diseases of unknown cause” by the World Health Organization (WHO) in 1980. This definition was characterized based on the pathological appearance of the heart and such diseases included dilated, hypertrophic, or restrictive features. A separate ”unclassified” cardiomyopathy category was considered for the class of cardiomyopathies that could not be easily placed in the above categories. With advancements in diagnostic techniques providing more information about cardiac function, it was determined that a different classification for diseases was needed (Keren and Popp, 1992). In 1995, the World Health Organization defined cardiomyopathies based upon more distinct pathophysiological features or detailed data about its specific cause (Richardson et al., 1996). These classifications included: dilated, hypertrophic and restrictive forms, as before, but now also included arrhythmogenic right ventricular cardiomyopathy, cardiomyopathies due to ”known causes,” and unclassified forms. With advancements in the identification of molecular and genetic causes of cardiac muscle diseases, cardiomyopathies have been reclassified in primary categories as genetic, acquired, or mixed forms and secondary cardiomyopathies include disorders that affect multiorgan systems (Maron et al., 2006). Within the group of ”mixed” (genetic/nongenetic) forms of cardiomyopathy, there exist cardiomyopathies originating from dysfunctional proteins of the cytoskeleton, cell-matrix and cell-cell ad-

hesion junctions (Towbin and Bowles, 2006; Bowles et al., 2000; Towbin and Bowles, 2000).

1.1 Organization of cardiac myocyte cytoskeletal-architecture

Normal myocardial and cardiomyocyte function is dependent upon the function of the sarcomere and the arrangement of thick and thin filaments. The muscle fibers in the heart consist of a staggered arrangement of myocytes that are separated by intercalated disks at the end of each individual myocyte. Within the intercalated disks are gap junctions necessary for electric coupling and structures necessary for mechanical stability: fascia adherens which dock the cytoskeleton to the membrane and contractile components and desmosomes which link intermediate filaments to the muscle termini (Figure 1). Proteins found within the intercalated disks include, but are not limited to: α–actinin, connexins, desmins, desmoplakin, desmocolliln, desmoglein, plakoglobin, N-cadherin, αE-catenin, αT-catenin, N-RAP, muscle LIM protein, talin, and vinculin (Towbin et al., 2006; Clark et al., 2002; Perriard et al., 2003).

The extracellular matrix surrounds the cardiac myocyte and consists of laminin, collagen, and fibronectin. Integrins bridge the extracellular matrix to the actin cytoskeleton and the interaction of the extracellular matrix with integrins, provides adhesive support for the myocyte and allow for adhesive and mechanical signaling. Previous work with integrins in both cell culture and in mice supports its role in maintaining myocyte integrity (Babbitt et al., 2002; Keller et al., 2001; Ross et al., 1998). Costameres are complex multi-protein structures which flank the Z-disk of myocytes and link the sarcomere, through the cytoskeleton, to the extracellular matrix (Figure 2). Therefore, the costameres play an important role in maintaining cell structure and mechanotransduction in contracting cardiomyocytes (Clark et al., 2002; Samarel, 2005). Costameres have been shown to be the site where forces generated by cardiac myocytes are trans-

mitted to the external extracellular matrix (inside-out) (Danowski et al., 1992) as well as the site where forces externally applied by the extracellular matrix are transmitted into the cardiac myocyte (outside-in) (Mansour et al., 2004). Similar to other linkage sites, costameres contain a large number of proteins which include, but are not limited to tropomodulin, syntrophin, ankyrin, spectrin, syncolin, γ-actin, desmin, filamin, myopalladin, calsarcins, cypher, melusin, integrins, dystroglycan complex, caveolin-3, α-actinin, talin, and vinculin (Ervasti, 2003). Understanding the role of these proteins in the cardiac myocyte, in normal cardiac function and how they might be linked to development of cardiomyopathies is important and may potentially lead to the identification of novel therapeutics (Zemljic-Harpf et al., 2009). Here, we briefly review cardiac mechanotransduction and expand upon new directions for studying cardiac mechanotransduction, with specific attention to the study of the role of vinculin in cardiac mechanotransduction.

1.2 Cardiac mechanotransduction in the heart

Mechanotransduction is the process by which mechanical signals are transduced into biochemical signals. Consequences of mechanotransduction in the cardiac myocyte include but are not limited to: increased protein synthesis, hypertrophic markers, and effects on the beta-adrenergic receptor function, ion channel function, cell shape changes, cell-cell communication, sarcomeric protein assembly, and cell survival (Samarel, 2005).

Cardiac mechanotransduction might occur through a range of proteins including stretch-activated channels, integrins, second messengers, titin, T-cap, MLP, melusin, calcineurin, calsarcins, enigma, ENH, cipher family, and other additional Z-disc proteins (Knoll et al., 2003). Through the use of a variety of knockout and mutation studies, the role of an assortment of proteins implicated in mechanotransduction have been studied.

1.3 Current methods to study cardiac mechanotransduction

The current methods for studying cardiac mechanotransduction include, but are not limited to: membrane stretch via an elastic substrate, shear stress by fluid flow, optical trapping, magnetic tweezers, and magnetic twisting (Huang et al., 2004). These varieties of methods allow the mechanistic study of various branches of cardiac mechanotransduction. Here we will focus on the use of biophotonics to study cardiac mechanotransduction.

Biophotonics are photon-based techniques for imaging, sensing, manipulation, and characterization of biological tissues, and cells. Their applications include therapeutics, diagnostics, and life sciences research. An important technique of interest is optical trapping, also termed laser tweezers. This technique is used for minimally invasive mechanical manipulation of living cells and their organelles (Berns, 1998). Optical trapping utilizes a continuous focused laser beam and can trap micron-sized particles (Ashkin, 1992).

Another important technique stemming from biophotonics is the development fluorescence resonance energy transfer (FRET) used in imaging. FRET is quantum mechanical process, which occurs when a donor fluorophore is excited and radiationless transfer of energy from the donor to an acceptor fluorophores occurs. FRET can occur when the emission spectrum of the donor fluorophore significantly overlaps ($>$ 30%) the absorption spectrum of an acceptor. FRET biosensors have been engineered to study processes such as microclustering of integrins and the enzyme substrate dynamics (Chodniewicz et al., 2004; Wang et al., 2005). As the conformation of the FRET biosensor changes such that there is a strong overlap of the donor emission spectrum and acceptor excitation spectrum, the fluorescence emissions provide information about these interactions (Gaits and Hahn, 2003).

The ability to study mechanotransduction in single cells using laser tweezers and

FRET was first described for primary human umbilical vein endothelial cells (HUVEC) in 2004 (Wang et al. 2005). These studies showed the power of using FRET reporters to study mechanically activated signaling pathways. This study used a Src reporter in human umbilical vein endothelial cells (HUVECs) in conjunction with fibronectin-coated beads and laser tweezers. The result was the discovery that the transmission of mechanically induced Src activation was a dynamic process that directed signals via the cytoskeleton to spatial destinations within the cell distal from the site of force application.

By using ligand coated beads for receptors implicated in mechanical signaling in conjunction with the force pulling ability of optical traps, this method provides a means to study cardiac mechanotransduction. As such, we will focus on the integrin branch of cardiac mechanotransduction and even more specifically on the role of vinculin within this branch.

1.4 Integrins

A hypertrophic response, in which the heart compensates for dysfunction (Grossman et al., 1975), has been detected in cardiomyocytes after application of mechanical forces. As such, the existence of a cell mechanotransducer apparatus has been implicated in cardiac myocytes and a large subset may be linked to integrins.

Integrins are transmembrane proteins that serve as cell-surface receptors, consisting of alpha and beta subunits. Each integrin heterodimer binds to a specific extracellular matrix protein or cell surface counter receptor including: collagen, E-cadherin, fibrinogen, fibronectin, laminin, tenascin, vascular cell adhesion molecule, and vitronectin. When integrins are not bound to the extracellular matrix (ECM), the integrin is found in an inactive conformation, in which the ECM-binding pocket is masked. Upon talin recruitment to the plasma membrane and activation via phosphatidylinositol phosphate kinase type I γ, it binds to the cytoplasmic tail of β integrin, which separates the cytoplasmic domains and induces the integrin to become primed (Critchley, 2004). The

integrin extracellular domain extends, unmasks its ECM-binding pocket, and binding to the ECM can occur.

In embryonic cardiomyocytes, cells mainly express β1A, an isoforms of β1 integrin subunit, while newborn and adult cardiomyocytes mainly express β1D (Brancaccio et al., 2006). In adult cardiomyocytes, the laminin binding $\alpha 7\beta 1$ is the major integrin heterodimer. The characterization of the cytoplasmic domain of β1 isoforms have shown unique properties of interacting with cytoskeletal proteins and signaling molecules. The cytoplasmic domain of integrins and talin form a platform for recruiting other proteins including vinculin, integrin-linked kinase (ILK), PINCH, parvin, and paxillin (Legate et al., 2006). Upon integrin engagement and clustering, focal adhesion kinase (FAK) is recruited and binds to the β1 integrin tail (Liu et al., 2000). FAK is then activated by autophosphorylation at the Tyr-397 site, leading to downstream changes in signaling including activation of ERK1/2 (Domingos et al., 2002).

1.5 Vinculin

Vinculin is a 117 kDa, 1066 amino acid protein (Figure 3). It has a splice-variant isoform metavinculin, produced from the same gene (Weller et al., 1990). Vinculin is localized in cell-cell and cell-matrix junctions including intercalated disks, focal adhesions, Z bands, and costameres of cardiomyocytes (Shiraishi et al., 1997; Pokutta et al., 2002). Vinculin forms a molecular bridge between the extracellular matrix and the actin-based cytoskeleton of the cell via binding to talin, a-actinin, and actin. It also binds to other proteins including, but not limited to: talin and FAK (Ziegler et al., 2006; Ben Zeev et al. 1990; Bendori et al., 1989; Burridge et al., 1984; Ezzell et al., 1997; Goldmann et al., 1998; Johnson et al., 1994; Schlessinger et al., 1983). Vinculin has a head-to-tail intramolecular association (Bakolitsa et al., 2004; Borgon et al., 2004), which can lead to masking of its binding sites.

Using NIH3T3 cells, it has been shown that the vinculin head regulates integrin dynamics and the tail is involved in mechanotransduction (Humphries et al., 2007).

Vinculin is a component of the complex which mediates force transmission from the extracellular matrix to the cell interior through integrins and serves as lateral attachments at Z-bands of myofibrils to the plasma membranes and T-tubules (Danowski et al., 1992; Imanaka-Yoshida et al., 1999). Immunocytochemical studies in cell culture have suggested that vinculin may be important for cardiac myofibrillogenesis (Simpson et al., 1994). Reduction in vinculin expression in cultured fetal mouse cardiomyocytes by use of antisense oligonucleotides resulted in the disruption of normal cellular organization (Shiraishi et al., 1997). Studies in vinculin deficient cells support the primary importance of vinculin's role in orchestrating mechanical coupling between integrins on the cell surface and in the cellular cytoskeleton (Ezzell et al., 1997; Goldmann and Ingber, 2002).

In a mouse model, the vinculin gene has been deleted by Dr. Eileen Adamson's group (Xu et al., 1998). The construction of these mice ablated both vinculin and metavinculin protein expression. Homozygous vinculin knockout (KO) mice died by embryonic day (E) 10, with neural defects, aberrant forelimb developments, and hearts with reduced size and fewer than normal myocytes. Whether the cardiac phenotype was primary or secondary was not determined. The heterozygous vinculin KO mice (+/- Vcl KO) are viable, fertile, and do not have any obvious abnormalities but these mice are predisposed to cardiac failure when subjected to increased hemodynamic loading (Zemljic-Harpf et al., 2004). In another mouse model with cardiac myocyte specific excision of the vinculin gene (cVcl KO), mice showed disruption of cellular junctions, causing sudden death or dilated cardiomyopathy (Zemljic-Harpf, et al., 2007). Vinculin and metavinculin expression have also been found to be upregulated in normal functioning muscles in muscular dystrophy mouse models (Law et al., 1994). Here, as a result of the lack of dystrophin, the expression of vinculin and other proteins within its complex may occur as an alternative means for providing mechanical coupling and stable cellular structure.

In human heart failure and a bovine model of right ventricular failure caused by pulmonary hypertension (Heling et al., 2000; Lemler et al., 2000), the distribution of

vinculin and metavinculin within cardiomyocytes have been found to be disorganized and mobilization of vinculin from areas within intercalated disks and costameres to the cytoplasm was observed. Additionally, several recent reports have linked metavinculin mutations to cardiomyopathy in humans. Two mutations in the metavinculin exon included a missense mutation Arg975Trp and a 3bp deletion (Leu954del) (Olson et al., 2002). These mutations were detected in patients that presented with dilated cardiomyopathy and had heterozygous mutations, which suggest a dominant negative effect of this mutant allele or that approximate 50% reductions in cardiac metavinculin could predispose individuals to dilated cardiomyopathy. Recently, the Arg975Trp mutation and a mutation in the head region of Vcl (Leu277Met) were both associated with hypertrophic cardiomyopathy (Vasile et al., 2006a; Vasile et al., 2006b). These patients had a preserved ratio of vinculin and metavinculin expression in Z-lines of biopsy specimens, but were significantly reduced in the intercalated disks of the heart, which suggests that normal expression for metavinculin is necessary for maintaining cardiac function.

Despite this range of studies, it is still unclear as to vinculin's direct role in mechanotransduction and in the development of cardiomyopathy.

1.6 Conclusion and future directions

Currently, there exist a variety of methods used to study the various types of cardiac mechanotransduction. Despite extensive analyses of its structure, the mechanism of vinculin's interactions and its role in cardiac mechanotransduction still remains incompletely understood. With the development of new methods to study the spatial and temporal changes of signaling pathways using live-cell imaging, the roles of proteins involved in cardiac mechanotransduction may give insight on how mechanical signals are transduced into biochemical signals. Future directions include loss of function, gain of function, and molecular rescue studies and probing the anisotropy of mechanotransduction in cardiac cells from embryonic, neonatal, and adults. By utilizing new methods for studying mechanotransduction, a more mechanistic understanding of vinculin, its

role in cardiac mechanotransduction, and ultimately, in heart failure may provide key information useful for the development of future therapies for heart failure.

1.7 Scope of the dissertation

The objective of this dissertation is to investigate the role of vinculin in cardiac mechanotransduction. To study vinculin's role in mechanotransduction, we developed a method using laser tweezers and multifocal multiphoton fluorescence resonance energy transfer microscopy. We investigated the ability of our system to apply mechanical forces and detect changes in cell signaling in response to these forces. We also studied the effects of directionalized force application on isolated neonatal murine ventricular cardiac myocytes and investigated the effect of vinculin gene deletion/ protein deficiency on changes in cardiac mechanotransduction (Figure 4).

Chapter 2 introduces the theory behind optical trapping and multiphoton fluorescence microscopy.

Chapter 3 discusses the hardware, software, and optical design for studying cardiac mechanotransduction.

Chapter 4 describes the effects of optical trapping and multiphoton fluorescence microscopy on cardiac mechanotransduction. The discussion includes cell type considerations, wavelength selection, and control of experimental conditions.

Chapter 5 discusses the development of an adenovirus containing a FAK FRET reporter. The virus was constructed, verified, purified, titered, and the concentrations for use on neonatal murine cardiac ventricular myocytes and adult murine cardiac ventricular myocytes were determined.

Chapter 6 discusses the use of the combined laser tweezers and multifocal multiphoton fluorescence resonance energy transfer microscopy system to study cardiac mechanotransduction. The effects of force application on a ligand-coated bead on neonatal murine cardiac ventricular myocytes are measured and the effects of directionalized force application are measured.

Chapter 7 discusses the development and characterization of a tamoxifen inducible cardiac specific vinculin knockout mouse. This model is a temporally controlled cardiac specific vinculin knockout model. The time course and dosage of tamoxifen to gain sufficient vinculin knockdown is characterized. Time course for survival curve and development of cardiomyopathy is determined.

Chapter 8 discusses the role of vinculin in isolated neonatal murine cardiac ventricular myocytes. The effects of vinculin deletion on cardiac mechanotransduction are investigated. The mechanotransduction responses to directionally applied forces in both wildtype and knockouts are measured.

Chapter 9 summarizes these studies and their contributions to studying cardiac mechanotransduction and the role of vinculin in cardiac mechanotransduction. I will also discuss the custom system's limitations and possible solutions as well as hardware and software modifications that can optimize experiments and increase throughput. Finally, I will conclude with discuss the project's potential future directions.

The appendices include supplementary information including user manuals and discussion of pilot projects.

Appendix A is a Imspector user manual for multiphoton fluorescence excitation.

Appendix B is a Robolase III user manual for manipulating the laser tweezers.

Appendix C is a Dual view calibration user manual used to calibrate the images used in fluorescence resonance energy transfer studies.

Appendix D is a Laser tweezers force calibration user manual used to calibrate the laser tweezers.

Appendix E discusses the use of fluorescence correlation spectroscopy for the determination of ligand concentration per unit area of a polystyrene bead used in cardiac mechanotransduction experiments.

Appendix F discusses the use of Continuity to study the anisotropic stress and strain of a single cardiac myocyte.

1.8 Figures

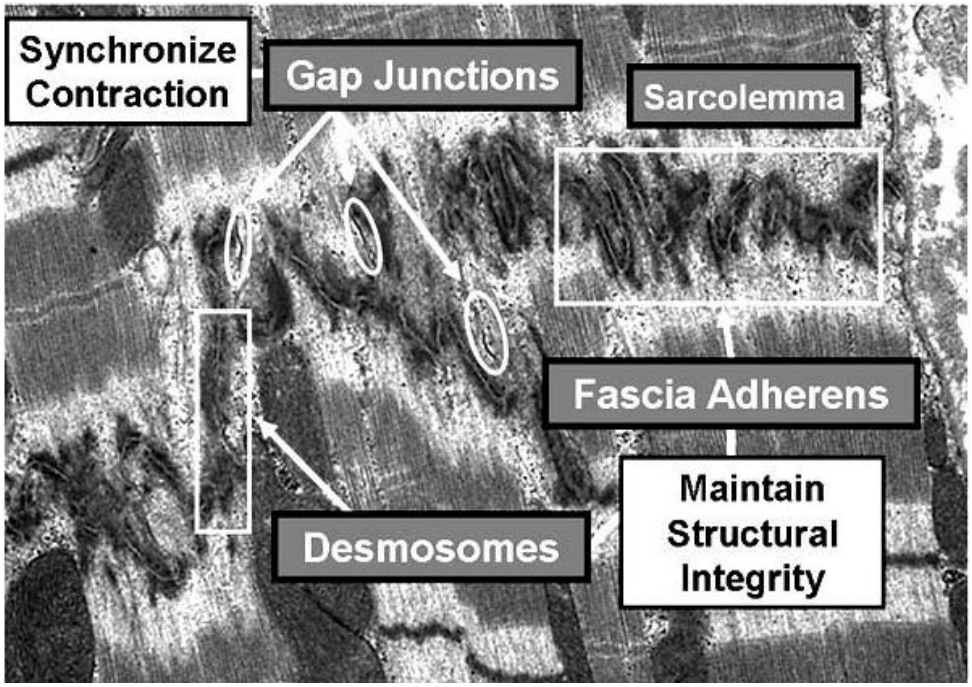

Figure 1.1: Arrangement of the intercalated disk. The cardiac myocytes are connected end to end by intercalated disks. The intercalated disks include gap junctions which are the sites of electrical coupling, fascia adherens, where myofilaments connect to the sarcolemma, and desmosomes which link intermediate filaments. Figure courtesy of Dr. Robert Ross.

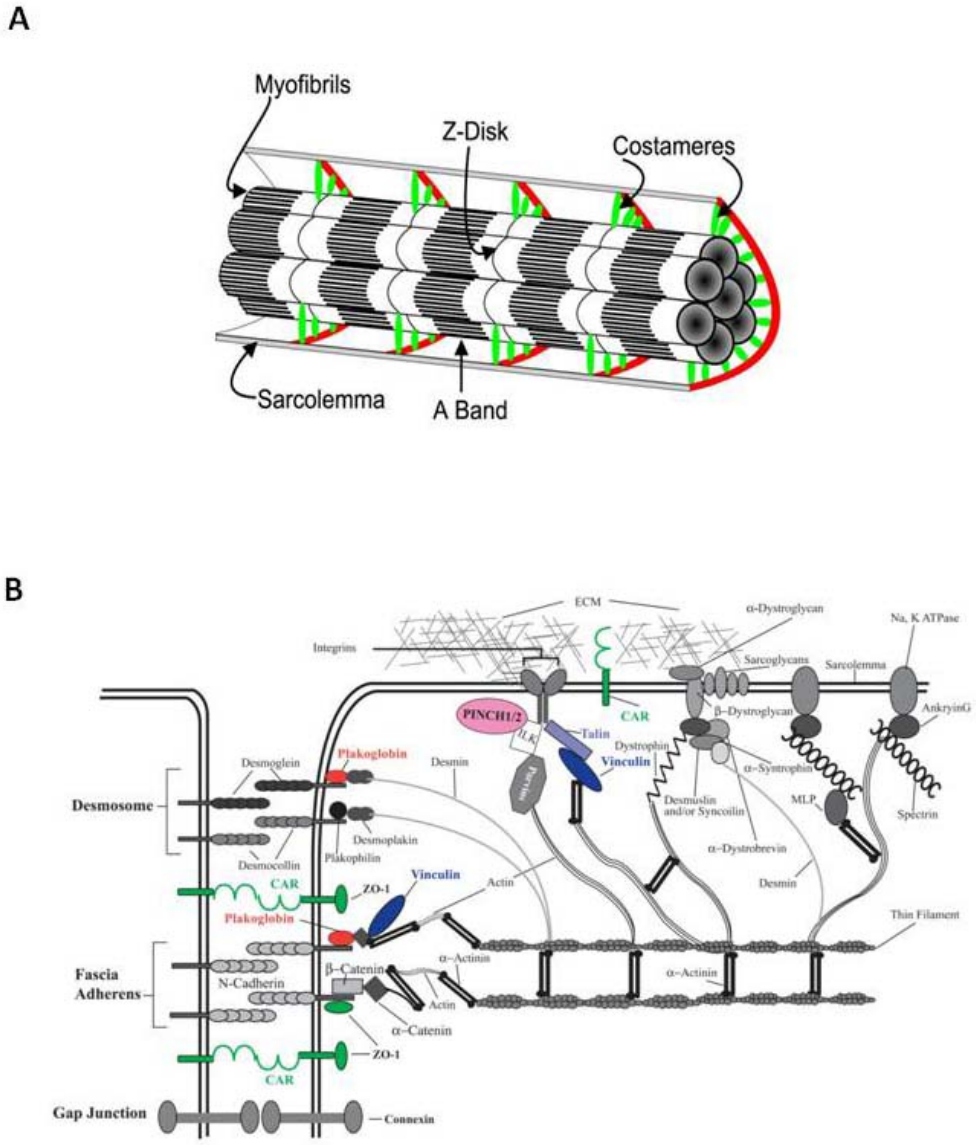

Figure 1.2: Cardiac myocyte cell and structure. A) Cartoon of a cardiac myocyte showing the location of the costameres relative to the cell axis (Ervasti, 2003). B) Cartoon of important proteins located in the intercalated disk and cell-extracellular matrix junction and how they connect to the myofilaments. Figure adapted from Clark et al., 2002 and courtesy of Dr. Robert Ross.

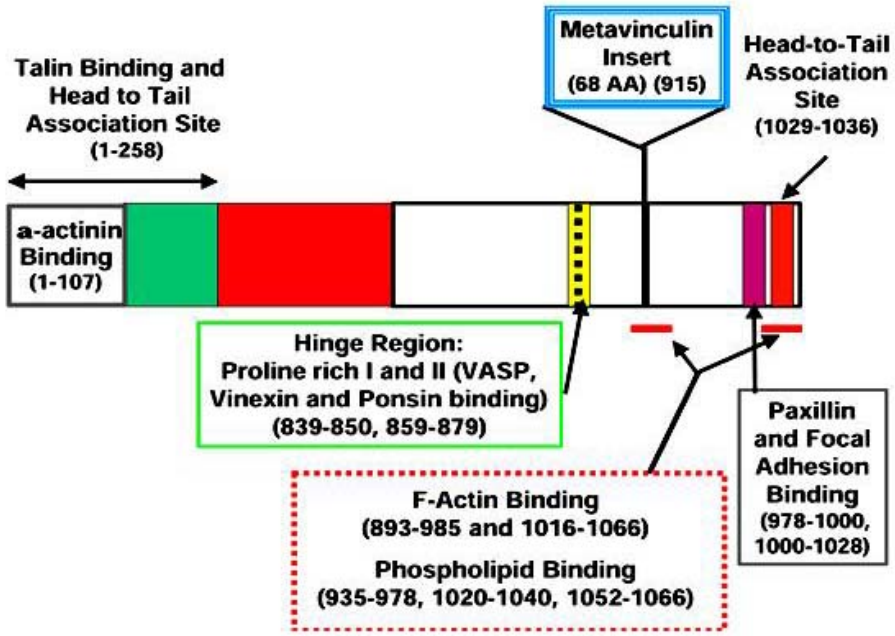

Figure 1.3: Important domains within the vinculin protein and the metavinculin insertion site. Figure courtesy of Dr. Robert Ross.

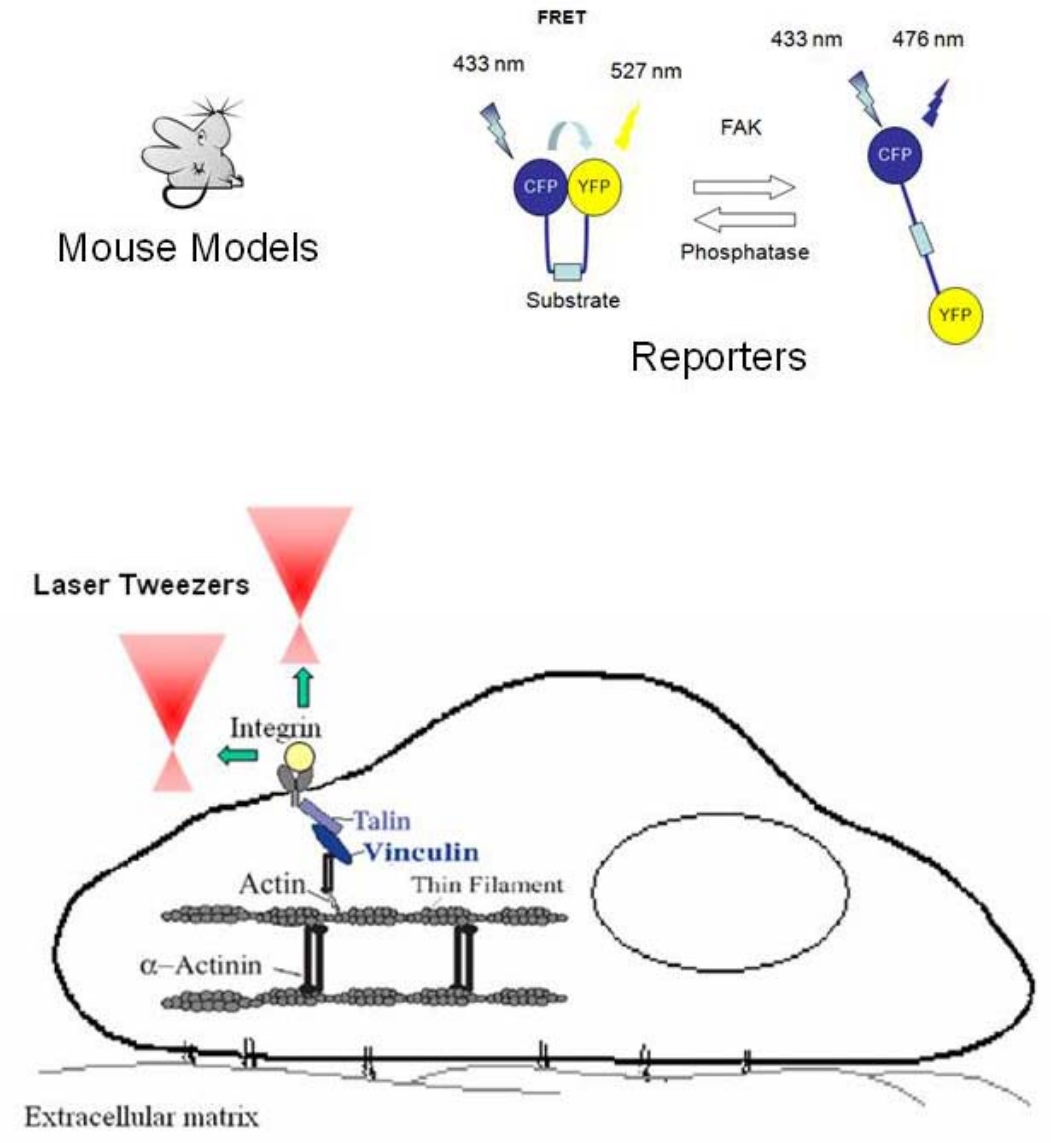

Figure 1.4: Overview of studying cardiac mechanotransduction using isolated single cells from genetically manipulated murine models in combination with laser tweezers and multiphoton fluorescence resonance energy transfer microscopy.

1.9 References

[1] Ashkin, A. (1992). Forces of a single-beam gradient laser trap on a dielectric sphere in the ray optics regime. Biophys J, 61, 569-582.

[2] Babbitt, C.J., Shai, S.Y., Harpf, A.E., Pham, C.G., and Ross, R.S. (2002). Modulation of integrins and integrin signaling molecules in the pressure-loaded murine ventricle. Histochem. Cell Biol. 118, 431-439.

[3] Bakolitsa, C., Cohen, D.M., Bankston, L.A., Bobkov, A.A., Cadwell, G.W., Jennings, L., Critchley, D.R., Craig, S.W., and Liddington, R.C. (2004). Structural basis for vinculin activation at sites of cell adhesion BAKOLITSA2004. Nature 430, 583-586.

[4] Ben Ze'ev, A., Reiss, R., Bendori, R., and Gorodecki, B. (1990). Transient induction of vinculin gene expression in 3T3 fibroblasts stimulated by serum-growth factors. Cell Regul. 1, 621-636.

[5] Bendori, R., Salomon, D., and Geiger, B. (1989). Identification of two distinct functional domains on vinculin involved in its association with focal contacts. J. Cell Biol. 108, 2383-2393.

[6] Berns, M.W. (1998). Laser scissors and tweezers. Scientific American 278, 62-67.

[7] Borgon, R.A., Vonrhein, C., Bricogne, G., Bois, P.R., and Izard, T. (2004). Crystal structure of human vinculin. Structure. 12, 1189-1197.

[8] Bowles, N.E., Bowles, K.R., and Towbin, J.A. (2000). The "final common pathway" hypothesis and inherited cardiovascular disease. The role of cytoskeletal proteins in dilated cardiomyopathy. Herz 25, 168-175.

[9] Brancaccio, M., Hirsch, E., Notte, A., Selvetella, G., Lembo, G., & Tarone, G. (2006). Integrin signalling: The tug-of-war in heart hypertrophy. Cardiovasc Res, 70(3), 422-433.

[10] Burridge, K. and Mangeat, P. (1984). An interaction between vinculin and talin. Nature 308, 744-746.

[11] Chodniewicz, D., & Klemke, R. (2004). Regulation of integrin-mediated cellular responses through assembly of a CAS/Crk scaffold. Biochim Biophys Acta, 1692, 63-76.

[12] Clark, K.A., McElhinny, A.S., Beckerle, M.C., and Gregorio, C.C. (2002). Striated muscle cytoarchitecture: an intricate web of form and function. Annu. Rev. Cell Dev. Biol. 18, 637-706.

[13] Critchley, D. R. (2004). Cytoskeletal proteins talin and vinculin in integrin-mediated adhesion. Biochem Soc Trans., 32, 831-836.

[14] Danowski, B.A., Imanaka-Yoshida, K., Sanger, J.M., and Sanger, J.W. (1992). Costameres are sites of force transmission to the substratum in adult rat cardiomyocytes. J Cell Biol. 118, 1411-1420.

[15] Domingos, P., Fonseca, P., Nadruz, W. J., & Franchini, K. (2002). Load-induced focal adhesion kinase activation in the myocardium: Role of stretch and contractile activity. Am J Physiol Heart Circ Physiol, 282, H556-H564.

[16] Ervasti, J.M. (2003). Costameres: the Achilles' heel of Herculean muscle. J. Biol. Chem. 278, 13591-13594.

[17] Ezzell, R.M., Goldmann, W.H., Wang, N., Parasharama, N., and Ingber, D.E. (1997). Vinculin promotes cell spreading by mechanically coupling integrins to the cytoskeleton. Exp Cell Res 231, 14-26.

[18] Gaits, F., & Hahn, K. (2003). Shedding light on cell signaling Interpretation of FRET biosensors. Sci STKE, 165, PE3.

[19] Goldmann, W.H., Guttenberg, Z., Tang, J.X., Kroy, K., Isenberg, G., and Ezzell, R.M. (1998). Analysis of the F-actin binding fragments of vinculin using stopped-flow and dynamic light-scattering measurements [published erratum appears in Eur J Biochem 1998 Sep 15; 256(3):603]. Eur. J. Biochem. 254, 413-419.

[20] Goldmann, W.H. and Ingber, D.E. (2002). Intact vinculin protein is required for control of cell shape, cell mechanics, and rac-dependent lamellipodia formation. Biochem. Biophys. Res. Commun. 290, 749-755.

[21] Grossman, W., D. Jones, and L. P. McLaurin. (1975) Wall stress and patterns of hypertrophy in the human left ventricle. J. Clin. Invest. 56: 56-64.

[22] Heling, A., Zimmermann, R., Kostin, S., Maeno, Y., Hein, S., Devaux, B., Bauer, E., Klovekorn, W.P., Schlepper, M., Schaper, W., and Schaper, J. (2000). Increased expression of cytoskeletal, linkage, and extracellular proteins in failing human myocardium. Circ. Res. 86, 846-853.

[23] Huang, H., Kamm, R., & Lee, R. (2004). Cell mechanics and mechanotransduction: Pathways, probes, and physiology. Am J Physiol Cell Physiol, 287, C1-C11.

[24] Humphries, J., Wang, P., Streuli, C., Geiger, B., Humphries, M., & Ballestrem, C. (2007). Vinculin controls focal adhesion formation by direct interactions with talin and actin. J Cell Biol, 179, 1043-1057.

[25] Imanaka-Yoshida, K., Enomoto-Iwamoto, M., Yoshida, T., and Sakakura, T. (1999). Vinculin, Talin, Integrin alpha6beta1 and laminin can serve as components of attachment complex mediating contraction force transmission from cardiomyocytes to extracellular matrix. Cell Motil. Cytoskeleton 42, 1-11.

[26] Johnson, R.P. and Craig, S.W. (1994). An intramolecular association between the head and tail domains of vinculin modulates talin binding. J. Biol. Chem. 269, 12611-12619.

[27] Keller, R.S., Shai, S.Y., Babbitt, C.J., Pham, C.G., Solaro, R.J., Valencik, M.L., Loftus, J.C., and Ross, R.S. (2001). Disruption of Integrin Function in the Murine Myocardium Leads to Perinatal Lethality, Fibrosis, and Abnormal Cardiac Performance. Am J Pathol. 158, 1079-1090.

[28] Keren, A. and Popp, R.L. (1992). Assignment of patients into the classification of cardiomyopathies. Circulation 86, 1622-1633.

[29] Knll, R., Hoshijima, M., & Chien, K. (2003). Cardiac mechanotransduction and implications for heart disease.81, 750-756.

[30] Law, D.J., Allen, D.L., and Tidball, J.G. (1994). Talin, vinculin and DRP (utrophin) concentrations are increased at mdx myotendinous junctions following onset of necrosis. J Cell Sci 107 (Pt 6), 1477-1483.

[31] Legate, K. R., M., E., Kudlacek, O., & Fssler, R. (2006). ILK, PINCH and parvin: The tIPP of integrin signalling. Nat Rev Mol Cell Biol., 7, 20-31.

[32] Lemler, M.S., Bies, R.D., Frid, M.G., Sastravaha, A., Zisman, L.S., Bohlmeyer, T., Gerdes, A.M., Reeves, J.T., and Stenmark, K.R. (2000). Myocyte cytoskeletal disorganization and right heart failure in hypoxia- induced neonatal pulmonary hypertension. Am. J. Physiol Heart Circ. Physiol 279, H1365-H1376.

[33] Liu, S., Calderwood, D., Ginsberg, (2000). M. Integrin cytoplasmic domain-binding proteins. J Cell Sci. 113, 3563-3571.

[34] Mansour, H., de Tombe, P.P., Samarel, A.M., et al. (2004) Restoration of resting sarcomere length after uniaxial static strain is regulated by protein kinase Cepsilon and focal adhesion kinase. Circ Res. 94, 642-649.

[35] Maron, B.J., Towbin, J.A., Thiene, G., Antzelevitch, C., Corrado, D., Arnett, D., Moss, A.J., Seidman, C.E., and Young, J.B. (2006). Contemporary definitions and classification of the cardiomyopathies: an American Heart Association Scientific

Statement from the Council on Clinical Cardiology, Heart Failure and Transplantation Committee; Quality of Care and Outcomes Research and Functional Genomics and Translational Biology Interdisciplinary Working Groups; and Council on Epidemiology and Prevention. Circulation 113, 1807-1816.

[36] Olson, T.M., Illenberger, S., Kishimoto, N.Y., Huttelmaier, S., Keating, M.T., and Jockusch, B.M. (2002). Metavinculin mutations alter actin interaction in dilated cardiomyopathy. Circulation 105, 431-437.

[37] Perriard, J.C., Hirschy, A., and Ehler, E. (2003). Dilated cardiomyopathy: a disease of the intercalated disc? Trends Cardiovasc. Med. 13, 30-38.

[38] Pokutta, S. and Weis, W.I. (2002). The cytoplasmic face of cell contact sites. Curr. Opin. Struct. Biol. 12, 255-262.

[39] Richardson, P., McKenna, W., Bristow, M., Maisch, B., Mautner, B., O'Connell, J., Olsen, E., Thiene, G., Goodwin, J., Gyarfas, I., Martin, I., and Nordet, P. (1996). Report of the 1995 World Health Organization/International Society and Federation of Cardiology Task Force on the Definition and Classification of cardiomyopathies. Circulation 93, 841-842.

[40] Ross, R.S., Pham, C., Shai, S.Y., Goldhaber, J.I., Fenczik, C., Glembotski, C.C., Ginsberg, M.H., and Loftus, J.C. (1998). Beta1 integrins participate in the hypertrophic response of rat ventricular myocytes. Circ. Res. 82, 1160-1172.

[41] Samarel, A.M. (2005). Costameres, focal adhesions, and cardiomyocyte mechanotransduction. Am. J. Physiol Heart Circ. Physiol 289, H2291-H2301.

[42] Schlessinger, J. and Geiger, B. (1983). The dynamic interrelationships of actin and vinculin in cultured cells. Cell Motil. 3, 399-403.

[43] Shiraishi, I., Simpson, D.G., Carver, W., Price, R., Hirozane, T., Terracio, L., and Borg, T.K. (1997). Vinculin is an essential component for normal myofibrillar arrangement in fetal mouse cardiac myocytes. J. Mol. Cell Cardiol. 29, 2041-2052.

[44] Simpson, D.G., Terracio, L., Terracio, M., Price, R.L., Turner, D.C., and Borg, T.K. (1994). Modulation of cardiac myocyte phenotype in vitro by the composition and orientation of the extracellular matrix. J. Cell Physiol. 161, 89-105.

[45] Terracio, L., Simpson, D.G., Hilenski, L., Carver, W., Decker, R.S., Vinson, N., and Borg, T.K. (1990). Distribution of vinculin in the Z-disk of striated muscle: analysis by laser scanning confocal microscopy. J Cell Physiol 145, 78-87.

[46] Towbin, J.A. and Bowles, N.E. (2000). Genetic abnormalities responsible for dilated cardiomyopathy. Curr. Cardiol. Rep. 2, 475-480.

[47] Towbin, J.A. and Bowles, N.E. (2006). Dilated Cardiomyopathy: A Tale of Cytoskeletal Proteins and Beyond TOWBIN2006. J. Cardiovasc. Electrophysiol. 17, 919-26.

[48] Vasile, V.C., Ommen, S.R., Edwards, W.D., and Ackerman, M.J. (2006a). A missense mutation in a ubiquitously expressed protein, vinculin, confers susceptibility to hypertrophic cardiomyopathy. Biochem. Biophys. Res. Commun. 345, 998-1003.

[49] Vasile, V.C., Will, M.L., Ommen, S.R., Edwards, W.D., Olson, T.M., and Ackerman, M.J. (2006b). Identification of a metavinculin missense mutation, R975W, associated with both hypertrophic and dilated cardiomyopathy. Mol. Genet. Metab 87, 169-174.

[50] Wang, Y., Botvinick, E., Zhao, Y., Berns, M., Usami, S., Tsien, R., and Chien, S. (2005). Visualizing the mechanical activation of src. Nature, 434, 1040-1045.

[51] Weller, P.A., Ogryzko, E.P., Corben, E.B., Zhidkova, N.I., Patel, B., Price, G.J., Spurr, N.K., Koteliansky, V.E., and Critchley, D.R. (1990). Complete sequence of human vinculin and assignment of the gene to chromosome 10. Proc Natl Acad Sci U S A 87, 5667-5671.

[52] Xu, W., Baribault, H., and Adamson, E.D. (1998). Vinculin knockout results in heart and brain defects during embryonic development. Development 125, 327-337.

[53] Zemljic-Harpf, A., Manso, A. M., & Ross, R. S. (2009). Vinculin and talin: Focus on the myocardium. J Investig Med., 57(8), 849-855.

[54] Zemljic-Harpf, A., Miller, J., Henderson, S., Wright, A., Manso, A., Elsherif, L., et al. (2007). Cardiac-myocyte-specific excision of the vinculin gene disrupts cellular junctions, causing sudden death or dilated cardiomyopathy. Mol Cell Biol, 27, 7522-7537.

[55] Zemljic-Harpf, A., Ponrartana, S., Avalos, R., Jordan, M., Roos, K., Dalton, N., et al. (2004). Heterozygous inactivation of the vinculin gene predisposes to stress-induced cardiomyopathy. Am J Pathol, 165, 1033-1044.

[56] Ziegler, W.H., Liddington, R.C., and Critchley, D.R. (2006). The structure and regulation of vinculin. Trends Cell Biol. 16, 453-460.

Chapter 2

Optical trapping and multiphoton fluorescence microscopy

2.1 Introduction

For this dissertation, we will develop a method to study cardiac mechanotransduction in isolated single cells. We will begin by describing the current methods for applying external mechanical signals to cells and the imaging modalities for providing readouts for mechanotransduction events. We will then discuss our selected method for force application and imaging modality for studying cardiac mechanotransduction events.

2.2 Methods for applying mechanical forces

Current methods for mechanical perturbation include, but are not limited to: anisotropic stretch application using an elastic substrate, shear stress by fluid flow, magnetic tweezers, and use of optical trapping (Huang et al., 2004).

Anisotropic stretch using an elastic substrate has been used previously to study cardiac mechanotransduction events in neonatal rat cardiac ventricular myocytes. In

Gopalan et al., 2003, anisotropic stretchers were used to study transverse and longitudinal effects on regulation of sarcomere organization, hypertrophy, and cell-cell junctions. Although this technique provides a powerful means to apply forces on a cell, results reported are representative of a population of cells and the transverse and longitudinal stretches were not uniaxial. This type of experiment is difficult to elucidate mechanistically how a protein may contribute to a mechanotransduction event. Alternatively, in Senyo et al., 2007, uniaxial strains were applied to cells, however, the results were representative of a population of cells, and it is difficult to tease out the contributions of a mechanical signal on a single cell's mechanotransduction events and how it contributes to an overall monolayer response.

In Lorenzen-Schmidt et al., 2006, shear stress by fluid flow was applied to cardiac ventricular myocytes. Results elucidated that the beta-adrenergic signaling pathway and integrin activation may play a role in mechanotransduction response to fluid shear. Although this setup provides a means to apply mechanical forces, it is difficult to use this setup to study an isolated mechanotransduction pathway because there is no means to control which mechanotransduction pathway is activated.

To allow for local stresses to be applied on a specific group of receptors on single cells, ligand coated beads for a specific group of receptors is typically used (Huang et al., 2004). One technique which utilizes ligand coated beads is magnetic tweezers. Magnetic tweezers use magnetic fields to generate magnetic forces on a bead, which when adhered to a cell, can cause mechanical forces to be applied on a cell. The advantage of using this system is that a constant force can be applied and it can be applied to a specific receptor system. Disadvantages of this system include the working distance requirements of incorporating the magnetic tweezers into the setup, the difficulty of creating a fine sharp tip capable of applying forces to a bead, and fabrication of magnetic beads.

Alternative to magnetic tweezers, laser tweezers, also known as optical trapping, provides a means to apply mechanical forces to a specific receptor system within a cell.

An advantage to using laser tweezers is the specificity of localized mechanical

forces, the ability to apply forces in various directions, and the ability to control the amount of forces. As such, we will discuss the theory behind optical trapping and discuss the application of laser tweezers in cardiac mechanotransduction studies.

2.3 Theory of optical trapping

A light beam is made up of many photons. Upon interaction of an incoming light beam focused by a microscope objective and a particle, the momentum change in the photon will be conserved by transferring it to the particle and the change in momentum of a photon per time is related to force.

For particles larger than the wavelength of light (Mie regime), the incident light beam is broken up into rays. The momentum flux of a ray of light can be calculated to be p = nP/c in the direction of the ray, where p is the magnitude of the momentum flux, P is the power (i.e. energy flux); n is the refractive index of the medium, and c is the speed of light in free space (Nieminen et al., 2007). These rays are then traced through the transparent sphere through infinite reflection and their direction changes when the ray reflects and refracts at the particle-medium interface. When light is refracted by the particle, the momentum of the photons is changed and since momentum is conserved, an equal and opposite momentum change is related the particle (Neuman and Block, 2004). Optical forces are generated because force is the time rate of change in the momentum flux of the beam (Nieminen et al., 2007). For particles whose index of refraction is greater than the surrounding media, the gradient force is in the direction of the maximum light intensity and the scattering force is caused by the reflections or refractions of the light pointing in an outward propagating direction. These forces are proportional to the intensity of light (Neuman and Block, 2004) and when the gradient force overcomes the scattering force, the particle becomes trapped (Figure 1).

For mechanotransduction studies, the laser tweezers can be calibrated by using microspheres visualized by a CCD camera (Wang and Botvinick, 2007). Using the Airy disk radius as an approximation of microscope resolution, the positioning of the bead

image obtained on the CCD camera can be calculated.

When a microsphere is stably trapped and the stage is moved to allow the bead to reach force equilibrium, the force exerted by the trap can be calculated. The force exerted by the trap is calculated because the viscous forces equal the light forces. The viscous force can be calculated from the stage velocity using the Stokes flow approximation: $F_{viscous} = 6\pi\mu r v_{stage}$, where μ is the viscosity of the surrounding fluid, r is the microsphere radius, and vstage is the microscope stage velocity (Figure 2). Using images captured by the CCD camera when the stage is moved and a bead is stably trapped, the displacement between the center of the bead and the center of the trap can be calculated and a force-displacement curve can be generated. By varying the power of the laser or size of a bead, a variety of forces can be achieved (Figure 3).

Overall, laser tweezers provides a means to study cardiac mechanotransduction by applying mechanical forces to specific receptor systems in a controlled manner.

2.4 Imaging modalities for studying cardiac mechanotransduction

We discussed the use of laser tweezers to study cardiac mechanotransduction in isolated single cells, and now, we will discuss the various imaging modalities that exist to record readouts of reporters involved in mechanotransduction pathways.

For this dissertation, we are interested in studying mechanotransduction events in cardiac myocytes and to elucidate the role of vinculin in mechanotransduction. As such, reporters for biochemical signaling and imaging of these reporters are required. Current reporters for cell signaling include fluorescent reporters consisting of single fluorophore (i.e. Fura-2AM) or multiple fluorophore systems (i.e. FRET based systems).

To image cells that contain fluorescent markers, wide field fluorescence microscopy has been typically used. The advantages of wide field fluorescence are that a wide spectrum equivalent to the excitation spectrum of the chosen fluorescent marker

can be used to the excite the markers and that by changing excitation and emission filter sets, a variety of markers can be imaged with the same system. The disadvantage of wield field fluorescence that fluorescence excitation is not limited to a single plane, and emission occurs throughout the excited volume which obscures the resolution of the image that exists in the objective focal plane. Other disadvantages of wide field fluorescence is excitation of a large focal volume, also leads to an increased volume of photobleached molecules, and excitation with shorter wavelengths can be phototoxic for cells (Swedlow and Platani, 2002).

To overcome the phototoxicity and obscured resolution of wide field fluorescence, two photon, or multiphoton excitation fluorescence microscopy provides a means to image fragile cardiac myocytes.

2.5 Theory of multiphoton excitation

In fluorescence experiments, excitation occurs due to absorption of a single photon by each fluorophore. However, a fluorophore can absorb two or more long wavelength photons to reach the same first singlet excited state. Two photon or multiphoton excitation occurs when there is a simultaneous absorption of two or more lower energy photons to reach an excited state (Figure 4). For this to occur, it is essential to focus the exciting photons to obtain a high local intensity. Because of the intensity of short-pulsed lasers it is possible to focus a light beam to a near diffraction-limited spot that is small enough so that multiphoton absorption/excitation can occur.

Two photon absorption increases quadratically with illumination intensity and limits the excitation to a tiny focal volume. This limits the out of focus background excitation and provides confocality because only fluorophores in the focal volume of the beam will be excited. The use of longer excitation light (710 - 990 nm) slows the rate of photobleaching, allowing the use of higher magnification objectives, and reduces phototoxicity effects (Bewersdorf et al., 1998).

2.6 Discussion and conclusion

For this dissertation, we discussed the use of an optical trap for studying the anisotropy of cardiac mechanotransduction and investigate the role of vinculin in mechanotransduction.

Advantages to using laser tweezers are that forces applied to a cell can be applied in a specific plane and in a specific direction in a controlled manner and in a controlled amount. When studying mechanotransduction, ligand coated beads are placed onto the cells to allow mechanical stimulus to be applied to specific receptor systems. To apply directionalized forces, a free floating bead is confined with an optical trap. The trapped bead position within the depth of the dish is adjusted such that the position of the highest intensity of the laser beam is determined and aligned with the center position of the bead that is adhered to cell (Figure 5). This calibration allows only forces in the x-y plane to act on the bead that is adhered to the cell and allows the experimenter to probe the directional responses of a cell to mechanical forces.

Using laser tweezers allows a range of forces to be applied in directions specified by the user, but disadvantages to using laser tweezers are that a long infrared wavelength laser and optics are needed to guide the laser into the microscope and the time of force application may be limited due to thermal heating caused by laser. Thermal heating effects caused by laser tweezers will be discussed further in Chapter 4.

In addition to directional force application, for this dissertation, longer wavelength excitation of a fluorescent resonance energy transfer (FRET) reporter to study primary cell lines will be used. Two photon excitation has advantages such as minimizing phototoxicity and photobleaching, and eliminating background fluorescence. However, two photon excitation has disadvantages, including photobleaching within the plane of excitation and the requirement of a pulsed laser capable of generating photons for two photon excitation. To decrease the photobleaching effect caused by two photon excitation, we implement a beam multiplexing system which splits the main laser beam of the Ti:sapphire laser into 16 beams. This increases the imaging speed by illuminating

multiple points of the sample simultaneously, as well as decreasing photobleaching. The simultaneous application of N foci results in an N times longer pixel time and N times more photons reaching the point, while the laser power is kept to a minimum (LaVision BioTec). For our set up, the dwell time of each of 16 beamlets was 0.013ms.

In conclusion, we will be using laser tweezers for directional force application and a laser split into 16 beams for multifocal multiphoton excitation. These techniques combined provide a powerful tool for studying cardiac mechanotransduction.

2.7 Figures

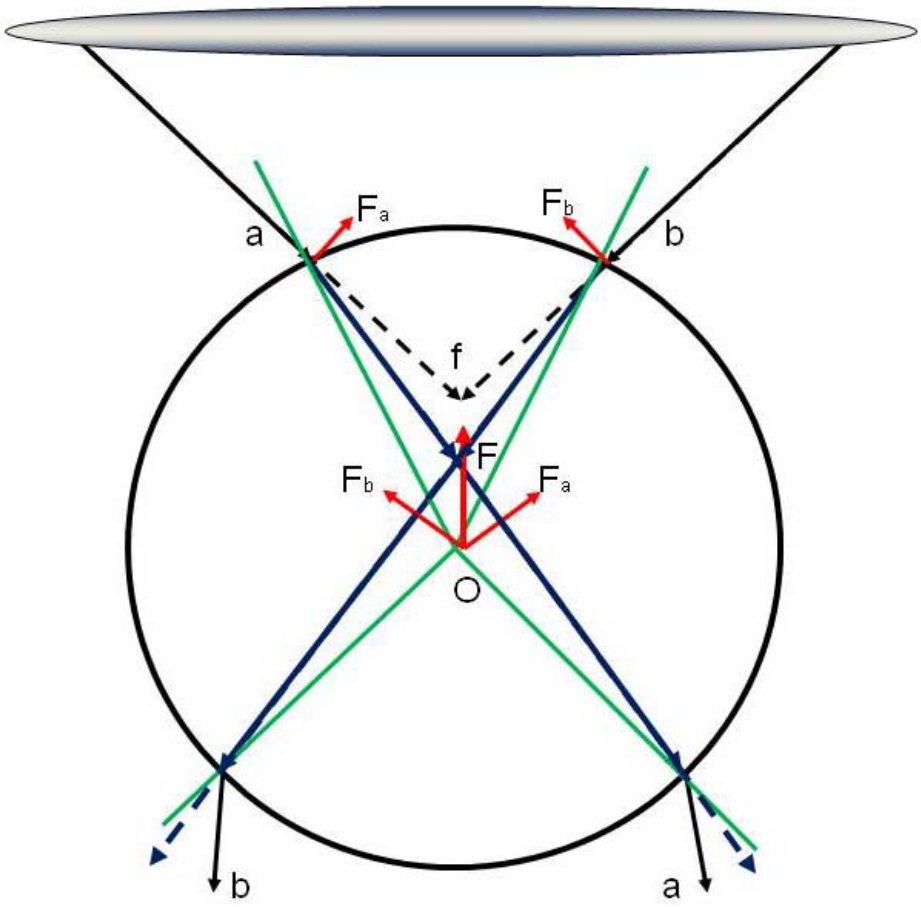

Figure 2.1: Ray optics diagram for a laser beam passed through a high numerical aperture lens and the positioning of a dielectric sphere in the trap. The diagram shows the displacement of the sphere from position O to the focus position, f. The rays drawn depict changes to the path of light due to the index of refraction of the sphere being greater than the index of refraction of the surrounding medium. The resulting net force, F, is due to the summation of forces Fa and Fb. This diagram shows the net force moving the bead in the z direction.

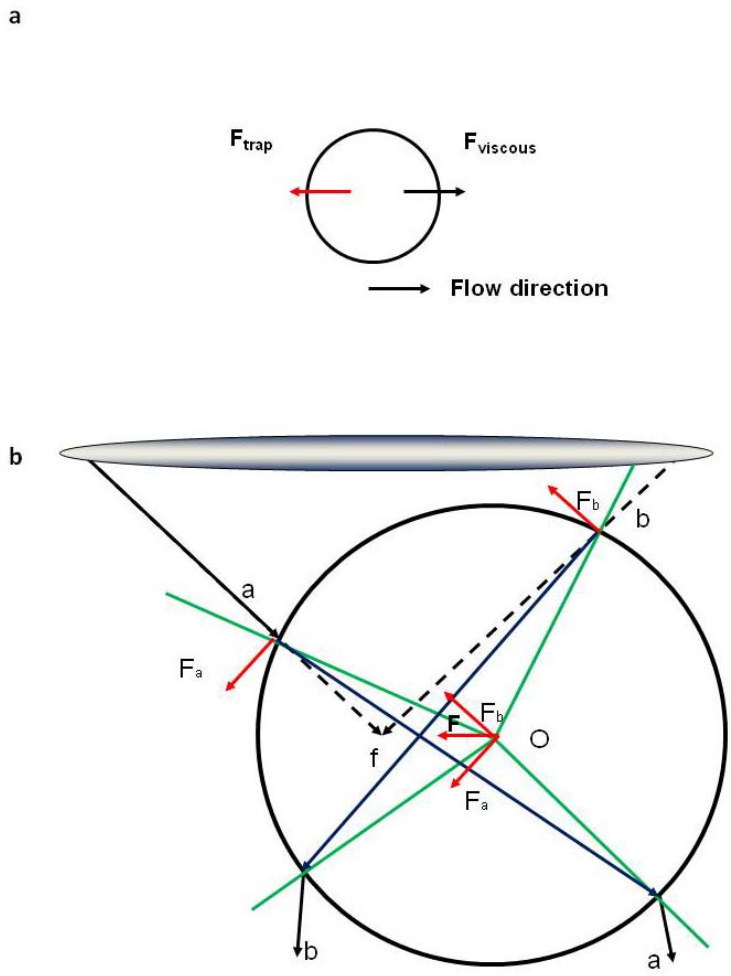

Figure 2.2: Calibration of laser tweezers. A) Force equilibrium for a sphere trapped by a laser tweezers and fluid flow passing over the sphere as a result of moving the stage. B) Ray optics diagram for a laser beam passed through a high numerical aperture lens and the positioning of a dielectric sphere in the trap. The diagram shows the displacement of the sphere from position O to the focus position, f. The rays drawn depict changes to the path of light due to the index of refraction of the sphere being greater than the index of refraction of the surrounding medium. The resulting net force, F, is due to the summation of forces Fa and Fb. This diagram shows the net force moving the bead in the x, y direction.

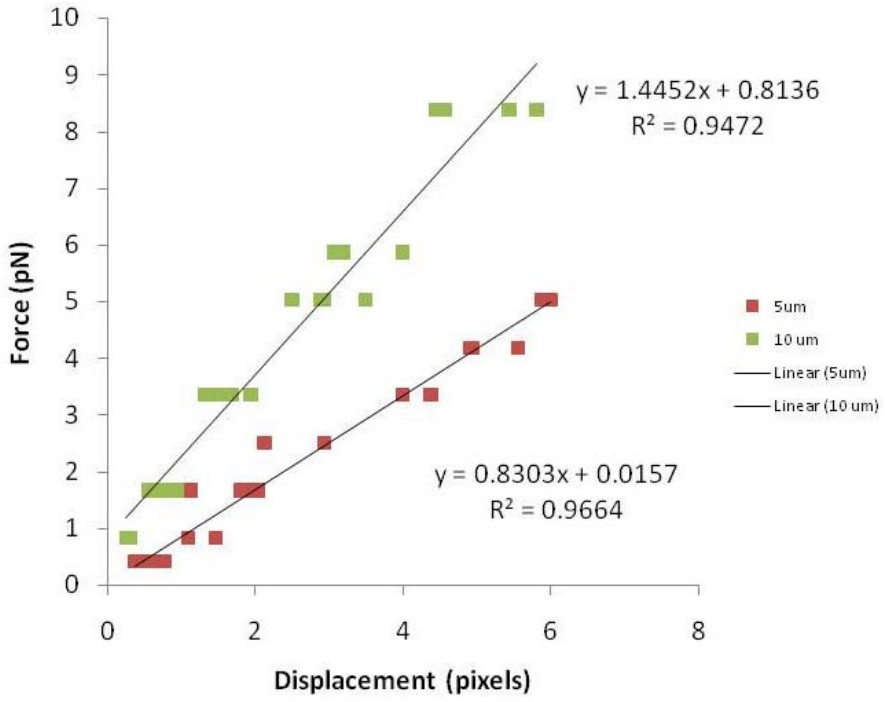

Figure 2.3: Force calibration curve. For a laser power setting of 18mW in the focal volume of the microscope, the force calibration curves were generated for a 5 micron and 10 micron bead.

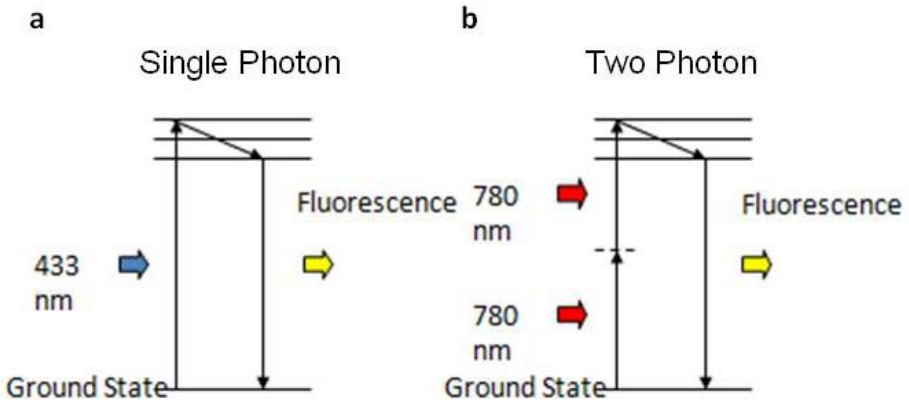

Figure 2.4: Jablonski diagram for single photon and two photon fluorescence. A) Single photon excitation, B) Two photon excitation

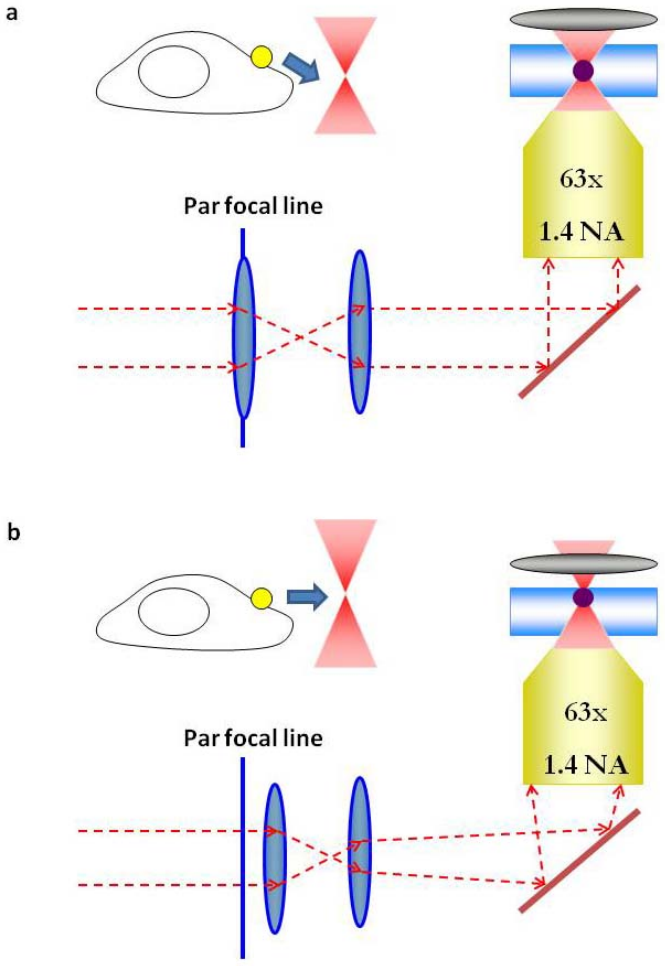

Figure 2.5: Preparing the laser tweezers position for force application. a) Laser tweezers setup shows that when a lens is positioned at the par focal line, the bead can be trapped in the focal plane of the laser tweezers. However, the center of the trap may be positioned lower than the center Z position of the bead that is adhered to the bead. b) To adjust the laser tweezers such that the center of the trap is lined up with the center Z position of the bead adhered to the cell, a lens is moved out of par focal alignment.

2.8 References

[1] Ashkin, A. (1992). Forces of a single-beam gradient laser trap on a dielectric sphere in the ray optics regime. Biophys J, 61, 569-582.

[2] Bewersdorf, J., Pick, R., & Hell, S. (1998). Multifocal multiphoton microscopy. Opt Lett., 23(9), 655-657.

[3] Gopalan, S., Flaim, C., Bhatia, S., Hoshijima, M., Knoell, R., Chien, K., et al. (2003). Anisotropic stretch-induced hypertrophy in neonatal ventricular myocytes micropatterned on deformable elastomers. Biotechnol Bioeng, 81(5), 578-587.

[4] Huang, H., Kamm, R., & Lee, R. (2004). Cell mechanics and mechanotransduction: Pathways, probes, and physiology. Am J Physiol Cell Physiol, 287, C1-C11.

[5] Lorenzen-Schmidt, I., Schmid-Schonbein, G. W., Giles, W. R., McCulloch, A. D., Chien, S., & Omens, J. H. (2006). Chronotropic response of cultured neonatal rat ventricular myocytes to short-term fluid shear. Cell Biochem Biophys, 46(2), 113-122.

[6] Neuman, K., & Block, S. (2004). Optical trapping. Rev Sci Instrum., 75(9), 2787-2809.

[7] Nielsen, T., Fricke, M., Hellweg, D., & Andresen, P. (2001). High efficiency beam splitter for multifocal multiphoton microscopy. J Microsc., 201, 368-376.

[8] Senyo, S., Koshman, Y., & Russell, B. (2007). Stimulus interval, rate and direction differentially regulate phosphorylation for mechanotransduction in neonatal cardiac myocytes. FEBS Lett., 581, 4241-4247.

[9] Swedlow, J. R., & Platani, M. (2002). Live cell imaging using wide-field microscopy and deconvolution. Cell Structure and Function, 27, 335-341.

Chapter 3

Hardware, software, and optical design for studying cardiac mechanotransduction

3.1 Introduction

For this dissertation, we developed a method to study cardiac mechanotransduction using laser tweezers and multiphoton fluorescence resonance energy transfer microscopy. By developing a custom hardware, software, and optical path setup, we can control parameters that we wish to manipulate, and minimize any disadvantages that exist in our setup.In this chapter, I will describe the hardware and software system that can be used to apply a force on cardiac myocytes with simultaneous fluorescence excitation.

3.2 Microscope system

The microscope used to do all laser tweezers and multiphoton fluorescence experiments is an Axiovert 200M (Zeiss, Thornwood, NY) with motorized objective turret, reflector turret, condensor turret, and a 63x plan-apochromat phase III, NA 1.4 oil im-

mersion objective. The motorized reflector turret is shift-free to allow repeat switching between filter cube positions and contains several filter cubes and a mirror for guiding the 1064nm infrared laser tweezers and the Ti:sapphire laser. Specimens were mounted in an X-Y servo stage controlled with ASI Automated Stage Controller (MS-2000 XYZ, Applied Scientific Instrumentation, Eugene, OR). Both microscope and stage controller are controlled by the main controller through serial port cable (COM). The temperature of the specimens was maintained at 37°C by a Temperature Controller stage holder (TC-324B, Warren Instrument Corporation).

The microscope system, hereafter referred to as "Robolase," utilizes two computer structures (Figure 1): a) main computer: controls the multiphoton fluorescence imaging system and microscope system, b) trapping computer: controls the optical tweezers and phase imaging. For capturing fluorescent images, a cooled digital 12 bit SensiCam CCD Camera (Applied Scientific Instrumentation, Eugene, OR) is connected to the top port of a Dual Video Adapter. Emission light from the microscope is guided into a dual view system where the collimating lens, gathers the divergent beams of light into a parallel beam. The light is then guided to a dichroic filter, where the light is split into ECFP and YPet emissions and the images are projected side by side on the CCD. This camera is connected to the main computer via a PCI imaging card. The Ti:sapphire femtosecond laser is controlled via the Imspector software and is connected to the computer via a serial port cable. For phase imaging, a red filter D680/60X is placed in front of the halogen light source and a short pass dichroic (600DCSP, Chroma, Bellows Falls, VT) is placed in the Dual Video Adapter to guide the long red wavelength to a Hamamatsu cooled charge-coupled device camera (C4742-98-24, Hamamatsu Photonics, K.K., Hamamatsu, Japan). This CCD Camera has high resolution (1344 x 1024 pixels), has a progressive scan interline readout with no mechanical shutter, and has an adjustable gain and exposure time for optical signal-to-noise characteristics. Robolase uses Hamamatsu's video capture Library for Labview plug-in to communicate with the camera controller through its Digital CAMera Application Programming Interface (DCAMAPI) driver. The infrared laser is controlled via Robolase and a serial port cable.

3.3 Laser and optical path

The 1064nm infrared laser power was controlled by the laser controller from the laser manufacturer. The beam was expanded using a beam expander made up of lenses from ThorLabs (biconvex, f = 35mm and f = 75mm) that has anti-reflective coating (650 - 1050 nm), but no other correction. A mechanical shutter (Uniblitz LS6ZM2, Vincent Associates, Rochester, NY) in the laser path is controlled by a shutter driver (Uniblitz VMM-D3, Vincent Associates) through two lines of digital input-output from the motion controller. Telecentric beam steering is achieved by placing a dual-axis fast scanning mirror (Newport Corp) at an image plane conjugate to the back focal plane of the microscope objective, producing a converging output beam parallel to the optical axis. This beam is then guided through relay lenses (f = 300mm), mirrors, a periscope, scan lens (f = 50mm), and a tube lens (f = 150mm). As the beam enters the microscope, it enters an empty filter cube position in the reflector turret, before entering the back of the objective lens (Figure 2).

The Ti:sapphire laser has a repetition rate of 76MHz and a pulse duration of 200fs. The main laser beam enters an attenuator and the beam diameter is adjusted by a telescope. The beam is then guided through a pre-chirp arrangement in which it compensates the pulse elongation introduced by lenses. The beam then enters a beam-multiplexer such that the beams are split to create 16 beams. These beams enter the same amount of glass and have identical pulse lengths. The beams then enter a nonresonant xy-scanner and the microscope objective focuses the beamlets into multiple foci on the object plane and allows for excitation of fluorescent molecules.

3.3.1 Measuring laser power

Laser power for each laser was measured before and after each experiment. These measurements were made by calibrating the photodiode output to the laser power measured in the specimen plane. To estimate laser power in the specimen plane, the objective is removed from the objective turret and the shutter for each laser is kept con-

tinuously open at a time, and the laser output was collected onto a pre-calibrated laser light meter (Newport Optical Meter, 1918 C). The transmission of the objective was measured using the established dual-objective method (Viana et al. 2006). This method corrects for total internal reflection losses at the objective oil-glass-water interfaces. The transmission coefficient of the Zeiss 63x1.4 NA objective for 780nm was determined to be 0.65 and for 1064nm was determined to be 0.25. The laser energy at the object focal plane was determined by measuring the input energy at the back aperture of the objective multiplied by the transmission coefficient of the objective at the wavelength of the laser used.

3.3.2 Dual View Calibration

Before each experiment, the DualView split images are aligned (Figure 3). A gridded slide is placed on the microscope setup and a custom-designed LabVIEW program is run to verify the alignment. The logic of the LabVIEW program is: to capture regions of interest from the two split image and check to see if there is a shift in the column and the row of the images. The program then outputs how much shift in pixels there exists in the images and allows the user to adjust the alignment of the DualView system and have the program check the changes until full image alignment is achieved. For detailed procedures on using this program, please refer to appendix C.

3.4 Robolase III microscope software system

3.4.1 Robolase III Software

The control software is programmed in the LabVIEW 8.2 (National Instruments) language and is responsible for control of the microscope, cameras, and trapping laser power. The control software also manages image and manage file storage. It communicates with the user through the graphic user interface or the ‘front panel’ in LabVIEW. The front panel receives user input and displays images and measurements. The control

software interprets commands sent by the user into appropriate hardware calls and returns the results of that action to the front panel and/or computer's hard drive. Emphasis was placed on the design of the front panel, such that it would be easy to learn while providing the features needed to search for a cell of interest and then to perform bead trapping on that cell (Figure 4). For more information on using this program, please refer to appendix B.

3.4.2 Imspector Software

Fluorescence imaging on the Sensicam is captured and translated to Imspector (LaVision Biotec, Germany). It controls various hardware devices such as the CCD Camera, the filter wheel, and the Ti:sapphire laser (Figure 5). For more information on using this program, please refer to appendix A.

3.5 Conclusion

For this dissertation, we designed and built a custom made optical system for studying cardiac mechanotransduction using laser tweezers and multifocal multiphoton fluorescence microscopy. Advantages of creating our own setup include designing our own software program for controlling hardware components, having control over experimental conditions such as force application, length of force application, and temperature control of specimens. Weaknesses to our setup include the maintenance of our lasers. However, by routinely testing the laser power in a controlled manner as described above, we can assess the laser power quality in a consistent manner. In conclusion, we have developed an optically based method for studying cardiac mechanotransduction in which we have optimized our experimental setup and minimized any disadvantages.

3.6 Figures

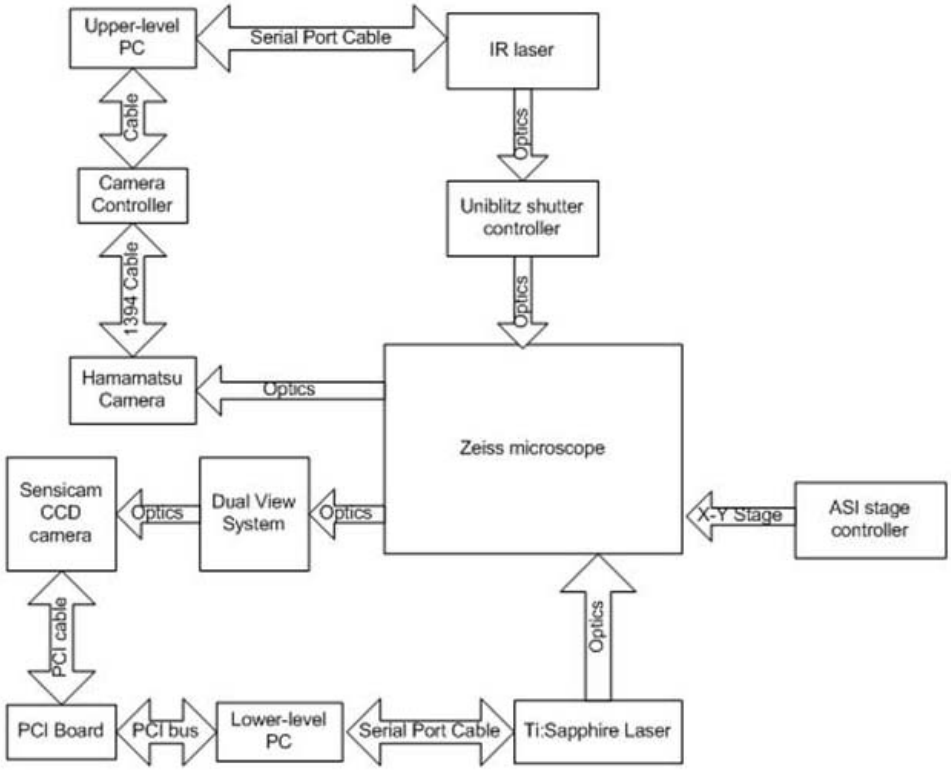

Figure 3.1: Hardware diagram of a system to study cardiac mechanotransduction

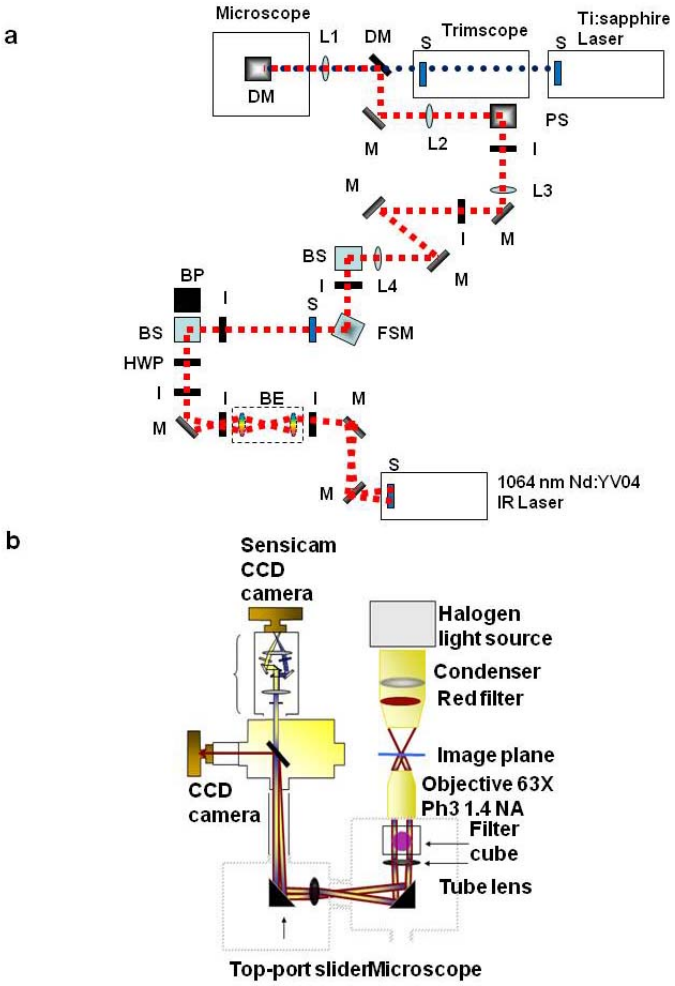

Figure 3.2: Diagram of microscope components for a multiphoton FRET-trapping system. a) A Ti:sapphire laser is divided into sixteen simultaneous laser spots using a TrimScope and combined with laser tweezers which enters an inverted microscope. Legend: 1.5x beam expansion system (BE), blocked path (BP), polarization beam splitter (BS), dichroic mirror (DM), fast steering mirror (FSM), iris (I), tube lens (f = 150mm) (L1), scan lens (f = 50mm) (L2), relay lenses (f = 300mm), mirror (M), periscope (PS), shutter (S), and half wave plate (HWP).

b) A red filter is placed before the microscope condenser to allow simultaneous imaging of phase contrast and separating the phase contrast light from the collected short wavelength fluorescence emissions. The shorter wavelength emissions of ECFP and YPet pass through a dual view system which splits the emissions and images simultaneously on the Sensicam CCD camera.

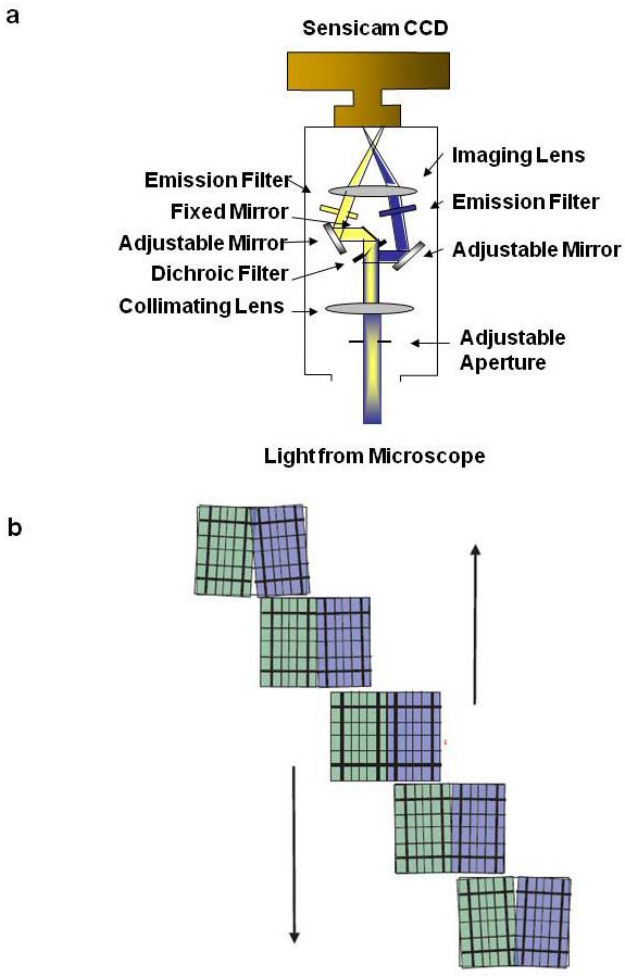

Figure 3.3: Dual View System. A) Emission light from the microscope is guided into the Dual View system where the collimating lens, gathers the divergent beams of light into a parallel beam. The light is then guided to a dichroic filter, where the light is split into ECFP and YPet emissions and the images are projected side by side on the CCD. B) A gridded slide is used to adjust the alignment of the Dual View system. The adjustable mirrors are adjusted right, left, up or down to achieve alignment between the two split images.

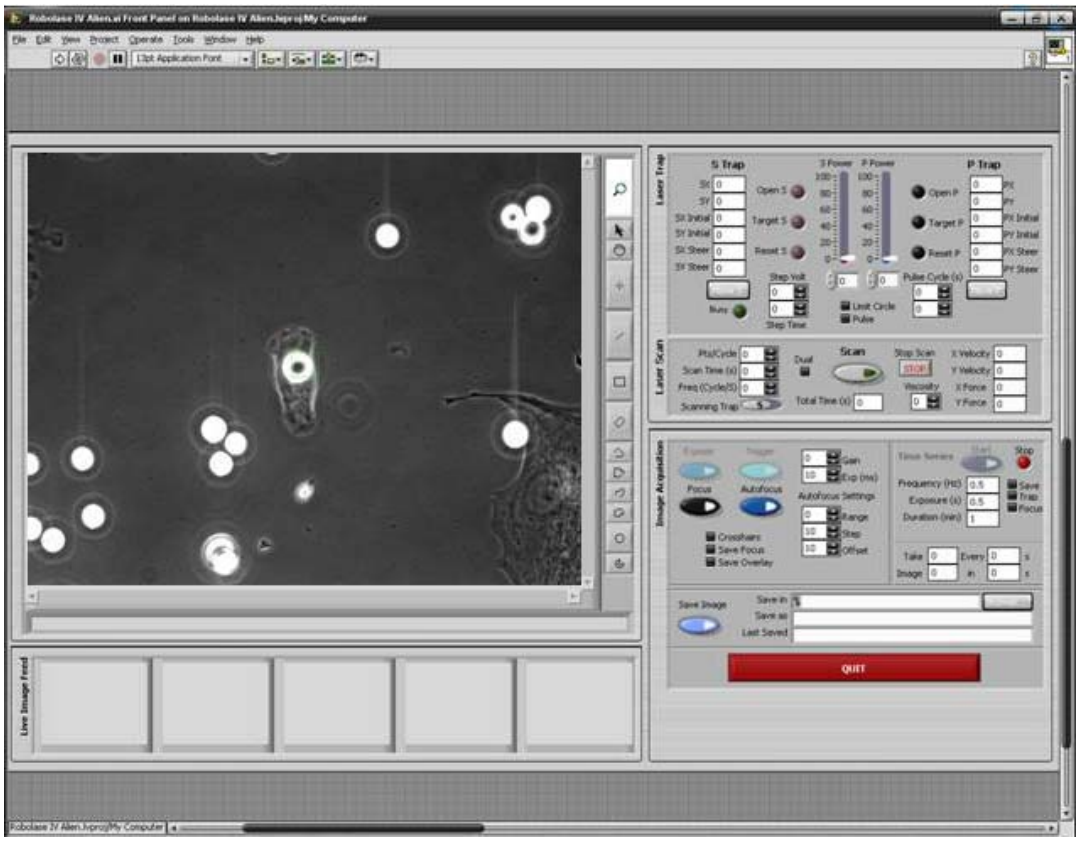

Figure 3.4: Front panel of Robolase III. Robolase III controls the laser tweezers (i.e. laser trap). When the laser trap, represented by the green square on the image interface, is on, the open S button is lit. Vice versa, when the laser trap is off, the open S button is off. The laser scan panel allows setting a duty cycle of on and off laser trap states. The image acquisition panel allows for real-time focusing of the cell, capturing, and saving of images. The lower panel below the current image panel shows previous images taken.

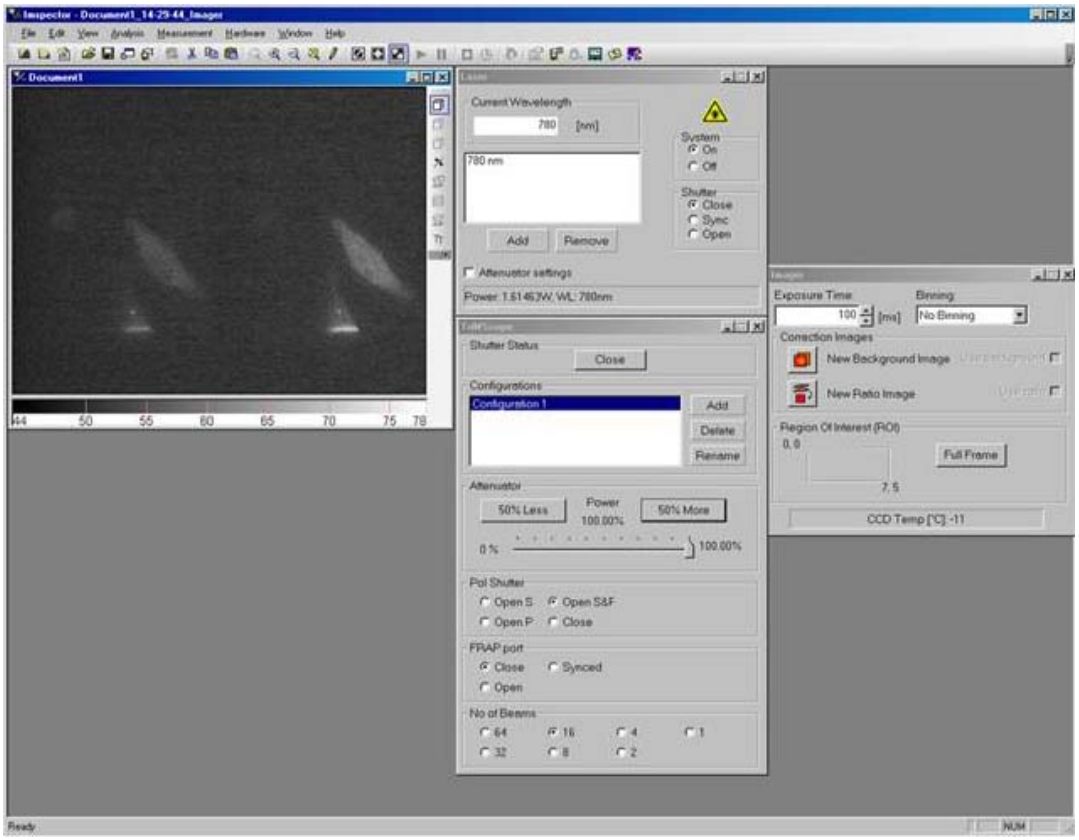

Figure 3.5: Imspector software layout. The Imspector software allows the user to control the wavelength, number of beamlets, the power of the laser, the shutter controls, and exposure time for the beamlets. Additionally, captured images from the Dual View system are displayed upon image acquisition.

3.7 References

[1] Viana, N., Rocha, M., Mesquita, O., Mazolli, A., & Maia Neto, P. (2006). Characterization of objective transmittance for optical tweezers. Appl Opt, 45(18), 4263-4269.

Chapter 4

Effects of optical trapping and multiphoton fluorescence microscopy on cardiac mechanotransduction

4.1 Introduction

In this chapter, I will describe the preliminary design considerations used to develop our system. Design considerations include: cell types, excitation wavelength for two photon fluorescence excitation, effects of two photon excitation, thermal heating effects of the trapping laser, and maintaining the temperature and pH of the cells during live cell imaging.

4.2 Cell type considerations

4.2.1 Neonatal rat ventricular cardiac myocytes

Neonatal rat ventricular cardiac myocytes (NRVMs) were harvested from freshly dissected ventricles of 1 to 3 day-old Sprague-Dawley rats using an isolation kit (Cellutron, Highland Park, NJ). Cells were plated on dishes coated overnight with 10 ug/mL

laminin (Sigma, L-2020) and cultured on 35 mm glass-bottom dishes (FluoroDish, World Precision Instruments, Sarasota, FL) in high-serum plating media (Dulbecco's Modified Eagle Media (DMEM), 17% M199, 10% horse serum (HS), 5% fetal bovine serum (FBS), 100 units/ml penicillin and 50 mg/ml streptomycin) at 100,000 cells/cm_2. After 18 hours, the cells were washed with Dulbecco's Phosphate-Buffered Saline (DPBS) and transferred to low serum maintenance media (DMEM, 18.5% M199, 5% HS, 1% FBS and antibiotics). 24 - 48 hours after transfection of a focal adhesion kinase fluorescence resonance energy transfer (FAK FRET) biosensor, cells were washed with DPBS and fresh maintenance media was added. Cell cultures were maintained at 37°C and 5% CO_2. All culture media was purchased from Invitrogen and sera was purchased from Gemini BioProducts. These animal studies were in accordance with University of California Institutional Animal Care and Use Committee (IACUC) guidelines.

Fibronectin coated beads were adhered to neonatal rat ventricular myocytes. Due to the intrinsic nature of cardiac myocytes, the NRVMs were beating before the experiment, or began beating during the experiment, thereby making varying the amount of force applied. The beating nature of the cell and the differences in beating in non-paced cells, made it difficult to apply a known force using the laser tweezers consistently across cell samples. Consequently, we implemented two inhibitors (Figure 1), a) 10mM 2,3-butanedione monoxime (Sigma, 31550), a myosin ATPase inhibitor, and b) 10uM blebbistatin (Sigma, B0560), myosin II inhibitor. Our FAK FRET biosensor consists of a FAK - tyrosine 397 substrate peptide fused with a cyan fluorescent protein and yellow fluorescent protein. Using this reporter, changes in biochemical signaling of FAK can be observed. Both groups showed an increase in focal adhesion kinase phosphorylation in response to a mechanical stimulus in areas that were in contact to the ligand coated bead.

4.2.2 Neonatal mouse ventricular cardiac myocytes

Neonatal mouse ventricular cardiac myocytes were harvested from freshly dissected ventricles of 0 to 2 day-old mice using a standard isolation kit (Cellutron, Highland Park, NJ). Cells were plated and maintained following the protocol for isolation of the neonatal rat ventricular cardiac myocytes as previously described.

Due to the availability of genetically manipulated murine lines, studies were changed from investigating neonatal rat ventricular cardiac myocytes to studying neonatal mouse ventricular cardiac myocytes (NMVMs). Due to the intrinsic nature of the cells to beat, we implemented 10mM 2,3-butanedione monoxime (BDM) and 10uM blebbistatin as previously described for the NRVMs (Figure 2). Upon addition of BDM, autophagy of the cells was noted immediately. As such, all studies following this experiment utilized blebbistatin.

Blebbistatin has been implicated previously to disrupt vinculin and focal adhesion activity after long periods of time, so we studied the effects of blebbistatin on our reporter over short periods of time (Figure 3). Application of blebbistatin for short periods of time (5, 10, 20, 30 minutes) did not interfere with the ability to use the fluorescent reporters to investigate signalling events. For all subsequent studies, incubation times were limited to 15 minutes or less.

The use of genetically manipulated mice allows furthering of our understanding of the roles of specific proteins in cardiac mechanotransduction. Upon isolation of neonatal mouse ventricular cardiac myocytes, the cells exist in a variety of maturity states (Figure 4) and it has been noted that mouse ventricular cardiac myocytes had elongated cell bodies (Deng et al., 2000). Due to the similarity between the rod-shaped NMVMs and isolated adult murine cardiac ventricular myocytes, future experimental groups focused on the rod-shaped NMVMs.

4.3 Wavelength selection for two photon fluorescence excitation

Two photon excitation occurs when there is a simultaneous absorption of two lower energy photons to reach an excited state equivalent to the absorption of one higher energy photon. Using the Ti:sapphire laser, which has a repetition rate of 76MHz and a pulse duration of 200fs, the two photon excitation effect is achieved. The Ti:sapphire laser (MaiTai laser, Spectra physics, Mountain View, CA) is tunable over 710 - 990nm in wavelength. For our experiments, we plan to use a FAK FRET biosensor, which has a cyan fluorescent protein and yellow fluorescent protein. To excite the cyan fluorescent protein, the wavelengths were tuned to determine the best wavelength of excitation of the cyan fluorescent protein of THE FAK FRET biosensor (Figure 5). Results showed that the wavelengths less than 800nm resulted in more fluorescence intensity measured by the FAK FRET biosensor. To avoid two-photon wavelengths that were near ultraviolet wavelengths due to possible DNA damage, 780nm was chosen for excitation of the FAK FRET biosensor.

4.4 Effects of two photo excitation

At initiation of this project, it was noted that the fluorescence intensity of normal cells exhibited a decrease in fluorescence intensity over a few illumination cycles and then leveled off. One possible mechanism for explaining this drop in fluorescence is a reversible photobleaching of the cyan fluorescent protein (ECFP) (Sinnecker et al., 2005)

Previous work has characterized changes in photophysical properties of GFP variants including ECFP and citrine (Sinnecker et al., 2005; Henderson et al., 2007). These results showed that the fluorescence intensity decreased only during the first few illumination cycles and reaches a stable level afterward. In addition, it was noted that a dependence of photobleaching kinetics on ECFP occurred in the presence of a FRET

acceptor. In previous work shown by Sinnecker et al., 2005, the distance between the donor and acceptor resulted in a varying decay of fluorescence over time as a result of reversible photobleaching. In comparing to results observed in our study (Figure 6), the time for these fluorescence traces were normalized to gain insight as to how the distance between the donor and acceptor of a FRET construct are affected by reversible photobleaching. The results showed that when a donor and acceptor were incorporated into a cell as free plasmids, a kinetic constant, tau, of 42 seconds was observed for the decay in fluorescence over time. In addition, when the donor and acceptor fluorophores were linked directly, a tau of 46 seconds was observed. In comparison, for our FAK FRET construct, the donor and acceptor fluorophore are linked through a binding domain and a sequence of amino acids. A tau of 45 seconds was observed. These results show that the decay in fluorescence observed in our control cells may depend on the photobleaching kinetics of ECFP in the presence of its FRET acceptor, YPet.

4.5 Thermal heating effects of the laser tweezers

For our experiments, laser tweezers will be used to apply forces. The forces applied by the laser tweezers are dependent on the power of the laser, however, with increased power, the laser tweezers can lead to localized heating (Liu et al., 1995). In previous work, it was noted that an increase of 1.0 ± 0.30°C/100mW was observed for cells stably trapped with laser tweezers using up to 400 mW. In these studies there appeared to be no alterations in DNA structure or cellular pH (Liu et al., 1996).

Based on these observations, we applied forces with a trapping power of 300mW. For our studies, the cell is not held with the laser tweezers, but the cell can be vulnerable to the thermal heating caused by the laser tweezers being applied to the bead at the cell membrane-bead interface. However in the experiments reported here the power of the 1064nm infrared laser before the objective was only 300 mW. Since the measured transmission through the microscope optics was 25%, the final tweezers laser power in the focal plane was 75mW.

Using the mathematical model developed previously (Liu et al., 1995), the changes at the cellular membrane-bead interface was calculated as a function of time (Figure 7). It was noted that as time progressed, an exponential change in temperature was observed. These results show that force application experiments on cells should be limited to a few minutes because after a few minutes, the temperature at the cell membrane-bead interface may lead to heating of the cells and possibly alterations in DNA and cell structure.

4.6 Temperature and pH control

To maintain the cells at 37°C, the cells were placed on a temperature control stage holder (TC-324B, Warren Instrument Corporation) that maintained the cell temperature at 37 $\pm$ 0.1 °C. In addition, to maintain the pH of the cellular environment during live cell imaging, the cells were incubated in CO_2 independent media that maintained the pH at 7.4 $\pm$ 0.1 (Invitrogen, 18045-088).

4.7 Conclusion

In this chapter, several design considerations were discussed that were used to create a system for studying cardiac mechanotransduction. Fully understanding the design limitations of the system and understanding which conditions can be controlled, will facilitate our understanding of key proteins involved in mechanotransduction

4.8 Figures

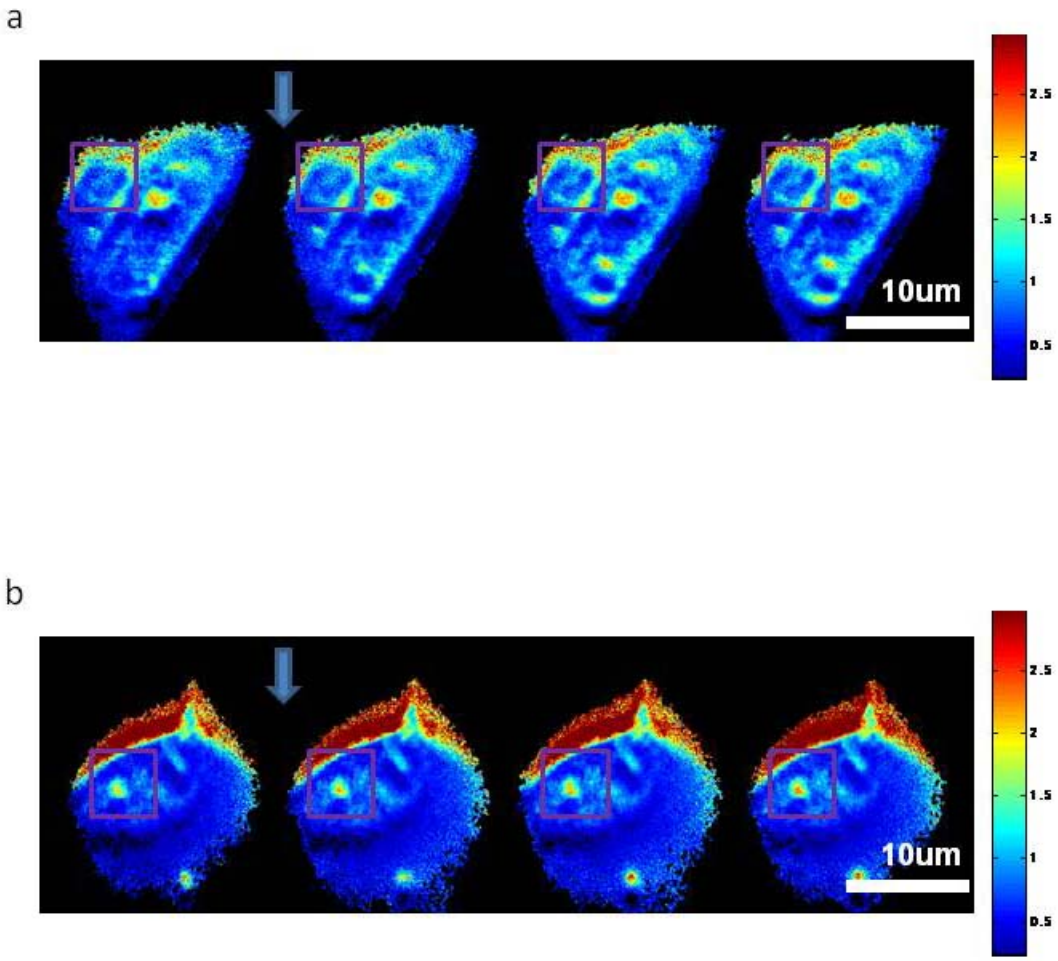

Figure 4.1: Ratio of ECFP/YPet ratio of force application experiment using neonatal rat ventricular myocytes. Neonatal rat ventricular cardiac myocytes were incubated with a) 10mM 2,3-butanedione monoxime and b) 10uM blebbistatin. The arrow indicates when force application is applied and the square indicates the area in which the bead-cell interact.

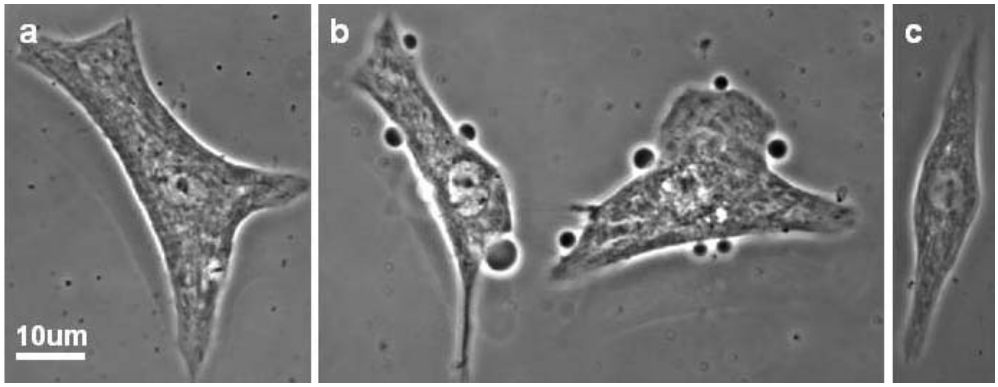

Figure 4.2: Phase contrast images of neonatal mouse ventricular cardiac myocytes. These cells were a) not exposed to an inhibitor, b) incubated with 10mM 2,3-butanedione monoxime, and c) incubated with 10uM blebbistatin.

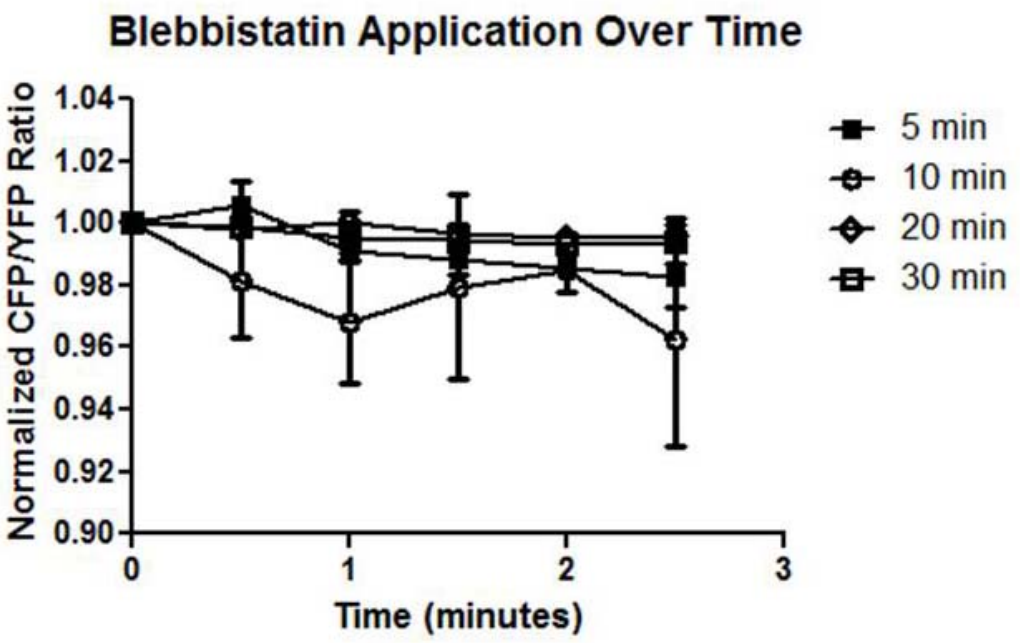

Figure 4.3: Normalized ECFP/YPet Ratio time course of NMVMs incubated with blebbistatin.

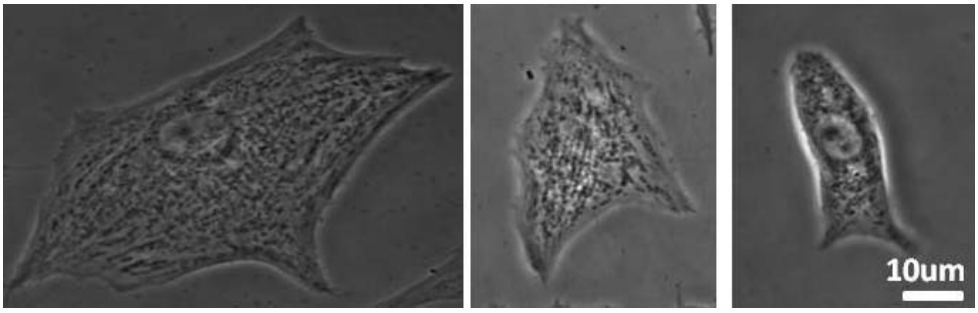

Figure 4.4: Phase contrast images of neonatal mouse ventricular cardiac myocytes.

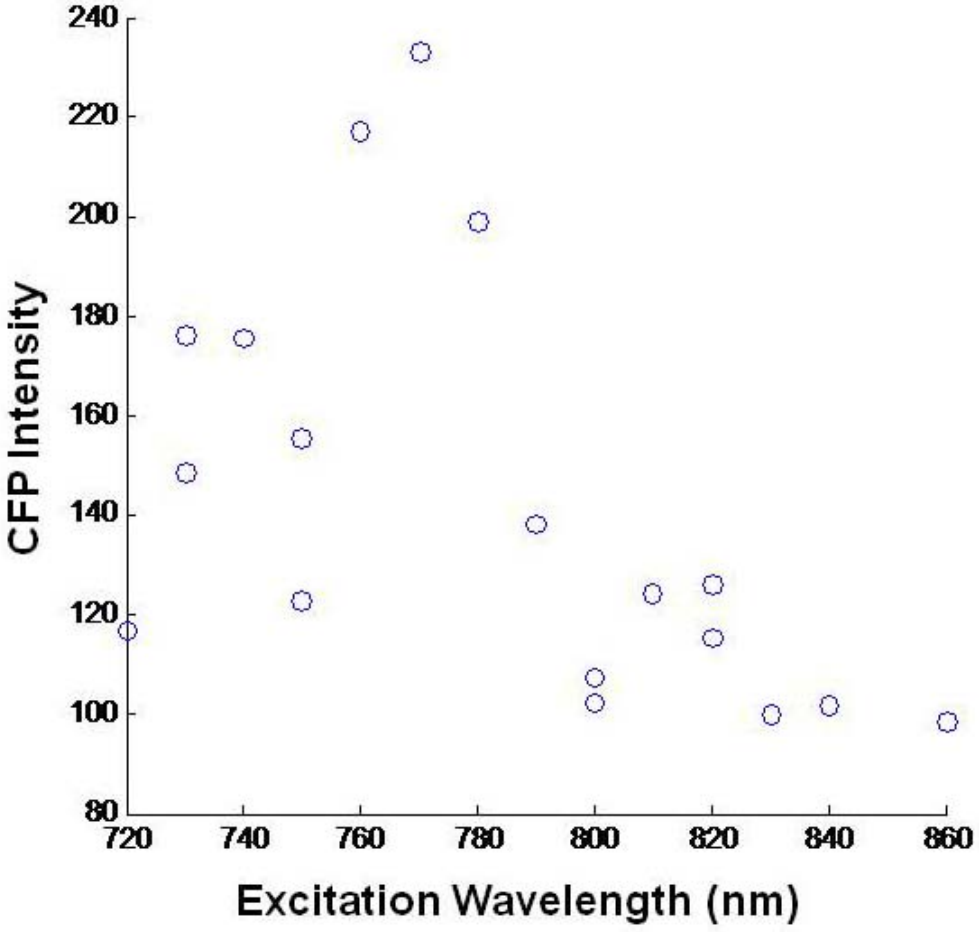

Figure 4.5: CFP intensities measured for two photon excitation using wavelengths 720-860nm.

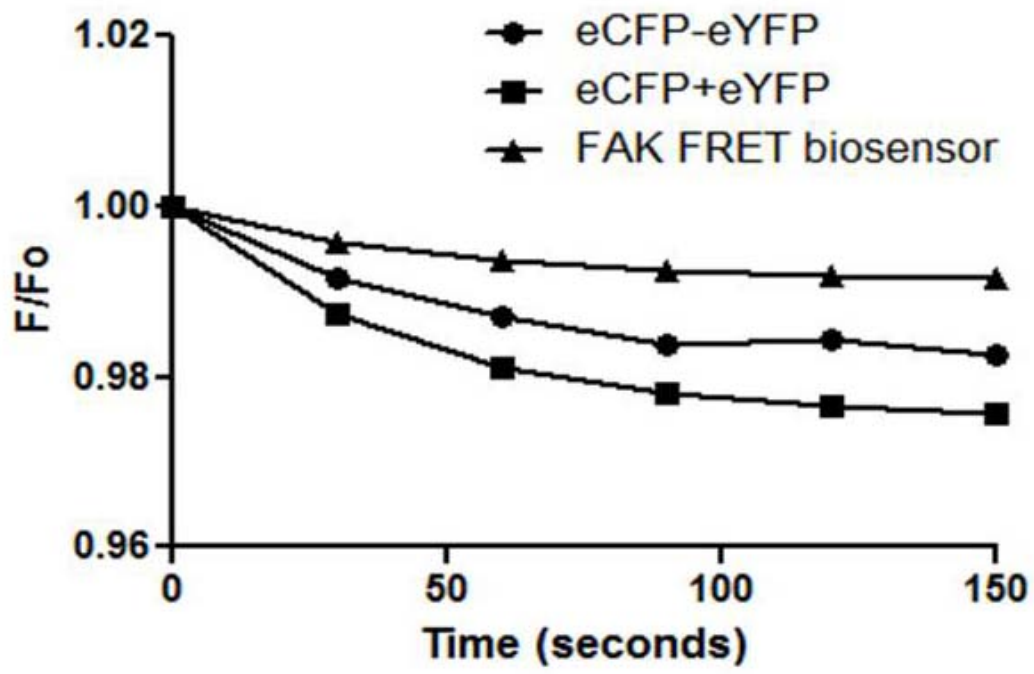

Figure 4.6: Dependence of photobleaching kinetics of eCFP in the presence of a FRET acceptor. Data was for photobleaching experiments for our FAK FRET biosensor, and data extracted from Sinnecker et al., 2005. For data from Sinnecker et al., 2005, HEK 293 cells were transfected with eCFP and eYFP (eCFP + eYFP) or a tandem protein where eCFP was fused directly to eYFP (eCFP-eYFP).

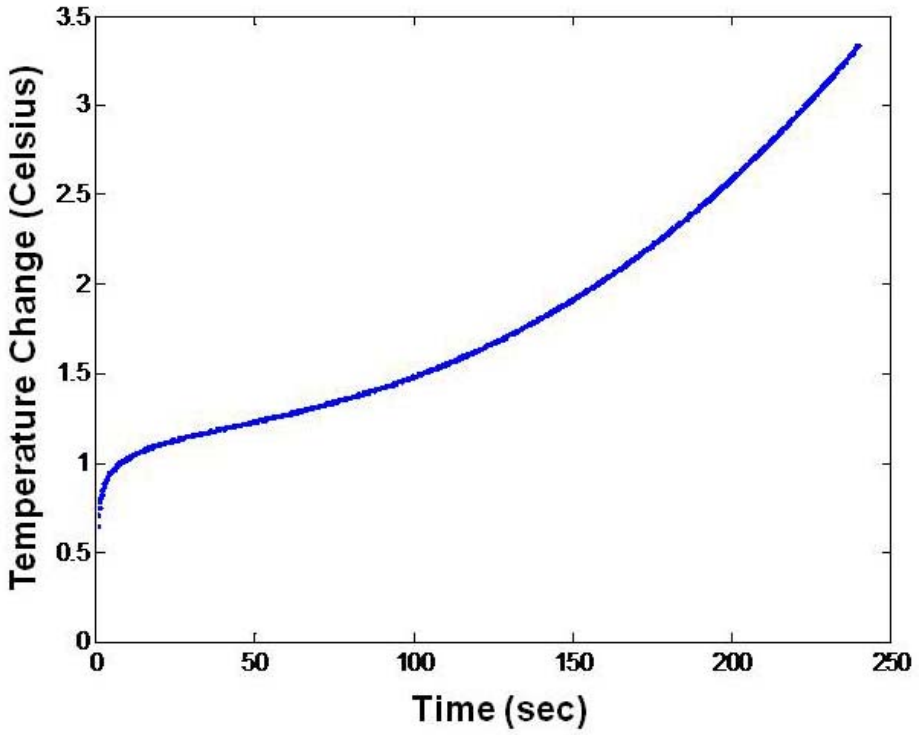

Figure 4.7: Transient temperature change at the bead-cell interface as a function of time for a bead adhered to a cell and stably trapped by laser tweezers.

4.9 References

[1] Deng, X. F., Rokosh, D. G., & Simpson, P. C. (2000). Autonomous and growth Factor-Induced hypertrophy in cultured neonatal mouse cardiac myocytes. Circulation Research, 87, 781-788.

[2] Henderson, J., Ai, H., Campbell, R., & Remington, S. (2007). Structural basis for reversible photobleaching of a green fluorescent protein homologue. Proc Natl Acad Sci U S A, 104(16), 6672-6677.

[3] Liu, Y., Cheng, D. K., Sonek, G. J., Berns, M. W., Chapman, C. F., & Tromberg, B. J. (1995). Evidence for localized cell heating induced by infrared optical tweezers. Biophys J., 68(5), 2137-2144.

[4] Liu, Y., Sonek, G. J., Berns, M. W., & Tromberg, B. J. (1996). Physiological monitoring of optically trapped cells: Assessing the effects of confinement by 1064-nm laser tweezers using microfluorometry. Biophys J., 71(4), 2158-2167.

[5] Sinnecker, D., Voigt, P., Hellwig, N., & Schaefer, M. (2005). Reversible photobleaching of enhanced green fluorescent proteins. Biochemistry, 44(18), 7085-7094.

Chapter 5

Methods for developing an adenoviral FAK FRET reporter

5.1 Introduction

Fluorescence resonance energy transfer (FRET) reporters have opened new means to study the spatiotemporal real time behavior of cell systems (Botvinick and Wang, 2007; Wang et al., 2005). With the development of a variety of FRET reporters used to study cell signaling including, but not limited to reporters for focal adhesion kinase (Cai et al. 2008), Src (Wang et al. 2005), and RhoA (Nakamura et al. 2005), signal transduction mechanisms may be probed mechanistically.

The combination of genetically manipulated murine lines with FRET reporters provides a means to study cell signaling systems under loss of function, gain of function, or rescue of function conditions. Additionally, the use of genetically manipulated murine lines allows the study of cell signaling systems in a variety of cell stages including embryonic, neonatal, and adult cells.

To combine the use of fragile primary cell lines with FRET reporters, a gene delivery method that allows the FRET reporter to be highly expressed in a cell without leading the cell to necrosis and apoptosis is necessary. Possible methods of gene

delivery include transient transfection (Saucerman et al. 2006), TAT-mediated protein transduction (Becker-Hapak et al. 2001), and viral delivery methods. To study fully differentiated primary cell lines, it is difficult to use transient transfection as the cells usually do not survive such an assault on its cell membrane. Use of TAT-mediated transduction may be a possibility as it uses some viral components to bring the protein into the cell. Viral delivery methods include adenoviruses and retroviruses which can effectively bring genes into a cell, however, retroviruses involve actively dividing cells and cannot be used for gene delivery in fully differentiated cell lines. As such, we describe the method used to create an adenoviral vector containing a focal adhesion kinase FRET reporter.

5.2 Methods

Construction. The FAK FRET reporter adenovirus was constructed first, by cutting out the reporter fragment from the original pcDNA 3.1 expression plasmid (received from Dr. Yingxiao Wang, U. Illinois - Urbana/Champaign) with KpnI (New England Biolabs, Ipswich, MA) and XbaI (New England Biolabs, Ipswich, MA) (Figure 1a). Following digestion, the DNA was analyzed by agarose gel electrophoresis, and the correct size fragment was extracted from the gel using the QIAGEN gel extraction kit (QIAGEN, Valencia, CA) (Figure 2a). Similarly, pACCMV.PLPASR(+), the parent vector used to create the recombinant adenovirus was processed in a similar fashion (Figure 1b). pACCMV.PLPASR(+) contains fragments of adenovirus type 5 DNA, a cytomegalovirus immediate early enhancer and promoter, simian virus 40 fragment, and a pUC19 polylinker. The resulting two fragments were then ligated with the Roche Rapid Ligation Kit (Indianapolis, IN) (Figure 1c).

Transformation. The ligated adenoviral shuttle vector was incubated with electrically competent bacteria cells (Invitrogen, Carlsbad, CA). The cells were electroporated and spread on agar plates with ampicillin. Colonies were purified using the QIAfier Mini Prep kit (QIAGEN, Valencia, CA).

Verification. The vectors were collected and fragment sizes were verified following KpnI and XbaI digestions and agarose gel electrophoresis to ensure the proper length of the final adenoviral shuttle vector (8.8kb) and that the original ligation fragments (1.7kb) were found (Figure 2a). The vector was also verified by polymerase chain reaction to ensure that the insert fragment matched the original reporter fragment intended and the vector was sequenced by Eton Biosciences (San Diego, CA), using primers defined by the FAK FRET reporter and the pACCMV.PLPASR(+) (Figure 2b). Primers were purchased from Operon (Huntsville, AL). (Figure 2)

Cotransfection and amplification. The pacCMV-FAK FRET reporter plasmid was cotransfected with JM17 into HEK293 cells using the Roche FuGENE 6 Transfection Reagent (Indianapolis, IN). The DNA of the JM17 vector serves as a recipient of DNA from the left hand end of the genome and allows the crossover between the shuttle vector and the JM17 vector to create a genome capable of being packaged into a virus (Young et al., 1998). (Figure 3) The cells were allowed to incubate with the viral DNA fragment for 1 hour and extra cell media (DMEM, 10% FBS, 1%PS) was added over a several of days. The cells and media were then collected, spun down, resuspended with fresh media, and frozen with liquid nitrogen.

Purification and extraction. The collected cells were purified using the Clontech Adenovirus Purification kit (Madison, WI) and resuspended with 10% glycerol, aliquoted into stock vials and frozen at -80°C.

Titering. The adenoviral FAK FRET reporter (Ad-FAK FRET) was tittered using the plaque formation assay. A 6-well plate was coated with fibronectin (10ug/mL) and HEK293 cells were plated. At 90% confluency, the cells were infected with various dilutions of the Ad-FAK FRET for 1 hour and after 1 hour, an agarose gel mixture was overlayed over the cells. After 7 days, plaques were counted and the viral particles per milliliter were calculated.

Western blotting. 293 cells were infected with the Ad-FAK FRET and incubated for 72 hours. Cells were lysed with IP lysis buffer and homogenized. Protein lysates were resolved by sodium dodecyl sulfate-polyacrylamide gel electrophoresis and

Western blots were performed to detect GFP, and alpha-tubulin levels. Blots were incubated with primary antibodies overnight at 4°C. Dilutions for anti-GFP (1:1000) and anti-GAPDH (1:4000). Densitometric quantification of protein bands were performed digitally (ImageJ, NIH, Bethesda, MD).

Infection of neonatal murine cardiac ventricular myocytes. Neonatal murine cardiac ventricular myocytes were isolated, as previously described (Chapter 4) and infected with 2.5 MOI of FAK FRET biosensor. The viral containing media was taken off after 24 hours and the cells were incubated for an additional 48 hours. The cells were washed, then fixed with 100% ethanol, washed, coated with fluoromount-G, and cover slipped. Fluorescent images were taken and the ECFP/YPet ratio was calculated, as described in Chapter 3.

Infection of isolated murine adult cardiac ventricular myocytes. Adult murine cardiac ventricular myocytes were isolated, as previously described (O' Connell et al., 2007) and infected with 5 MOI of FAK FRET biosensor. The viral containing media was taken off after 24 hours and the cells were incubated for an additional 48 hours. The cells were washed, then fixed with 100% ethanol, washed, coated with fluoromount-G, and cover slipped. Fluorescent images were taken and the ECFP/YPet ratio was calculated, as described in Chapter 3.

5.3 Results

Development of adenoviral FAK FRET reporter

An adenoviral form of a FAK FRET reporter was developed by cutting the original pcDNA and incorporating it into a pAC CMV vector (Figure 1c). Results showed that the cut FAK FRET construct was 1.7kb and the cut adenoviral shuttle vector plasmid was 8.8kb (Figure 2a). Ligated vector constructs were selected from colonies and PCR verification of these constructs produced the FAK FRET biosensor in several colonies (Figure 2b). Positive control was obtained from PCR products from the original pcDNA 3.1 (Figure 2b left) and PCR products were obtained from colonies (Figure 2b right),

showing that several colonies contained the adenoviral shuttle vector construct. Western blot results show that the FAK FRET construct exists upon adenoviral infection with the Ad-FAK FRET (Figure 4). Titering of the virus determined that the concentration of the virus was 6.5 x 10^{12} pfu/mL.

Infection of neonatal murine cardiac ventricular myocytes

Adenoviral infection of neonatal murine cardiac ventricular myocytes with 2.5 MOI of FAK FRET biosensor show that reporter is incorporated (Figure 5).

Infection of isolated murine adult cardiac ventricular myocytes

Adenoviral infection of adult murine cardiac ventricular myocytes with 5 MOI of FAK FRET biosensor show that reporter is incorporated (Figure 6).

5.4 Discussion and Conclusion

We have shown the generation of an adenovirus containing a FAK FRET biosensor. Currently, the virus has been used in neonatal murine cardiac ventricular myocytes and in isolated murine adult cardiac ventricular myocytes. In previous experiments, it was shown that 5MOI was the maximum amount of virus that could be added to cells before viral toxicity was reached. As such, 2.5 MOI were used in neonatal murine ventricular myocytes because to study vinculin knockdown, we reserved 2.5 MOI for Cre adenovirus, whereas in adult cardiac myocytes, if we use the tamoxifen inducible cardiac specific vinculin knockout line, the cells have a reduced vinculin before any infection and do not require infection with Cre. Future studies include incorporating the virus in genetically manipulated myocytes to further our understanding of mechanotransduction.

5.5 Acknowledgements

I'd like to thank Dr. Yingxiao Wang for providing the original FAK FRET biosensor vector. I'd like to thank Atsushi Miyanohara for providing the original pAC CMV vector and the JM17 vector. I'd like to thank Hideshi Okada for his assistance in amplifying, purifying, and titering the FAK FRET adenovirus. I'd also like to thank Ruixia Li for isolating the adult murine cardiac ventricular myocyte.

5.6 Figures

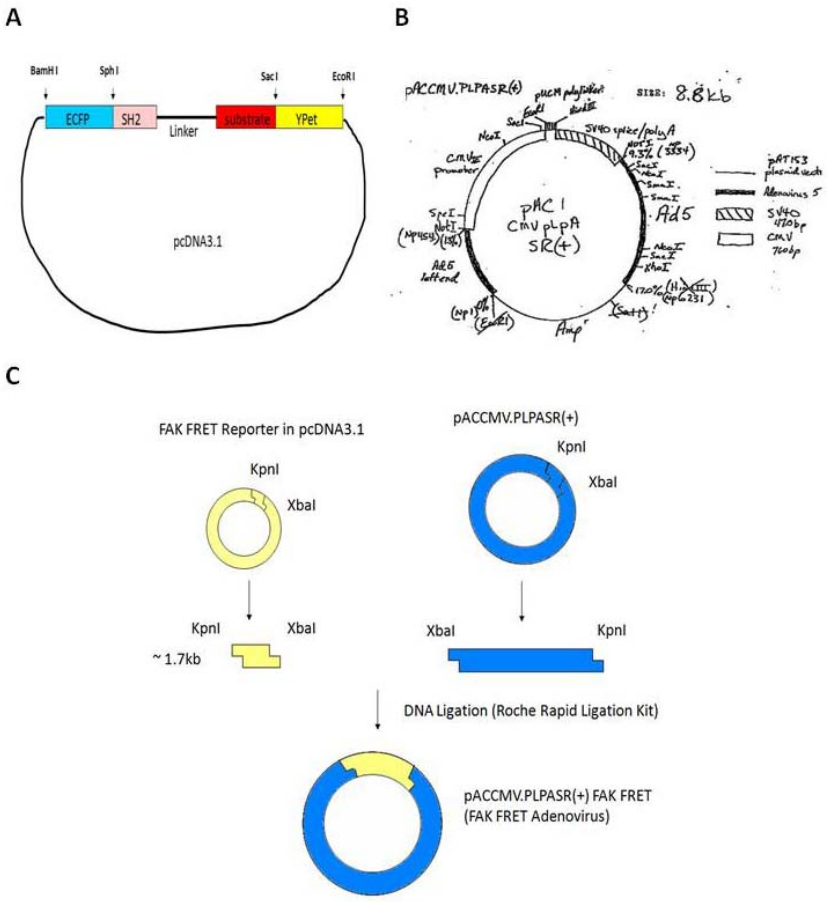

Figure 5.1: Construction of adenoviral FAK FRET reporter. A) Original plasmid for the FAK FRET biosensor. The FAK FRET biosensor construct was flanked inside a pcDNA3.1. B) Original pAC CMV Adenovirus Shuttle Vector. Cloning sites within this vector are located in the pUC19 polylinker (EcoRI, KpnI, BamHI, XbaI, SalI, HindIII). This vector contains the left end of Ad 5, which when co-transfected with JM17 can give rise to infectious virus very efficiently (McGrory et al., 1988). Figure courtesy of Dr. Atsushi Miyanohara. C) Creation of FAK FRET biosensor adenovirus shuttle vector. The FAK FRET biosensor was digested with KpnI and XbaI and the pAC CMV adenovirus shuttle vector was digested with KpnI and XbaI. The fragments were then ligated with the Roche Rapid Ligation Kit.

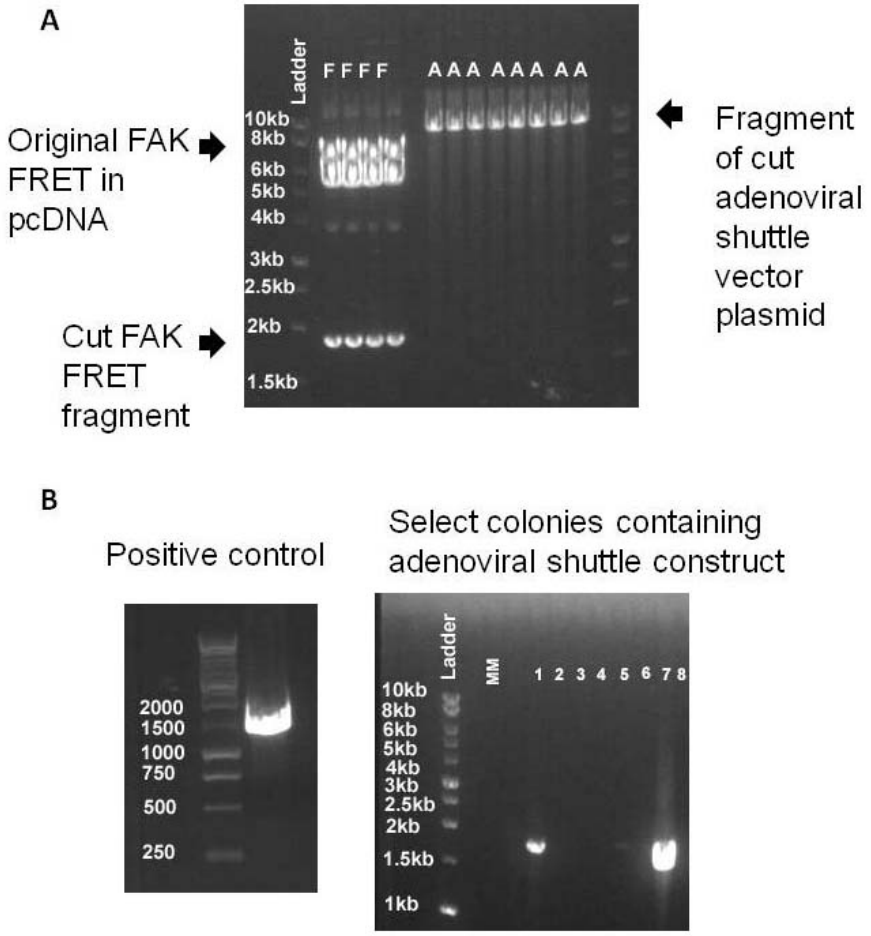

Figure 5.2: PCR verification of FAK FRET construct. A) Plasmids cut with KpnI and Xba I. Adenoviral shuttle vector plasmid when cut has a length of approximately 8.8kb. The FAK FRET biosensor plasmid when cut with KpnI and XbaI is approximately 1.7kb. B) PCR verification of ligated adenoviral construct of the FAK FRET reporter. Left panel: positive control, Right panel: PCR results of select colonies showing the fragment generated from the adenovirus FAK FRET shuttle vector construct.

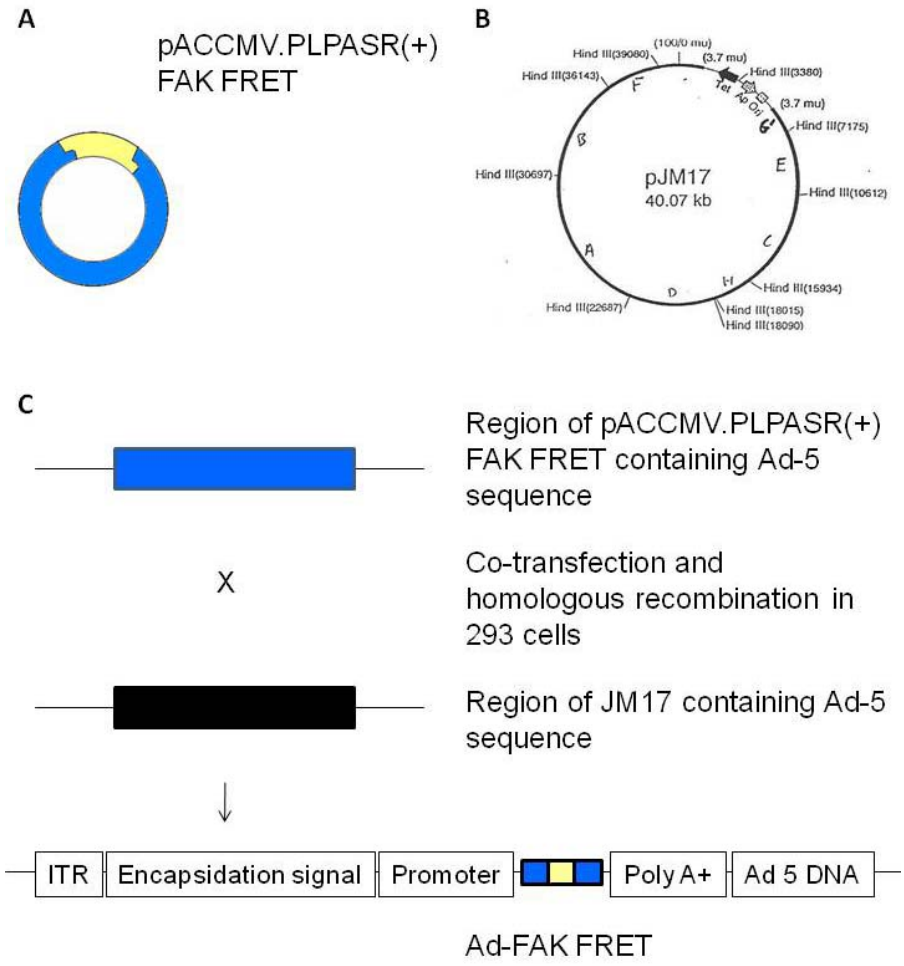

Figure 5.3: Construction of the adenovirus FAK FRET biosensor. A) Schematic representation of the pACCMV.PLPASR(+) FAK FRET. pACCMV.PLPASR(+) FAK FRET contains the inverted terminal repeat region (ITR), polyA+ (poly A tail), and essential packaging signals. B) Schematic representation of the JM17 vector. This plasmid can be used to construct adenovirus type 5 (Ad5) with inserts or mutations in early region 1 (E1). JM17 contains an insertion of a pBR322 derivative at bp 1339 (3.7 mu) in Ad5. Figure courtesy of Dr. Atsushi Miyanohara. C) pACCMV.PLPASR(+) FAK FRET is cotransfected with JM17. This allows construction of replication defective vectors with inserts in E1. Homologous recombination results in the generation of Ad-FAK FRET.

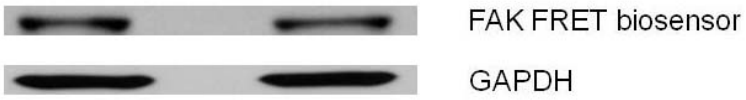

Figure 5.4: Western blot of FAK FRET infected 293 cells. Results show that the FAK FRET biosensor is detected in the lysed cells.

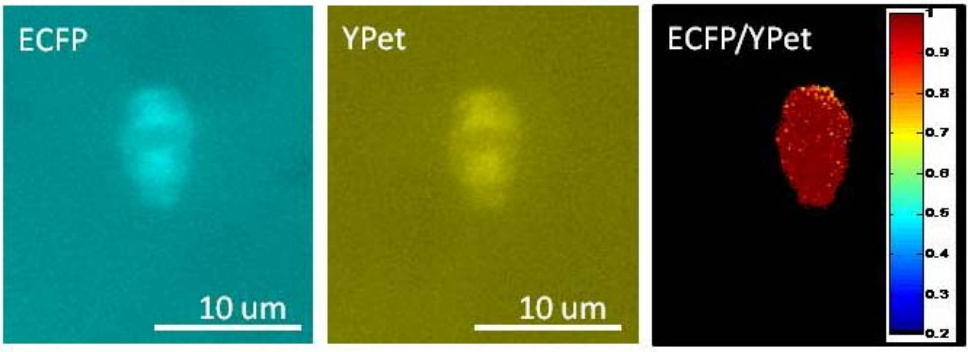

Figure 5.5: Infection of neonatal murine cardiac ventricular myocytes. Fluorescent images of a neonatal murine cardiac ventricular myocyte. ECFP (left) and YPet (center) images were taken and a ECFP/YPet ratio image (right) was calculated.

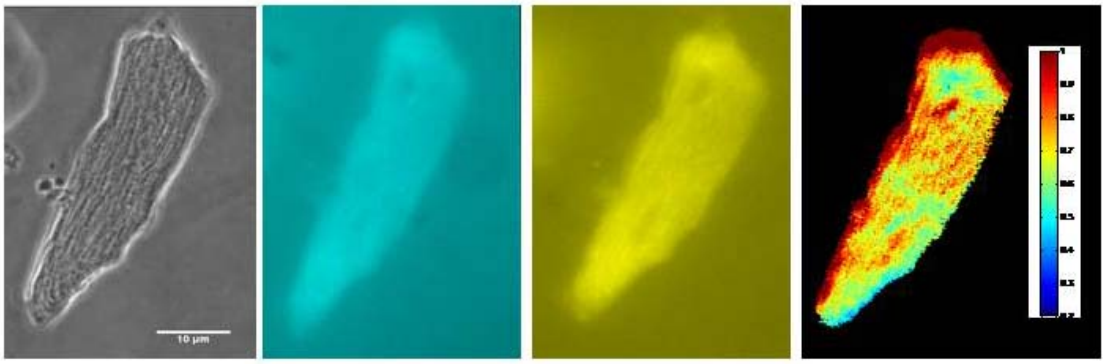

Figure 5.6: Infection of isolated adult murine cardiac ventricular myocytes. Phase contrast image of an adult murine cardiac ventricular myocyte (right). Fluorescent images of an adult murine cardiac ventricular myocyte: ECFP (center left) and YPet (center right) images were taken and a ECFP/YPet ratio image (right) was calculated.

5.7 References

[1] Becker-Hapak, M., McAllister, S. S., & Dowdy, S. F. (2001). TAT-mediated protein transduction into mammalian cells.. Methods, 24(3), 247-256.

[2] Botvinick, E. L., & Wang, Y. (2007). Laser tweezers in the study of mechanobiology in live cells. Methods Cell Biol., 82, 497-523.

[3] Cai, X., Lietha, D., Ceccarelli, D., Karginov, A., Rajfur, Z., Jacobson, K., et al. (2008). Spatial and temporal regulation of focal adhesion kinase activity in living cells. Mol Cell Biol, 28(201), 214.

[4] McGrory, W.J., Bautista, D.S., Graham, F.L. (1988). A simple technique for the rescue of early region I mutations into infectious human adenovirus type 5. Virology, 163(2), 614-617.

[5] Nakamura, T., Aoki, K., & Matsuda, M. (2005). FRET imaging in nerve growth cones reveals a high level of RhoA activity within the peripheral domain. Brain Res Mol Brain Res, 139(2), 277-287.

[6] Saucerman, J., Zhang, J., Martin, J., Peng, L., Stenbit, A., Tsien, R., et al. (2006). Systems analysis of PKA-mediated phosphorylation gradients in live cardiac myocytes. Proc Natl Acad Sci USA, 103(34), 12923-12928.

[7] Wang, Y., Botvinick, E., Zhao, Y., Berns, M., Usami, S., Tsien, R., et al. (2005). Visualizing the mechanical activation of src. Nature, 434, 1040-1045.

[8] Young, C. S., Nicolsvv, A. L., Lu, H., Munz, P.L. (1998). Methods for Creating and Analyzing Adenovirus Vectors that Express Proteins that Act on the Viral Genome. Adenovirus Methods and Protocols. 21, 61-83.

Chapter 6

A Mechanotransduction Response in Cardiac Myocytes Using Optical Tweezers and Multiphoton Fluorescence Resonance Energy Transfer

In this study we have combined laser tweezers with 16-point multiphoton fluorescence resonance energy transfer (MP-FRET) to study cardiac mechanotransduction. Isolated murine ventricular cardiac myocytes were transfected with a genetically constructed focal adhesion kinase fluorescent reporter (FAK FRET) to monitor integrin-mediated activation events. An integrin ligand-coated 10 micron diameter microsphere was adhered to the cell surface and laser tweezers were used to apply localized piconewton forces in either the long or short axis of the cell. Both phase contrast and fluorescent images were captured simultaneously, to study and quantify the effects of directionally applied forces on FRET ratio changes. The FAK autophosphorylation as reported by the biosensor FRET signal changed locally at the site of force application, but not dis-

tally from the site, and that these changes depended on the orientation of the local force with respect to the cell geometry. These data demonstrate that the use of laser tweezers combined with MP-FRET can be used to study integrin-mediated events in cardiac mechanotransduction.

6.1 Introduction

In this paper we combine laser tweezers with multi-point multiphoton imaging to study the molecular biology of cardiac mechanotransduction at the single cell level. Mechanotransduction is the process by which mechanical signals are transduced into biochemical signals. Key molecules involved in this process include integrins, receptor tyrosine kinases, and proteins interconnecting the extracellular environment with the intracellular environment (Schwartz, 2008, Samarel, 2005). In particular, recent evidence has suggested that defects in proteins involved in the cytoskeleton, cell-extracellular matrix, and cell-cell adhesion junctions can lead to a variety of diseases including cardiomyopathies (Towbin and Bowles, 2006; Bowles et al., 2000; Towbin and Bowles, 2000, Saffitz, 2006). Currently, the ability to investigate the specific interactions of various proteins involved in these processes on the molecular level has utilized either in vitro models of aligned cultures (Gopalan et al., 2002; Senyo et al., 2007), or cell spreading assays (Lu et al., 2008). The results of these approaches do not provide real time information on signal transduction in single cells.

We have developed a system that combines laser tweezers, multi-point multiphoton fluorescence resonance energy transfer (MP-FRET) microscopy, and genetically manipulated cardiomyocytes in order to study mechanotransduction-related signalling at the level of the single cardiac cell. This approach provides insight into the roles of structural linkers and key proteins involved in cardiac mechanotransduction, providing new information related to heart disease and ultimately heart failure.

6.2 Results

Proof of concept

A 16-point 760nm femtosecond laser array (see Methods section for instrument details) is scanned over single rectangular murine cardiomyocytes while they are simultaneously being subjected to a laser trapping force applied to 10 micron beads conjugated to the cell surface. Multiphoton induced fluorescence excitation/emission of a focal adhesion kinase (FAK) FRET-reporter occurs during application of the force. The following initial proof of concept experiments were conducted: i) transfected cells alone, ii) transfected cells with an active trapping laser, iii) transfected cells with a 10 micron integrin-ligand coated bead attached to the cell and exposed to the piconewton forces of the trapping laser.

The results (Figure 1) demonstrate that MP-FRET plus laser tweezers-induced forces can be used to study cardiac mechanotransduction in isolated single cells by monitoring FAK phosphorylation responses to force application.

Anisotropic properties of cardiac myocytes

The laser tweezers MP-FRET system was used to examine the anisotropic properties of cardiac myocytes in which a force was applied either i) in the longitudinal axis of the cell, or ii) in the transverse axis of the cell (Figure 2). The results demonstrate: (1) that FAK phosphorylation changes are localized to the site of force application and not distally from the location of force application, and (2) an increase in FAK autophosphorylation as reported by the FAK FRET biosensor when forces were applied in the transverse axis of the cell. In contrast, a decrease in FAK autophosphorylation was detected when forces were applied in the longitudinal axis of the cell. These results are consistent with anisotropic stretch studies in myocytes cultured on deformable membrane (Senyo et al., 2007), but unlike those studies, the studies reported here allowed discrete subcellular localization of mechanical signals in single cells as opposed to the ensemble responses previously seen only in large populations of cultured cells. In addition, our

results revealed that directionally applied forces lead to variances in biochemical signalling, not previously observed. These responses are also dependent on cytoskeletal components rather than actomyosin contractility.

6.3 Discussion and Conclusions

This is the first investigation in which isolated murine cardiomyocytes are studied using a combination of laser tweezers and multiphoton-FRET to detect localized mechanical events. In addition the use of 16 point MP-FRET permitted rapid scanning of the cardiac cell in order to gather functional intracellular information before substantial deterioration of the cell occurred. This method reduces the amount of time that the cell is exposed to the fluorescence excitation light resulting in less perturbation of cell function. This is especially important in fragile cells such as cardiac myocytes. The use of a longer wavelength to stimulate multi-photon fluorescence also reduces potential cellular phototoxicity.

From a biological perspective, the laser tweezers MP-FRET system has demonstrated that it is now possible to investigate how orientation affects mechanical signalling of single cells. This system differs from the aligned channel studies of groups of cells (Gopalan et al., 2002; Senyo et al., 2007) because those systems applied stretch in both orientations simultaneously and therefore could not test molecular signalling events in a single orientation. Additionally, the aligned channel systems require a large number of cells since the readout of signalling needed to be assayed by Western blot analyses. In the studies reported here, real time visualization of signalling changes is achieved, i.e., the results are immediately observed showing differences in biochemically signalling in response to directionally applied forces.

With the availability of many knockout and transgenic murine models, it should now be possible to use multipoint MP-FRET plus laser tweezers in combination with a variety of fluorescent reporter molecules, to study mechanotransduction in single cells.

6.4 Methods

Cell Culture. Cardiac myocytes were harvested from freshly dissected ventricles of 0 to 2 day-old mice using an isolation kit (Cellutron, Highland Park, NJ). Cells were plated on dishes coated overnight with 10 ug/mL laminin (Sigma, L-2020) and cultured on 35 mm glass-bottom dishes (FluoroDish, World Precision Instruments, Sarasota, FL) in high-serum plating media (Dulbecco's Modified Eagle Media (DMEM), 17% M199, 10% horse serum (HS), 5% fetal bovine serum (FBS), 100 units/ml penicillin and 50 mg/ml streptomycin) at 100,000 cells/cm^2. After eighteen hours, the cells were washed with Dulbecco's Phosphate-Buffered Saline (DPBS) and transferred to low serum maintenance media (DMEM, 18.5% M199, 5% HS, 1% FBS and antibiotics). Twenty-four to forty-eight hours after transfection, cells were washed with DPBS and fresh maintenance media was added. Cell cultures were maintained at 37°C and 5% CO_2. All culture media was purchased from Invitrogen and sera was purchased from Gemini BioProducts. These animal studies were in accordance with University of California Institutional Animal Care and Use Committee (IACUC) guidelines.

Laser tweezers. The laser tweezers system is a 1064 nm Nd:YVO4 Millenia IR Laser (Spectra Physics, Mountain View, CA) directed into an inverted microscope through a series of optics consisting of beam expansion (1.5x telescope), power adjustment (half wave plate - polarizer), and beam scanning (fast scanning mirror) (Figure 3). The beam enters a Zeiss Axiovert microscope and is focused by a 63X NA 1.4 phase objective to an estimated focal spot diameter of 0.48m. Laser power in the focal spot was 75 mW with an effective irradiance of 4.1x107 W/cm^2. Transmission through the objective was 25% as measured by the dual objective method as described in Viana et al. 2006.

Two photon excitation and Imaging. A femtosecond Ti:sapphire (MaiTai laser, Spectra physics, Mountain View, CA; 710-990nm) combined with a 16-64 multi-point generation system (TriM Scope, LaVision BioTec, Germany), was used for near-simultaneous

16 multi-point multiphoton fluorescence excitation/emission. The laser was tuned to 780 nm for these studies in order to match the two-photon absorption maximum wavelength of the ECFP fluorescent probe. Images are captured by a cooled CCD camera and processed using custom imaging software. Multiphoton excitation/emission was chosen not only because of the increased spatial resolution and sensitivity afforded by MP-induced fluorescence (Zipfel et al. 2003) but also because the dwell time of the excitation beam at any of the 16 focused laser points was so short (0.013ms) with an average of 17 mW per spot, that cells were exposed to a low amount of excitation energy in a relatively short period of time. This feature of the method is crucial because of the known fragility of many cultured cells, especially the cardiac myocytes used in this study. In addition MP-excitation allowed the use of longer wavelengths to activate the cyan fluorescent protein. Time points were taken at 30 second intervals as to reduce the total amount of photons that the cells would be subjected to. The ECFP/YPET ratio FRET measurements were made by splitting the fluoresce emission using a dual-view prism system (480DF30 for ECFP and 535DF25 for YPet) and projecting the YPET and ECFP emissions onto separate halves of the cooled digital 12 bit SensiCam CCD Camera.

Ligand-receptor signaling and bead coatings. The system described here has the ability to probe specific pathways of interest by coating beads with a ligand that activates a specific receptor implicated in mechanotransduction signaling events. One pathway of interest is the integrin family pathways: a large family of heterodimer receptors involved in complex signaling cascades (Brancaccio et al., 2006; Geiger et al., 2009). A bead coated with a ligand specific to a specific receptor system is placed on the cardiac cell surface and the laser tweezers are then used to apply a force that is specific the receptor system. Using a signalling molecule reporter downstream of the mechanical activation sight allows for the detection and monitoring of the changes in the myocyte signal transduction events. In this study we have discovered a variation in FAK signal transduction following application of force to the surface of single myocardial cells. The amount of FAK activation appears to be related to the orientation of the force applica-

tion.

Focal adhesion kinase fluorescence resonance energy transfer reporter. In this study, cardiac myocytes were transfected, using FuGene6 transfection reagent (Roche Diagnostics, Indianapolis, IN) with a focal adhesion kinase fluorescence resonance energy transfer reporter. The FAK FRET reporter transiently transfected into the cardiac myocytes consisted of a tyrosine 397 substrate peptide fused with cyan fluorescent protein and yellow fluorescent protein. The FAK FRET biosensor contains the SH2 domain derived from c-Src, a flexible linker peptide, and a specific sequence from FAK which encompasses Tyr-397. A FAK FRET reporter was chosen because in cardiac myocytes FAK has been implicated in the transduction of mechanical signals (Samarel, 2005).

Evaluation of two photon excitation in combination with laser tweezers. In the initial experiments the cells began to beat in a nonrhythmic manner when beads were attached to the surface and a laser force was applied. Since the cell motion interfered with the ability to record the FRET signals, the cells were treated with 2.5uM of blebbistatin, a myosin II inhibitor, for short periods of time (5, 10, 20, 30 minutes) prior to application of the laser tweezer force (See supplemental information on the blebbistatin incubation study).

A series of studies was conducted to examine the effects of laser-induced forces on FAK activation under the following conditions: i) FAK-FRET reporter transfected cells alone, ii) FAK-FRET reporter transfected cells with the trapping laser on within the vicinity of the cell, and iii) FAK-FRET reporter transfected cells with a bead attached and a static laser trapping force applied. Each of the above conditions was tested in the presence of blebbistatin. Beads were coated with fibronectin and attached to the cells for several minutes before application of the laser trapping force.

Evaluation of directionally localized force application. Cardiac myocytes are typically rod-shaped and have an orientation in which there is a defined longitudinal and

short axis. Forces were applied in the x and y direction. Each orientation correlates to in-vivo situations during systole, including longitudinal stretch along the fiber organization, and transverse stretch perpendicular to the fiber. Neonatal murine cardiac ventricular myocytes were prepared as described above. To probe the anisotropic properties of cardiac myocytes, the laser tweezers were adjusted such that directionally localized forces would be applied either in the transverse or in the longitudinal axis of the cell.

Image Processing. Image analysis was performed using the Otsu Method as described in Wang et al., 2005 and Botvinick and Wang, 2007. Using a customized Matlab program, mean intensity values were calculated for ECFP/YPet in regions of interest located at the site of bead attachment and distant from the bead attachment site.

Statistical Analysis. Data were compiled and are shown as means $\pm$ standard errors of the means. Each N represents a single cell. Statistical significance was determined by using Student's t test using GraphPad Prism 5 software (GraphPad Inc, San Diego, CA). A P value of <0.05 was considered significant.

6.5 Supplemental Information

Blebbistatin. Although this testing system provides the ability to study cardiac mechanotransduction at the single cell level, we note that a limitation of this setup is the use of blebbistatin, a myosin II inhibitor. Our studies currently show that it does not interfere with the ability to use our fluorescent reporters to investigate signalling events due to the short incubation times and as such, we will continue to use these methods to study mechanotransduction in cardiac myocytes.

Reversible photobleaching of the FAK FRET reporter. Previous work has characterized changes in photophysical properties of GFP variants including ECFP and citrine (Sinnecker et al., 2005; Henderson et al., 2007). These results showed that the fluo-

rescence intensity decreased only during the first few illumination cycles and reaches a stable level afterward. In addition, it was noted that a dependence of photobleaching kinetics on ECFP occurred in the presence of a FRET acceptor. In previous work shown by Sinnecker et al., 2005, the distance between the donor and acceptor resulted in a varying decay of fluorescence over time as a result of reversible photobleaching. In comparing to results observed in our lab, the time for these fluorescence traces were normalized to gain insight as to how distance between the donor and acceptor of a FRET construct are affected by reversible photobleaching. The results showed that when a donor and acceptor were incorporated into a cell as free plasmids, a kinetic constant, tau, of 42 seconds was observed for the decay in fluorescence over time. In addition, when the donor and acceptor fluorophores were linked directly, a tau of 46 seconds was observed. In comparison, for our FAK FRET construct, the donor and acceptor fluorophore are linked through a binding domain and a sequence of amino acids, tau of 45 seconds was observed. These results show that the decay in fluorescence observed in our control cells may be due to a dependence of the photobleaching kinetics of ECFP in the presence of its FRET acceptor, YPet.

6.6 Acknowledgements

We would like to thank M. Kim, A. Liu, M. Chen, Z. Shi, E. Botvinick, and the members of the Berns Lab, Chien Lab, Cardiac Mechanics Research Group, and the Ross Lab for their assistance. This study has been supported by an American Heart Association Pre-doctoral Fellowship (to A.L.H.), the University of California, San Diego, Cardiovascular Science Scholarship (to A.L.H.), National Institutes of Health, National Heart Lung and Blood Institute 5P01HL46345 (K.U.K., to A.D.M. and R.S.R. (Project 3)), the National Science Foundation (BES-0506252; to A.D.M), and the Air Force Office of Scientific Research (F9620-00-1-0371; to M.W.B).

Chapter 6 is being prepared for publication titled ”A Mechanotransduction Response in Cardiac Myocytes Using Optical Tweezers and Multiphoton Fluorescence

Resonance Energy Transfer" by Amy L. Hsieh, Tiffany W. Hsu, Qingyuan Zhu, Marcellinus S. Harsono, Yingxiao Wang, Alice Zemljic-Harpf, Robert S. Ross, Andrew D. McCulloch, Michael W. Berns for submission. The dissertation author is the primary investigator of this paper.

6.7 Figures

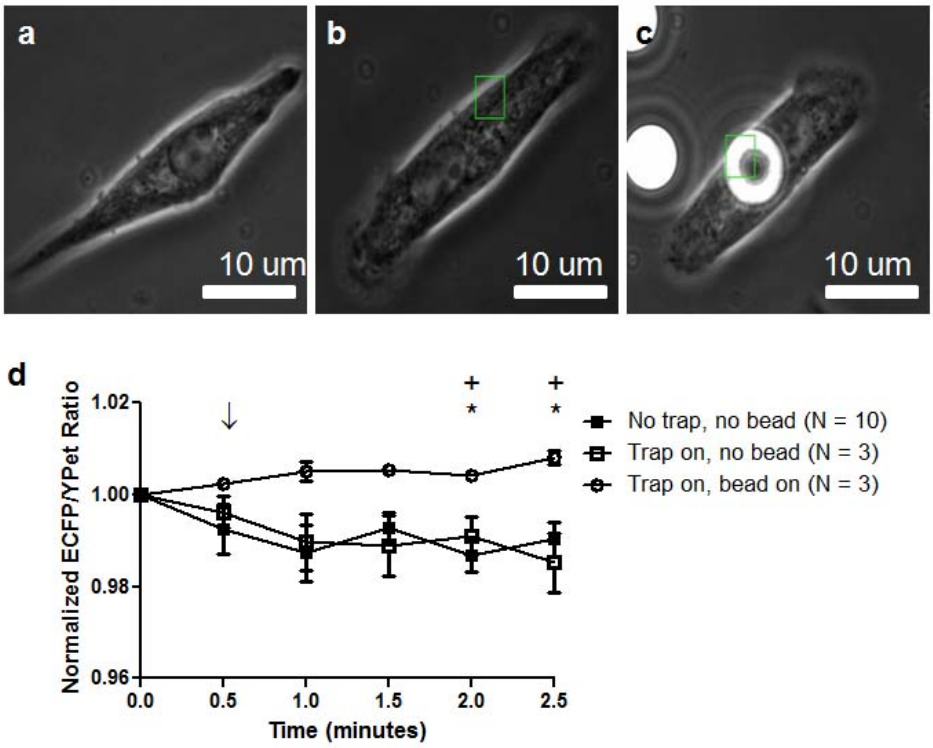

Figure 6.1: Characterization of the MP FRET-trapping system. The ECFP/YPet emission ratio time courses (d) of the FAK FRET reporter in neonatal murine cardiac ventricular myocytes under the following conditions: a) transfected cells alone (N = 10), b) active trapping laser on (N = 3), c) transfected cells with an integrin ligand coated bead attached to the cell and exposed to the force of the trapping laser (N = 3). Arrow indicates time point in which the trapping laser is turned on. (* $P < 0.05$, t-test comparison between transfected cells alone (no trap, no bead state) and transfected cells with integrin ligand coated bead attached (trap on, bead on), P values from left to right are 0.0332, 0.0299; + $P < 0.05$, t-test comparison between transfected cells in the presence of an active trapping laser (trap on, no bead) and and transfected cells with integrin ligand coated bead attached (trap on, bead on), P values from left to right are 0.0363, 0.0249)

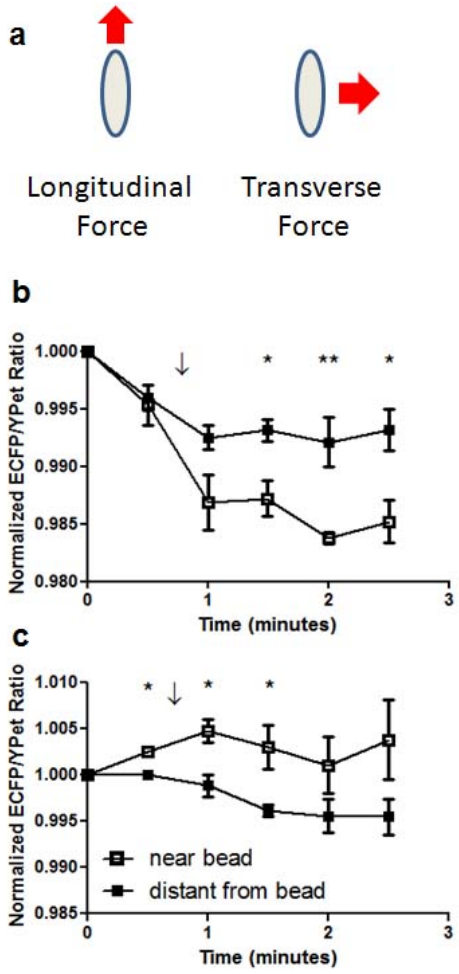

Figure 6.2: FAK FRET reporter changes in response to directionally localized force application. a) Pictorial diagram of the two orientations of force application. i) Longitudinal force applied parallel to the plane of the cell and along the long axis of the cell. ii) Transverse force applied parallel to the plane of the cell and along the short axis of the cell. b) Normalized ECFP/YPet Ratio time courses were obtained, (arrow) represents when the laser tweezers are turned on and a static force is applied in the longitudinal direction. (N = 4) (* $P < 0.05$, ** $P < 0.01$; P values from left to right: 0.017, 0.0094, 0.0217) c) Normalized ECFP/YPet Ratio time courses were obtained, (arrow) represents when the laser tweezers are turned on and a static force is applied in the transverse direction. (N = 3) (* $P < 0.05$; P values from left to right: 0.0123, 0.0265, 0.0481)

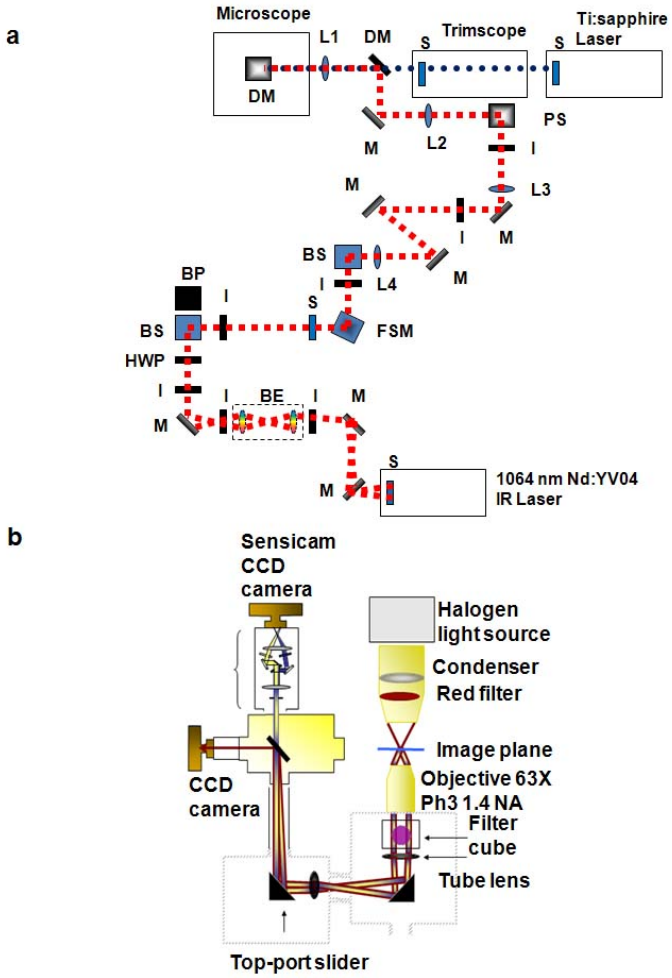

Figure 6.3: Diagram of microscope components for a multiphoton FRET-trapping system. a) A Ti:sapphire laser is divided into sixteen simultaneous laser spots using a TrimScope and combined with laser tweezers which enters an inverted microscope. Legend: 1.5x beam expansion system (BE), blocked path (BP), polarization beam splitter (BS), dichroic mirror (DM), fast steering mirror (FSM), iris (I), tube lens (f = 150mm) (L1), scan lens (f = 50mm) (L2), relay lenses (f = 300mm), mirror (M), periscope (PS), shutter (S), and half wave plate (HWP). b) A red filter is placed before the microscope condenser to allow simultaneous imaging of phase contrast and separating the phase contrast light from the collected short wavelength fluorescence emissions. The shorter wavelength emissions of ECFP and YPet pass through a dual view system which splits the emissions and images simultaneously on the Sensicam CCD camera.

6.8 References

[1] Schwartz, M., & DeSimone, D. (2008). Cell adhesion receptors in mechanotransduction. Curr Opin Cell Biol., 20(5), 551-556.

[2] Samarel, A.M. (2005). Costameres, focal adhesions, and cardiomyocyte mechanotransduction. Am. J. Physiol Heart Circ. Physiol 289, H2291-H2301.

[3] Towbin, J., & Bowles, N. (2006). Dilated cardiomyopathy: A tale of cytoskeletal proteins and beyond. J Cardiovasc Electrophysiol., 17, 919-926.

[4] Bowles, N.E., Bowles, K.R., and Towbin, J.A. (2000). The "final common pathway" hypothesis and inherited cardiovascular disease. The role of cytoskeletal proteins in dilated cardiomyopathy. Herz 25, 168-175.

[5] Towbin, J.A. and Bowles, N.E. (2000). Genetic abnormalities responsible for dilated cardiomyopathy. Curr. Cardiol. Rep. 2, 475-480

[6] Saffitz, J. (2006). Adhesion molecules: Why they are important to the electrophysiologist. J Cardiovasc Electrophysiol, 17, 225-229.

[7] Gopalan, S. et al. (2003). Anisotropic stretch-induced hypertrophy in neonatal ventricular myocytes micropatterned on deformable elastomers. Biotechnol Bioeng, 81(5), 578-587.

[8] Senyo, S., Koshman, Y., & Russell, B. (2007). Stimulus interval, rate and direction differentially regulate phosphorylation for mechanotransduction in neonatal cardiac myocytes. FEBS Lett., 581, 4241-4247.

[9] Lu, S., & Horowits, R. (2008). Role of nonmuscle myosin IIB and N-RAP in cell spreading and myofibril assembly in primary mouse cardiomyocytes. Cell Motil Cytoskeleton, 65(9), 747-761.

[10] Zipfel, W., Williams, R., & Webb, W. (2003). Nonlinear magic: Multiphoton microscopy in the biosciences. Nat Biotechnol, 21(11), 1369-1377.

[11] Brancaccio, M. et al. (2006). Integrin signalling: The tug-of-war in heart hypertrophy. Cardiovasc Res, 70(3), 422-433.

[12] Geiger, B., Spatz, J., & Bershadsky, A. (2009). Environmental sensing through focal adhesions. Nat Rev Mol Cell Biol, 10(1), 21-33.

[13] Wang, Y. et al. (2005). Visualizing the mechanical activation of Src. Nature 434, 1040-1045.

[14] Botvinick, E. L., & Wang, Y. (2007). Laser tweezers in the study of mechanobiology in live cells. Methods Cell Biol., 82, 497-523.

[15] Sinnecker, D., Voigt, P., Hellwig, N., & Schaefer, M. (2005). Reversible photobleaching of enhanced green fluorescent proteins. Biochemistry, 44(18), 7085-7094.

[16] Henderson, J., Ai, H., Campbell, R., & Remington, S. (2007). Structural basis for reversible photobleaching of a green fluorescent protein homologue. Proc Natl Acad Sci U S A, 104(16), 6672-6677.

Chapter 7

Development and characterization of a tamoxifen inducible cardiac specific vinculin knockout mouse

7.1 Introduction

Vinculin is a ubiquitously expressed protein found in muscle, and its isoform, metavinculin is found only expressed in striated muscle. Vinculin is an actin-linking protein which bridges the sarcomere to the cytoskeleton and is involved in cell-cell junctions and in cell-extracellular matrix adhesion.

In vivo models have shown that vinculin is necessary to maintain normal cardiac function. Global homozygous vinculin knockout (KO) mice died by embryonic day (E) 10, with neural defects, aberrant forelimb developments, and their hearts were reduced in size (Xu et al., 1998). Heterozygous vinculin KO mice (+/- Vcl KO) were viable, fertile, and did not have any obvious abnormalities. Upon increased hemodynamic loading, the heterozygous vinculin KO mice were predisposed to cardiac failure (Zemljic-Harpf et al., 2004). With the development of a cardiac myocyte specific vinculin KO model, it was discovered that these mice had disrupted cellular junctions, causing sudden death

or dilated cardiomyopathy (Zemljic-Harpf, et al., 2007).

Using these available knockout models has improved our understanding of vinculin's role in the heart, however, to further our understanding of the role of vinculin in the heart, we developed a tamoxifen inducible cardiac specific vinculin knockout. This mouse model will allow temporal control of vinculin excision, which can be used to understand the mechanistic role of vinculin in the heart and to evaluate the physiological role of vinculin in the cardiac myocyte.

7.2 Methods

Generation of the Tamoxifen Inducible Cardiac Specific Vinculin Knockout. To allow for detailed mechanistic analysis of the role of vinculin in cardiac myocytes, we generated a temporally controlled tamoxifen inducible cardiac specific vinculin knockout. A tamoxifen inducible cardiac myocyte specific, α-myosin heavy chain (αMHC) promoter Cre-recombinase (Sohal et al., 2001) was bred into the cardiac myocyte specific floxed vinculin mice (Zemljic-Harpf et al., 2007). These mice allow temporal control of Cre-recombinase function in cardiac myocytes upon tamoxifen administration to the mice. All animal study protocols were approved by the VA Healthcare San Diego Institutional Animal Care and Use Committee (IACUC).

Genotyping of Tamo cVclKO mice. The genotypes of the tamoxifen inducible cardiac specific vinculin knockout mice were determined by polymerase chain reaction as described previously in Zemljic-Harpf et al., 2007. In brief, when mice were weaned, tail DNA was retrieved, boiled in 50mM NaCl, cooled, and 1M Tris HCl was added. The subsequent DNA samples were used in PCR. Primers P3 (5'-CCTGCGCGGGATTACCTCATTGAC-3') and P2 (5'-TGCTCACCTGGCCCAAGATTCTTT-3') were used to detect the 843 bp band from the wildtype allele and the 960 bp from the floxed allele. CreF (5'-GTTCGCAAGAACCTGATGCACA-3') and CreR (5'-CTAGAGCCTGTTTTGCACGTTC-3') primers were used to assess Cre recombinase expression,

which produced a 350 bp Cre product. To check for Cre-mediated vinculin exon 3 excision, primers P1 (5'-TTACGCCTAGCACTTGAA-3') and P2 (as described above) are used.

Preparation and injection of tamoxifen. Tamoxifen stock solution (10mg/mL) was prepared fresh using 100mg tamoxifen (Sigma, T5648, St. Louis, MO), 200uL ethanol (Sigma, 459844, St. Louis, MO), and 10mL corn oil (Sigma, 8267, St. Louis, MO). Upon dissolution, the tamoxifen stock solution and control corn oil solution were filtered using a 0.45um syringe filter (Millipore, SLLHH04NL, Billerica, MA). Aliquots of the stock solution were made, wrapped in foil, and stored at 4^oC.

Animals were genotyped for the floxed allele, Cre product, and checked for exon 3 excision. Only animals that had no exon 3 excision prior to the experiment were used. Animal body weight was obtained and insulin syringes (Thermo Fisher Scientific, 14-826-79, Waltham, MA) were filled based on the dosages of 40 micrograms Tamoxifen/gram body weight of the animal. Animals were injected intraperitoneally for 5 days consecutively, alternating right and left side injections. At two, three, or four weeks after injection, hearts were collected for protein, histology, and immunofluorescence studies.

Adult murine cardiac ventricular myocyte isolation. Cardiac ventricular myocytes were isolated from mice at two, three, and four weeks after injection. Isolation procedures were performed as previously published in O'Connell et al., 2007.

In brief, animals were weighed and tamoxifen or corn oil filled syringes were prepared as described above. At the specified time point for harvest, the scientist performing the harvest was blinded as to the genotype and experimental group that the animal was in. The mouse was anesthetized with isoflurane and heparinized. The heart was then excised, cannulated, and perfused with perfusion buffer (120.4mM NaCl, 14.7mM KCl, 0.6mM KH_2PO_4, 0.6mM Na_2HPO_4, 1.2mM $MgSO_4$-$7H_2O$, 10mM Na-HEPES, 4.6mM $NaHCO_3$, 30mM Taurine, 10mM BDM, and 5.5mM glucose). The heart was then perfused with myocyte digestion buffer (perfusion buffer with 2.4 mg/mL colla-

genase II) and myocytes were dissociated. Enzyme digestion was then stopped with myocyte stopping buffer (perfusion buffer with 10% calf serum, and 12.5uM $CaCl_2$)

Immunofluorescence microscopy. For immunofluorescence microscopy, adult murine cardiac ventricular myocytes were isolated at 2 weeks, 3 weeks, and 4 weeks after tamoxifen injection as described previously in O'Connell et al., 2007. Cells were plated, fixed, and immunomicroscopy was performed as previously described in Zemljic-Harpf et al., 2007. Antibodies were diluted as follows: anti-vinculin (1:400) and the secondary antibody (1: 500).

Antibodies and fluorochromes. The following antibodies were used: mouse monoclonal anti-pan-vinculin (V 9131, Sigma, St. Louis, MO), anti-alpha-tubulin (T5168, Sigma, St. Louis, MO), anti-GAPDH (G8795, Sigma, St. Louis, MO), horseradish peroxidase-conjugated anti-mouse (115-175-146, Jackson Immunoresearch, West Grove, PA), Alexa Fluor 488 goat anti-mouse (A-11029, Molecular Probes, Invitrogen, Carlsbad, CA).

Western blotting. Freshly isolated hearts were immediately frozen in liquid nitrogen and homogenized in a lysis buffer (50mM Tris-HCl, 150mM NaCl, 1mM EDTA, 1% deoxycholate, 0.2% SDS, 1% IGEPAL, proteinase inhibitor) and analyzed as previously described in Zemljic-Harpf et al., 2007. Protein lysates were resolved by sodium dodecyl sulfate-polyacrylamide gel electrophoresis and Western blots were performed to detect vinculin, metavinculin, alpha-tubulin, or GAPDH levels. Blots were incubated with primary antibodies overnight at 4^oC. Dilutions for anti-vinculin (1:4000), anti-alpha-tubulin (1:4000), anti-GAPDH (1:40,000). Densitometric quantification of protein bands were performed digitally (ImageJ, NIH, Bethesda, MD).

Tissue acquisition, morphometry, histology, and morphometric analyses, the animals were sacrificed at 2 and 15 weeks after tamoxifen injection. At sacrifice, the hearts were arrested in diastole by injection of a high-potassium solution (25mM KCl and 5%

dextrose in phosphate-buffered saline). The heart tissue was collected for protein, DNA, and RNA analyses. Heart tissue was also preserved, sectioned, and stained with hematoxylin and eosin and trichrome stains.

Echocardiographic procedures. Echocardiographic procedures (M-mode, B-mode, two-dimensional, and Doppler) were performed on animals under isoflurane anesthesia and measured by investigators blinded to the genotype of the animal, as previously described in Zemljic-Harpf et al., 2004. In brief, animals are treated with Nair to remove the hair on their chest and placed in the echocardiography set up, induced with 2% isoflurane, and anesthetized with 1% isoflurane during imaging. Images were taken using B-mode ultrasound, to locate the best imaging plane and then switched to M-mode ultrasound to images changes in the left ventricle during diastole and systole. Doppler mode recordings were measured to determine aortic ejection time.

Papillary muscle isolation and testing. Papillary muscles were excised from animals 4 weeks after injection as described previously (Chuang et al., 2010). In brief, the animals were anesthetized, cervical dislocation was performed, the heart was dissected, cannulated, and perfused with cardioplegic solution. The right ventricle was opened and titanium oxide markers were placed on the papillary muscle. The papillary muscle was dissected and mounted in a tissue culture chamber via a titanium hook and force transducer. The muscle was paced and stretched while a uniaxial force was recorded. Stresses were calculated by dividing passive force data by the initial cross-sectional area of each muscle. Lagrangian strain measurements were calculated with respect to slack length and exponential fits were used to produce stress-strain curves.

Generation of the Double reporter Tamoxifen Inducible Cardiac Specific Vinculin Knockout. To allow for further detailed mechanistic analysis of the role of vinculin in isolated cardiac myocytes, we generated a temporally controlled tamoxifen inducible cardiac specific vinculin knockout and double fluorescent reporter knockin. A tamox-

ifen inducible cardiac myocyte specific, α-myosin heavy chain (αMHC) promoter Cre-recombinase was bred into the cardiac myocyte specific floxed vinculin mice (Zemljic-Harpf et al., 2007). The cardiac specific tamoxifen inducible floxed vinculin mice were bred with Gt(ROSA)26Sor$^{tm1Luo,\, tm2Luo,\, tm3Luo,\, tm4ACTB-tdTomato,-EGFP)Luo}$ obtained from Jackson Labs (Sacramento, CA). These mice were bred to homozygosity to produce a floxed vinculin double fluorescent reporter tamoxifen inducible Cre mouse line.

Genotyping of Tamo Tom cVclKO mice. The genotypes of the tamoxifen inducible double fluorescent reporter cardiac specific vinculin knockout mice were determined by PCR as described previously in Zemljic-Harpf et al., 2007 and Muzumdar et al., 2007. Detection of the floxed allele and Cre recombinase expression are described above. For detection of the double reporter system, a wildtype forward primer (5'-CTC TGC TGC CTC CTG GCT TCT-3'), wildtype reverse primer (5'- CGA GGC GGA TCA CAA GCA ATA-3'), and mutant reverse primer (5'- TCA ATG GGC GGG GGT CGT T-3') are used to detect a 330 bp wildtype allele or a 250 bp mutant allele.

Statistical methods. Data were compiled and are shown as mean $\pm$ standard errors of the mean. Data were evaluated using unpaired, two-tailed t tests (95% confidence interval) and GraphPad Prism 5 (GraphPad Inc, San Diego, CA). A P value of < 0.05 was considered significant. Specifically, for papillary muscle experiments, measurements are presented as mean $\pm$ standard deviation and stress-strain curves were compared by two way repeated measures ANOVA ($P < 0.05$ was considered significant).

7.3 Results

Vinculin gene excision occurs upon tamoxifen injection of tamoxifen inducible cardiac myocyte specific vinculin knockout mice

Breeding cardiac myocyte specific floxed vinculin mice (Zemljic-Harpf et al.,

2007) with a tamoxifen inducible cardiac myocyte specific, α-myosin heavy chain (αMHC) promoter Cre-recombinase (Sohal et al., 2001) has generated a tamoxifen inducible cardiac specific vinculin knockout mice (Tamo cVcl KO).

Polymerase chain reaction (PCR) studies verified the genotype of the mice (Figure 1). Both tamoxifen inducible Cre positive (TCre+) and Cre negative (TCre-) mice were injected with corn oil or tamoxifen. Results showed that exon 3 excision was detected in heart DNA of TCre+, but not in TCre- mice.

Tamoxifen inducible cardiac myocyte specific vinculin knockout mice allows temporal control of vinculin excision

Both tamoxifen inducible Cre positive (TCre+) and Cre negative (TCre-) mice were injected with corn oil or tamoxifen. Four weeks after injection, whole heart lysates were obtained and protein levels were assessed via Western blotting (Figure 2a). Results show a decrease in vinculin and metavinculin in tamoxifen injected Tamo cVcl KO mice as compared to controls (corn oil injected controls, corn oil injected knockouts, and tamoxifen injected control mice). Densitometric analysis of controls versus tamoxifen injected knockouts showed an overall 25.2% reduction in vinculin and 47.7% reduction in metavinculin (Figure 2b). Both expression levels for vinculin and metavinculin were assessed because vinculin is found in both myocytes and nonmyocytes, whereas, metavinculin is only expressed in myocytes. By looking at metavinculin expression in the heart, we can gain more information about the levels of vinculin and metavinculin expression in cardiac myocytes.

To investigate the role of vinculin in cardiac myocytes, adult murine cardiac ventricular myocytes were isolated from animals two weeks, three weeks, and four weeks after injection (Figure 3a). Densitometric analysis results showed an overall 11.8% reduction in vinculin in cells isolated two weeks after injection. In cells isolated three weeks after injection had a 12.9% reduction in vinculin and in cells isolated four weeks after injection, a 16.2% reduction in vinculin was detected. Immunofluorescence also shows the loss of vinculin in cells isolated three weeks after injection (Figure 3b).

Cardiac myocyte vinculin knockout in mature mice lead to dilated cardiomyopathy

Cardiac function of Tamo cVclKO mice were examined via echocardiography at discrete time points. (Figure 4) Results showed progressive dilation of the left ventricle in systole and diastole, an overall decrease in ventricular function as noted by a reduction in the percent of fractional shortening (%FS) and velocity of circumferential fiber shortening (Vcf). These results correlate with the development of dilated cardiomyopathy which occurs after injections. Figure 4e shows representative echocardiograms of control and knockout mice 15 weeks after tamoxifen injection. Results show dilation of the ventricular wall in knockout mice as compared to controls as denoted by LVIDd/BW (left ventricular internal dimension in diastole with respect to body weight) and LVIDs/BW (left ventricular internal dimension in systole with respect to body weight). Histological samples of the heart show evidence of mild fibrosis (Figure 5).

Tamo cVcl KO exhibit less stiffness in the fiber direction Tamo cVcl KO mice injected with tamoxifen were harvested 4 weeks after injection for papillary muscle experiments. At this time point, these mice do not exhibit functional differences as determined by echocardiography, however, they have reduced vinculin and metavinculin expression as compared to controls. Preliminary results obtained by Chuang et al., 2010 indicate that Tamo cVcl KO mice injected with tamoxifen, exhibit less stiff papillary muscles as compared to mice injected with corn oil (Figure 6).

Generation of the Tom Tamo cVcl KO allows visualization of the cells with active Cre-recombinase

Floxed vinculin double fluorescent reporter tamoxifen inducible Cre mouse was bred to allow visualization of cells that contained active Cre excision. Under no Cre conditions, the cells from this mouse exhibit a mTomato marker, whereas, under Cre excision, the cells exhibit a EGFP marker (Figure 7). Immunofluorescence images of

isolated cardiac myocytes, isolated 1 week after injection, taken with the same exposure time show that the double reporter of the mTomato and EGFP tag, provides a means of identifying cells that have Cre excision and the ability to separate the cells from those with no Cre excision.

7.4 Discussion and Conclusions

Vinculin is a component of the cell-extracellular matrix adhesion and cell-cell interaction sites. Its position within a cell may play a critical role in maintaining normal mechanotransduction and cytoskeletal integrity in the myocyte. Whole animal studies of global, heterozygous, and cardiac specific vinculin knockout mice have shown that vinculin is necessary to maintain normal cardiac function, but vinculin's role in a cardiac myocyte and the role it plays in progression of development is not fully understood. As such we aimed to develop a mouse model capable to allow the investigation of vinculin in an isolated cell, which lead to the development of the tamoxifen inducible cardiac specific vinculin knockout mouse.

Cardiac myocytes specific vinculin excision occurs upon tamoxifen administration in Tamo cVcl KO mice and Tamo cVcl KO mice develop dilated cardiomyopathy

Tamoxifen and corn oil injections of the Tamo cVcl KO mice showed that vinculin gene excision occurs and vinculin knockdown can be controlled using tamoxifen. After injection and over time, Tamo cVcl KO mice develop dilated cardiomyopathy as similarly noted to the cardiac specific floxed vinculin knockout mouse (MLC2v cVcl KO) (Zemljic-Harpf et al., 2007). Although small differences include the absence of noted arrhythmias in the Tamo cVcl KO as compared to the MLC2v cVcl KO (data not shown) via electrocardiograms, which could be attributed to the difference of when vinculin knockdown occurs as MLC2v cVcl KO have vinculin excision immediately after birth, whereas Tamo cVcl KO mice have physiologically normal function before injection and vinculin excision only occurs when injections are begun.

Other differences include the lack of sudden death in Tamo cVcl KO as compared to MLC2v cVcl KO. These results could be attributed again to when vinculin excision occurs, or to the fact that the Tamo cVcl KO males were housed in separate caging, thereby decreasing fighting between males which could stress the animal and cause sudden death.

Reduction in vinculin over time after injections in Tamo cVcl KO

Isolated adult cardiac myocytes from time points: two, three, and four weeks after injection show decreases in overall vinculin, however, there was no statistical difference between the two, three, and four week time points. These results could be attributed to the isolation procedure and anoikis due to the loss of vinculin and β1D integrin.

In addition, protein reduction of vinculin was noted to be less than in the whole heart because during the isolation procedure of calcium reintroduction, only cells that were pelleted were lysed. This selection of cells that could be pelleted could represent only a group of cells that had small amounts of vinculin reduction, but is not representative of total vinculin reduction because cells that could have more vinculin reduction were discarded during the isolation procedure. Given the echo results, in which at four weeks, there were no visible differences in cardiac function, one would pursue choosing later time points for isolation. However, given that we are actually selecting against cells with vinculin reduction via the calcium reintroduction process, it does not seem feasible at this time to pursue isolating cardiac myocytes at later timepoints, until adjustments to the isolation procedure are made.

Vinculin deletion of Tamo cVcl KO leads to less stiff papillary muscles

Previous studies of MLC2v cVcl KO mice indicated that vinculin deletion led to less passive stiffness in the fiber direction of the heart (Chuang et al., 2010). Similarly, vinculin deletion of Tamo cVcl KO resulted in less stiff papillary in tamoxifen injected animals as compared to controls. These results indicate that the Tamo cVcl KO mice are

more compliant in the fiber direction as similarly found in the MLC2v cardiac myocyte specific vinculin knockout (Chuang et al., 2010).

Tom Tamo cVcl KO mice provide a means to investigate the role of vinculin in isolated cardiac myocytes

The generation of the Tom Tamo cVcl KO mouse has shown that tamoxifen administration intraperitoneally may lead to a heterogenous excision of Cre within cells of the heart. Additionally, this mouse model provides a means to determine which cells have Cre excision. Having the ability to identify which cells are Cre excised will provide a means to perform single cell studies with the knowledge of whether the cell is normal or knocked down.

In conclusion, we have developed a tamoxifen inducible cardiac myocyte specific vinculin knockout mouse and a double reporter tamoxifen inducible cardiac myocytes specific vinculin knockout mouse. In the heart and in isolated myocytes, it has been shown that vinculin knockdown can be controlled temporally. The dilated cardiomyopathy phenotype in response to vinculin excision in the adult myocytes has been observed similarly as previously noted in the cardiac specific vinculin knockout mouse, but whether the means to the development of the disease is the same requires further investigation. Our results show that it is now possible to study the effects of vinculin deletion in an intact adult cardiac myocyte.

7.5 Acknowledgements

I'd like to acknowledge Steve Padilla, Dr. Alice Zemljic-Harpf, and Dr. Robert Ross for their preliminary work in breeding and injection pilot studies with the Tamo cVcl KO mice. I'd like to acknowledge Ruixia Li for the adult cardiac myocyte isolations. I'd like to acknowledge Joyce Chuang for the papillary muscle experiment.

7.6 Figures

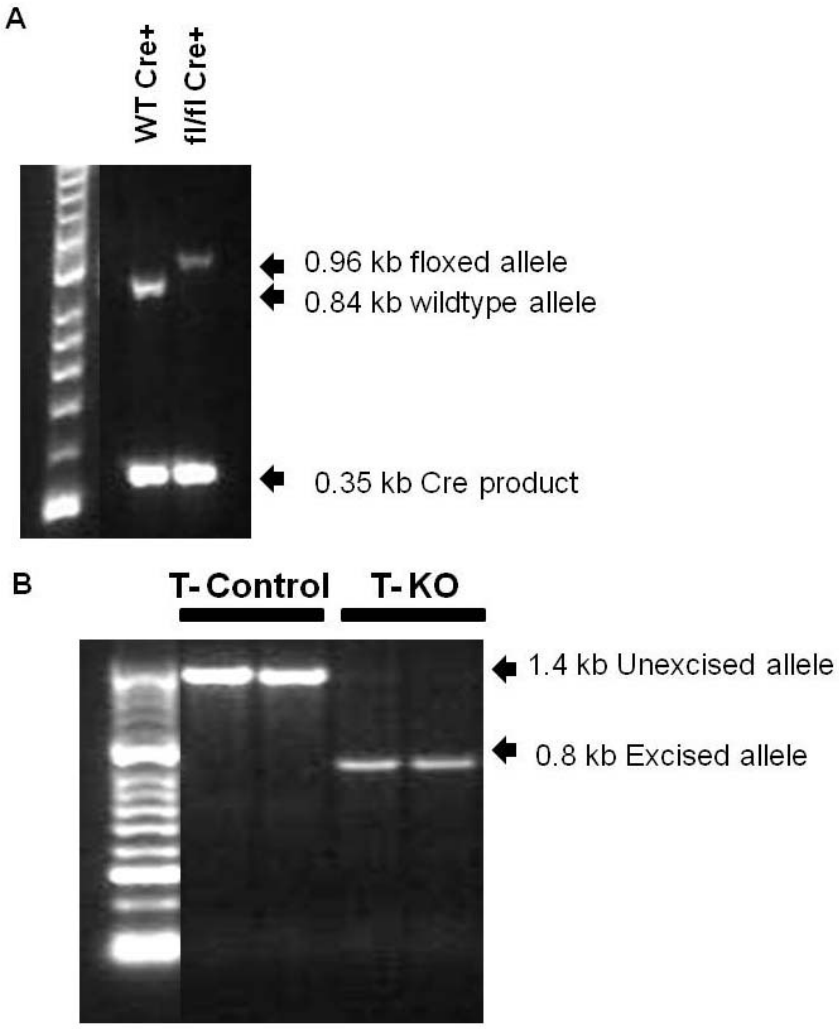

Figure 7.1: PCR was performed on DNA extracted from tails and heart tissue. A) The PCR for DNA obtained from tails confirms the 0.96 kb band generated from the gene-targeted floxed vinculin allele and the presence or absence of the Cre recombinase (350bp). B) T-Control are fl/fl TCre- animals injected with tamoxifen and T-KO are fl/fl TCre+ animals injected with tamoxifen. The PCR performed from DNA extracted from the heart shows the 0.8 kb band for the excision of exon 3 and it exists only when Cre is induced by injection of tamoxifen in TCre+ animals.

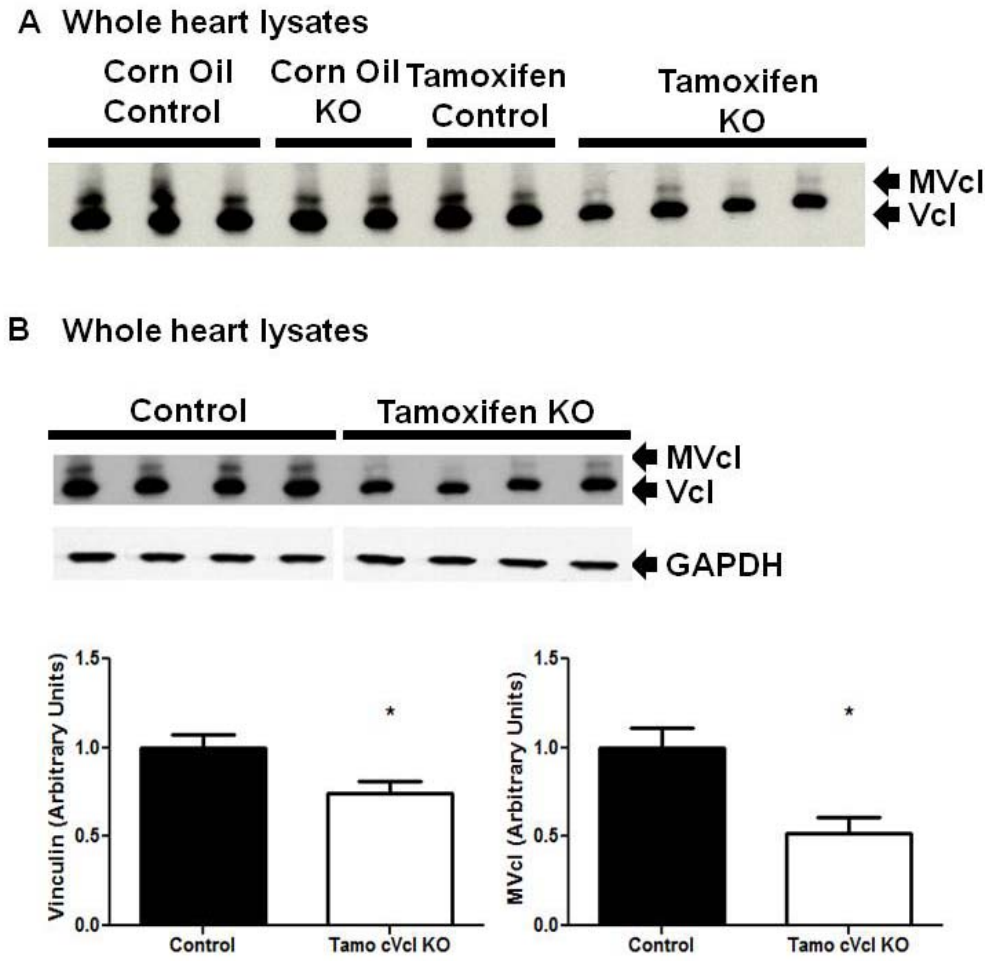

Figure 7.2: Western blot for whole heart tissue lysates collected four weeks after injection. A) The injection groups included: i) control mice ($Vcl^{fl/fl}$ TCre-) injected with corn oil (N = 3) (Corn Oil Control), ii) knockout mice ($Vcl^{fl/fl}$ TCre+) injected with corn oil (N = 2) (Corn Oil KO), iii) control mice ($Vcl^{fl/fl}$ TCre-) injected with tamoxifen (N = 2) (Tamoxifen Control), and iv) knockout mice ($Vcl^{fl/fl}$ TCre+) injected with tamoxifen (N = 4) (Tamoxifen KO). B) Controls (N = 4) vs. knockouts (N = 4). Vinculin expression was normalized to GAPDH expression. Tamo cVcl KO hearts showed a 25.2% reduction of vinculin, as compared to controls and a 47.7% reduction of metavinculin as compared to controls.

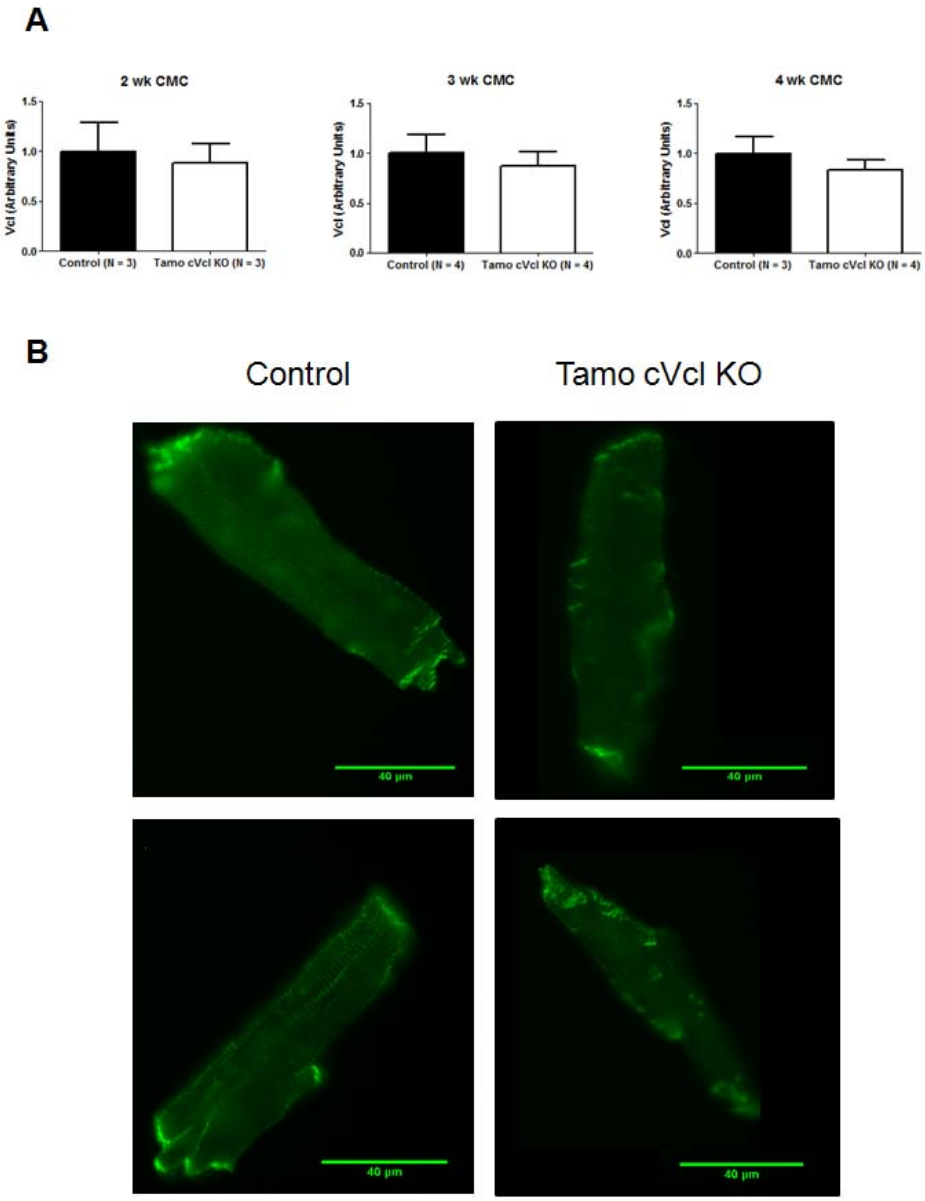

Figure 7.3: A) Western blot for isolated cardiac myocyte lysates. Cardiac myocytes were isolated two, three, and four weeks after injection. Densitometric analysis results showed an overall 11.8% reduction in vinculin in cells isolated two weeks after injection. In cells isolated three weeks after injection had a 12.9% reduction in vinculin and in cells isolated four weeks after injection, a 16.2% reduction in vinculin was detected. B) Anti-vinculin immunofluorescence also shows a decrease in vinculin in isolated cells three weeks after injection.

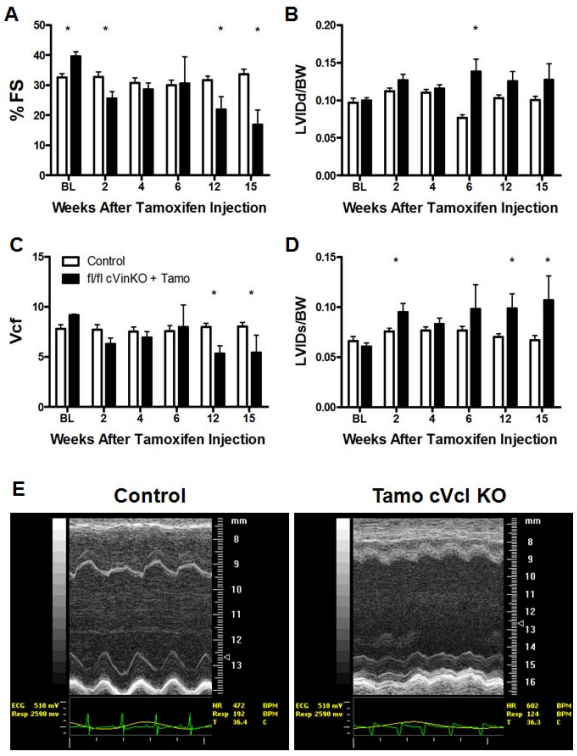

Figure 7.4: Echocardiographic data was obtained at baseline, 2, 4, 6, 12, and 15 weeks after tamoxifen injection. Hearts of the tamoxifen inducible cardiac specific vinculin knockout mice (Tamo fl/fl cVclKO) show left ventricular dilation and impaired cardiac function. At baseline, control = 12, KO = 3; after 2 weeks, control = 17, KO = 7; after 4 weeks, control = 24, KO = 11; after 6 weeks, control = 12, KO = 3; after 12 weeks, control = 12, KO = 3; after 15 weeks, control = 12, KO = 2. A) %FS, percent of fractional shortening (at baseline and after 2 and 12 weeks, * $P < 0.02$; after 15 weeks, * $P < 0.004$ between control versus KO), B) LVIDd/BW, left ventricular internal dimension in diastole with respect to body weight (after 6 weeks, * $P < 0.0002$ between control versus KO), C) Vcf, velocity of circumferential fiber shortening (after 12 weeks, * $P < 0.008$ between control versus KO, after 15 weeks, * $P < 0.05$ between control versus KO), D) LVIDs/BW, left ventricular internal dimension in systole with respect to body weight (after 2 weeks, * $P < 0.02$ between control versus KO, after 12 weeks, * $P < 0.008$ between control versus KO, after 15 weeks, * $P < 0.01$ between control versus KO). E) Representative echocardiograms from control and tamoxifen inducible vinculin knockout (Tamo cVcl KO) mice.

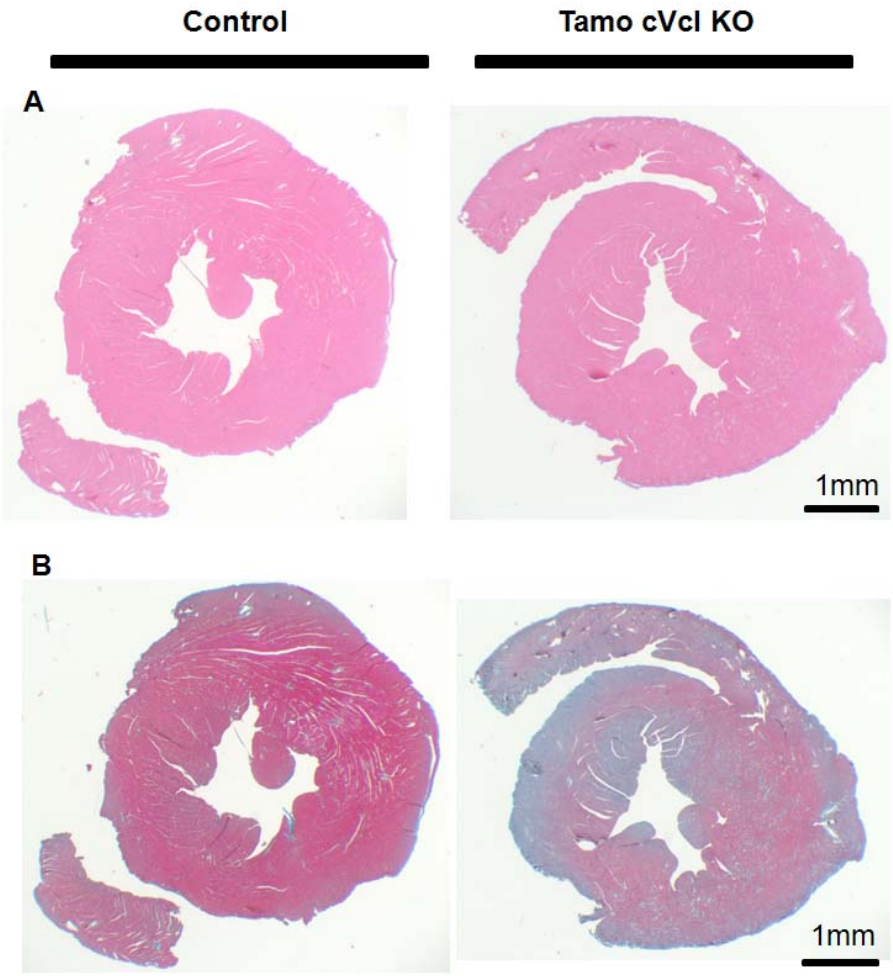

Figure 7.5: Tamoxifen inducible cardiac myocyte specific vinculin knockout (Tamo cVcl KO) mice exhibit dilated cardiomyopathy. Histological analysis of myocardial tissue collected 4 weeks after tamoxifen injection were stained with hematoxylin and eosin (A) and trichrome (B). Tamo cVcl KO injected with tamoxifen exhibit mild fibrosis as compared to controls.

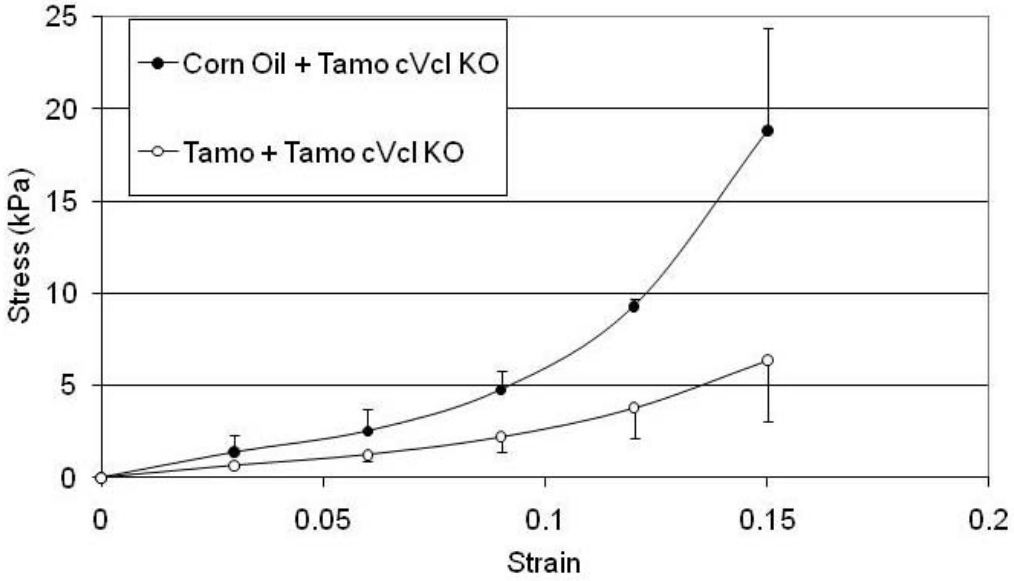

Figure 7.6: Stress-strain curves of muscles from Tamo cVcl KO (courtesy of Joyce Chuang). Papillary muscles were isolated from mice four weeks after tamoxifen injection. Tamo cVcl KO were injected with corn oil (•) (N = 2) and Tamo cVcl KO were injected with tamoxifen (○) (N = 2) at a dose of 40 micrograms tamoxifen/gram of body weight. The stress-strain curve reveals that the papillary muscle of the Tamo cVcl KO that was injected with tamoxifen is more compliant in the fiber direction as compared to the corn oil injected controls.

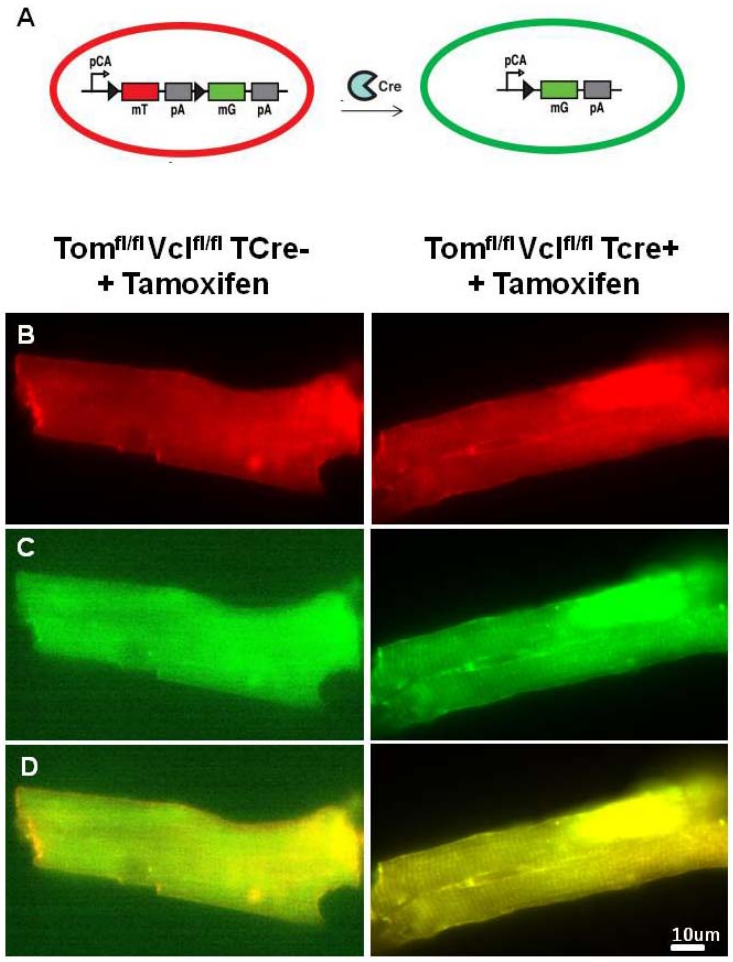

Figure 7.7: Tamoxifen inducible double reporter vinculin knockout (Tom Tamo cVcl KO) mice exhibit Cre expression upon administration of tamoxifen. A) Schematic diagram showing that before Cre excision, the cells exhibit the mTomato marker, whereas, when Cre excision occurs, the cells exhibit the EGFP marker. Immunofluorescence also shows that identification of Cre-activated cells in intact isolated cardiac myocytes is possible. Red fluorescing cells have no Cre activation and green fluorescing cells identify the cells as having activated Cre and Cre excision of floxed genes. Fluorescence images taken with the same exposure times, show results obtained from the B) red channel, C) green channel, and D) merged images from tamoxifen injected control (Tom$^{fl/fl}$ Vcl$^{fl/fl}$ TCre-) and knockout (Tom$^{fl/fl}$ Vcl$^{fl/fl}$ TCre+). Results indicate that the introduction of tamoxifen leads to increase of the EGFP signal and Cre excision in the tamoxifen inducible Cre positive mice, as compared to its Cre negative control.

7.7 References

[1] Chuang, J. S. (2010). The role of costameric proteins in cardiac force transmission and signaling. (Doctoral dissertation). Retrieved from ProQuest Dissertations and Theses Database. (AAT 3390089)

[2] Muzumdar, M. D., Tasic, B., Miyamichi, K., Li, L., & Luo, L. (2007). A global double-fluorescent cre reporter mouse. Genesis, 45(9), 593-605.

[3] O'Connell, T. D., Rodrigo, M. C., & Simpson, P. C. (2007). Isolation and culture of adult mouse cardiac myocytes. Methods Mol Biol., 357, 271-296.

[4] Sohal, D., Nghiem, M., Crackower, M., Witt, S., Kimball, T., Tymitz, K., et al. (2001). Temporally regulated and tissue-specific gene manipulations in the adult and embryonic heart using a tamoxifen-inducible cre protein. Circ Res, 89, 20-25.

[5] Xu, W., Baribault, H., and Adamson, E.D. (1998). Vinculin knockout results in heart and brain defects during embryonic development. Development 125, 327-337.

[6] Zemljic-Harpf, A., Manso, A. M., & Ross, R. S. (2009). Vinculin and talin: Focus on the myocardium. J Investig Med., 57(8), 849-855.

[7] Zemljic-Harpf, A., Miller, J., Henderson, S., Wright, A., Manso, A., Elsherif, L., et al. (2007). Cardiac-myocyte-specific excision of the vinculin gene disrupts cellular junctions, causing sudden death or dilated cardiomyopathy. Mol Cell Biol, 27, 7522-7537.

[8] Zemljic-Harpf, A., Ponrartana, S., Avalos, R., Jordan, M., Roos, K., Dalton, N., et al. (2004). Heterozygous inactivation of the vinculin gene predisposes to stress-induced cardiomyopathy. Am J Pathol, 165, 1033-1044.

Chapter 8

Vinculin mediates anisotropic mechanotransduction responses of focal adhesion kinase in neonatal cardiac ventricular myocytes

Vinculin is an actin-linking protein which bridges the sarcomere to the cytoskeleton and has been implicated to play a role in mechanotransduction events. Neonatal cardiac ventricular myocytes were isolated from cardiac myocyte specific floxed vinculin mice (fl/fl cVcl). Cells were plated on stretcher membranes, treated with Ad-LacZ or Ad-Cre, and subjected to 10% transverse and 5% longitudinal strain to the myofibrils. Cells were harvested and assayed after 20 minutes of stretch, for activation of FAK by western blotting. Results indicate that FAK is an indicator of mechanotransduction events in knockdown vinculin cells. To study how directionally applied localized forces affected mechanotransduction in these cell types, fluorescence resonance energy transfer (FRET) biosensors for FAK were incorporated into wildtype and cVcl KO cells. These cells were subjected to forces applied by an optical trap and changes in mechanotransduction events were monitored by our FAK FRET biosensor. Results show that a

reduction in vinculin led to a decrease in mechanotransduction through integrins, leading to a greater decrease in FAK phosphorylation when cells are subjected to forces applied transversely compared to wildtype cells. In comparison, vinculin knockdown cells subjected to forces applied along the longitudinal axis of the cell showed an increase in focal adhesion kinase phosphorylation as compared to the responses observed in the wildtype NMVMs. In conclusion, heterozygous vinculin KO cells had a decreased mechanotransduction response as reported by the FAK FRET biosensor in response to mechanical force application, and anisotropic responses to mechanotransduction as reported by FAK FRET biosensor is mediated by vinculin.

8.1 Introduction

Cardiac mechanotransduction is the process by which mechanical signals are transduced into biochemical signals in cardiac myocytes. Mechanotransduction signaling pathways help to maintain normal cardiac function and these pathways include, but are not limited to regulating protein synthesis, cell survival/apoptosis, cell-cell communication, sarcomeric protein assembly, cell shape changes, ion channel function, and hypertrophy (Samarel, 2005). Cardiac cells are connected to each other via cell junction proteins including gap junctions, desmosomes, and adherens junctions, and cells are connected to the extracellular matrix.

Within the cardiac myocyte there exist costameres, which are muti-protein structures which flank the Z-disk of myocytes and link the sarcomere, through the cytoskeleton to the extracellular matrix. Costameres have been shown to be the site where forces generated by cardiac myocytes are transmitted to the external extracellular matrix (”inside-out”) (Danowski et al., 1992) as well as the site where forces externally applied by the extracellular matrix are transmitted into the cardiac myocyte (”outside-in”) (Mansour et al., 2004). Two main protein complexes within the costamere site include the integrin complex and the dystrophin-glycoprotein complex (Lapidos et al., 2004).

Integrins are heterodimeric cell surface receptors compose of α and β subunits that bridge the cytoskeleton and possibly the sarcomere within the extracellular matrix. As such, they have been implicated as mechanotransducers (Ingber, 2006). In newborn and adult cardiomyocytes, β1D integrin is the main isoform expressed in the heart (Brancaccio et al., 2006). Previous work done by our group has shown that β1 has been linked to a hypertrophic phenotype in neonatal rat cardiac myocytes (Ross et al., 1998). In addition, transgenic and knockout mouse models have shown the importance of integrin function within the myocyte to preserve normal cardiac function (Shai et al., 2002, Keller et al., 2001, Valencik et al., 2002, Valencik et al., 2006). This work shows that the integrin complex and the proteins involved in connecting the extracellular matrix with the cytoskeleton and possibly the sarcomere through the integrin complex are essential in transmitting mechanical signals within the cardiac myocyte.

Several structural proteins involved in connecting integrins with the actin cytoskeleton include, but are not limited to talin, vinculin, α-actinin, and integrin linked kinase (Legate et al., 2009). Integrin also plays a role in recruiting signaling proteins such as focal adhesion kinase (FAK) and src (Wiesner et al., 2005). Upon integrin clustering, FAK becomes phosphorylated at the FAK-Y397 site (Sieg et al., 2000).

Vinculin is an actin-linking protein which bridges the sarcomere to the cytoskeleton and is involved in cell-cell junctions and in cell-extracellular matrix adhesion. The vinculin head regulates integrin dynamics and the tail is involved in mechanotransduction (Humphries et al., 2007). Vinculin also contains a focal adhesion binding domain in which it can interact with FAK. Because of vinculin's involvement with integrin and FAK, in addition to vinculin's anisotropic localization within a cell, we hypothesize that vinculin is required for normal cardiac mechanotransduction responses involving FAK.

8.2 Methods

Genotyping of cardiac specific floxed vinculin mice. The genotypes of the cardiac specific floxed vinculin knockout mice were determined by polymerase chain reaction

as described previously in Zemljic-Harpf et al., 2007.

Genotyping of the heterozygous vinculin knockout mice. The genotypes of the heterozygous vinculin knockout mice were determined by polymerase chain reaction as described previously in Zemljic-Harpf et al., 2004.

Cell Culture. Cardiac myocytes were harvested from freshly dissected ventricles of 0 to 2 day-old mice using an isolation kit (Cellutron, Highland Park, NJ). For the adenoviral studies, cardiac myocytes were isolated from neonatal mice that contained floxed alleles for vinculin (fl/fl cVcl Cre-). For studies using heterozygous vinculin knockout mice, cardiac myocytes were isolated from neonatal mice ventricles and atrias were used in genotyping. Cells were plated on dishes coated overnight with 10 ug/mL laminin (Sigma, L-2020) in high-serum plating media (Dulbecco's Modified Eagle Media (DMEM), 17% M199, 10% horse serum (HS), 5% fetal bovine serum (FBS), 100 units/ml penicillin and 50 mg/ml streptomycin) at 100,000 cells/cm^2. After eighteen hours, the cells were washed with Dulbecco's Phosphate-Buffered Saline (DPBS) and transferred to low serum maintenance media (DMEM, 18.5% M199, 5% HS, 1% FBS and antibiotics). Twenty-four to forty-eight hours after transfection, cells were washed with DPBS and fresh maintenance media was added. Cell cultures were maintained at 37°C and 5% CO_2. All culture media was purchased from Invitrogen (Carlsbad, CA) and sera was purchased from Gemini BioProducts (West Sacramento, CA). These animal studies were in accordance with VA Healthcare San Diego Institutional Animal Care and Use Committee (IACUC) guidelines.

Adenoviral treatment of neonatal murine ventricular myocytes. Stocks of LacZ adenovirus (Ad-LacZ) or Cre adenovirus (Ad-Cre) were previously titered and titer to infect cells in the various groups with equal MOIs. Cells were treated with Ad-LacZ or Ad-Cre for 24 hours and after 24 hours, the media was changed. Cells were washed with DPBS, lysed with a protein lysis buffer (50mM Tris-HCl, 150mM NaCl, 1mM EDTA, 1% de-

oxycholate, 0.2% SDS, 1% IGEPAL, and proteinase inhibitor), and stored in the -80°C).

Western blotting. Protein lysates were resolved by sodium dodecyl sulfate-polyacrylamide gel electrophoresis and western blots were performed to detect vinculin, metavinculin, alpha-tubulin, or GAPDH levels. Blots were incubated with primary antibodies overnight at 4°C. Dilutions for anti-vinculin (V9131, Sigma, St. Louis, MO,1:4000), anti-alpha-tubulin (T5168, Sigma, St. Louis, MO,1:4000), anti-GAPDH (sc-32233, Santa Cruz Biotechnology, 1:40,000). Densitometric quantification of protein bands were performed digitally (ImageJ, NIH, Bethesda, MD).

Anisotropic membrane stretch. Transversely aligned membranes were created and sterilized using a modified protocol (Camelliti et al., 2006). The membrane stretcher was assembled and placed in a non-stretched position. A layer of vacuum grease was placed to surround the aligned area of the membrane and the membrane was exposed to ultraviolet light for 15 minutes. Membranes were coated with laminin 10ug/mL at 37°C for several hours before plating. Neonatal murine cardiac ventricular myocytes (NMVMs) were isolated as described above. NMVMs were plated at a concentration of 3 million cells per stretcher. Cell media was changed from plating media to maintenance media one day after plating. Cells were treated with adenoviruses (Ad-Cre or Ad-LacZ) for 24 hours and then the virus was removed from the media. 72 hours after virus treatment, fresh media was added to the stretchers and the cells were stretched for 20 minutes at 10% transverse stretch and 5% longitudinal stretch or left unstretched for 20 minutes. The cells were lysed with lysis buffer and collected for western blot analysis as described above.

Focal adhesion kinase fluorescence resonance energy transfer reporter. In this study, cardiac myocytes were transfected, using FuGene6 transfection reagent (Roche Diagnostics, Indianapolis, IN) with a focal adhesion kinase fluorescence resonance energy transfer (FAK FRET) reporter. The FAK FRET reporter transiently transfected

into the cardiac myocytes consisted of a tyrosine 397 substrate peptide fused with cyan fluorescent protein and yellow fluorescent protein. The FAK FRET biosensor contains the SH2 domain derived from c-Src, a flexible linker peptide, and a specific sequence from FAK which encompasses Tyr-397. A FAK FRET reporter was chosen because in cardiac myocytes FAK has been implicated in the transduction of mechanical signals (Samarel, 2005).

Endothelin-1 stimulation. To determine difference in the FAK FRET reporter activity between wildtype and heterozygous vinculin knockouts, the cells were stimulated with endothelin-1 and changes in reporter activity were determined. Both control and endothelin-1 stimulation groups were serum starved for 24 hours and a time course of FAK FRET activity was observed under control and a 100mM endothelin-1 stimulation conditions (Sigma E7764) for both wildtype and endothelin-1 stimulation groups.

Force application with laser tweezers and monitoring of FAK FRET dynamics. The microscope used to do all laser tweezers and multiphoton fluorescence experiments of the FAK FRET biosensor is an Axiovert 200M (Zeiss, Thornwood, NY) with motorized objective turret, reflector turret, condensor turret, and a 63x plan-apochromat phase III, NA 1.4 oil immersion objective. The motorized reflector turret is shift-free to allow repeat switching between filter cube positions and contains several filter cubes and a mirror for guiding the 1064nm infrared laser tweezers and the Ti:sapphire laser. Specimens were mounted in an X-Y servo stage controlled with ASI Automated Stage Controller (MS-2000 XYZ, Applied Scientific Instrumentation, Eugene, OR). Both microscope and stage controller are controlled by the main controller through serial port cable (COM). The temperature of the specimens was maintained at 37°C by a Temperature Controller stage holder (TC-324B, Warren Instrument Corporation).

For capturing fluorescent images, a cooled digital 12 bit SensiCam CCD Camera (Applied Scientific Instrumentation, Eugene, OR) is connected to the top port of a Dual Video Adapter. Emission light from the microscope is guided into a dual view system

where the collimating lens, gathers the divergent beams of light into a parallel beam. The light is then guided to a dichroic filter, where the light is split into ECFP and YPet emissions and the images are projected side by side on the CCD. This camera is connected to the main computer via a PCI imaging card. The Ti:sapphire femtosecond laser is controlled via the Imspector software and is connected to the computer via a serial port cable.

For phase imaging, a red filter D680/60X is placed in front of the halogen light source and a short pass dichroic (600DCSP, Chroma, Bellows Falls, VT) is placed in the Dual Video Adapter to guide the long red wavelength to a Hamamatsu cooled charge-coupled device camera (C4742-98-24, Hamamatsu Photonics, K.K., Hamamatsu, Japan). This CCD Camera has high resolution (1344 x 1024 pixels), has a progressive scan interline readout with no mechanical shutter, and has an adjustable gain and exposure time for optical signal-to-noise characteristics. Robolase, a user-friendly Labview software/hardware system (Botvinick and Berns, 2005) uses Hamamatsu's video capture Library for Labview plug-in to communicate with the camera controller through its Digital CAMera Application Programming Interface (DCAMAPI) driver. The infrared laser is controlled via Robolase and a serial port cable.

Analysis of laser tweezers experiments. Image analysis was performed using the Otsu Method as described in Wang et al., 2005 and Botvinick and Wang, 2007. Using a customized Matlab program, mean intensity values were calculated for ECFP/YPet in regions of interest located at the site of bead attachment and distant from the bead attachment site. Results comparing wildtypes and knockouts were determined by normalizing bead attachment site changes by distant to the bead attachment site changes. Heterozygous vinculin knockouts have an overall decrease in β1D integrin (data not shown). β1D density was determined via immunofluorescence staining in both wildtype and heterozygous knockouts. To compare the wildtypes to the vinculin knockouts, areas for bead attachment were determined for each cell and comparison groups were determined based on overall average area normalized by β1D densities.

Statistical methods. Data were compiled and are shown as mean $\pm$ standard errors of the mean. Data were evaluated using unpaired, two-tailed t tests (95% confidence interval) and GraphPad Prism 5 (GraphPad Inc, San Diego, CA). A P value of < 0.05 was considered significant.

8.3 Results

Cre adenovirus treated cardiac specific floxed vinculin neonatal murine ventricular myocytes have reduced vinculin levels

Cardiac specific floxed vinculin neonatal murine cardiac myocytes were isolated, plated, and treated with 5 MOI LacZ adenovirus (Ad-LacZ) or Cre adenovirus (Ad-Cre). Lysates collected from Ad-LacZ fl/fl Vcl (N = 3) and Ad-Cre fl/fl Vcl (N = 3) cells were used for western blotting with an anti-vinculin antibody and alpha-tubulin protein expression was used as an internal loading control. Densitometric analyses showed a 57% reduction of vinculin in the Ad-Cre fl/fl Vcl cells as compared to Ad-LacZ fl/fl Vcl cells. (Figure 1)

Focal adhesion kinase activity is altered in vinculin deficient neonatal murine cardiac ventricular myocytes in response to anisotropic stretch

Cardiac specific floxed vinculin neonatal murine cardiac myocytes were isolated, plated, and mounted onto an elliptical cell stretcher system (Camelliti et al., 2006). Cells were treated with 5 MOI LacZ adenovirus (Ad-LacZ) or Cre adenovirus (Ad-Cre). Lysates were collected from cells that were unstretched (Ad-LacZ fl/fl Vcl (N = 3); Ad-Cre fl/fl Vcl cells (N = 3)) and subjected to a 20 minute 10% transverse, 5% longitudinal stretch (Ad-LacZ fl/fl Vcl (N = 3); Ad-Cre fl/fl Vcl cells (N = 3)). Cells from each of the groups were use for western blotting with an anti-focal adhesion kinase tyrosine 397 phosphorylation, anti-focal adhesion kinase, and anti-vinculin antibodies. GAPDH protein expression was used as an internal loading control. Densitometric analyses showed

a 33% reduction of baseline FAK-P/FAK ratio in the Ad-Cre fl/fl Vcl cells as compared to Ad-LacZ fl/fl Vcl cells and that a decrease in vinculin resulted in an overall increase of focal adhesion kinase phosphorylation in response to stretch (Figure 2). Densitometric analyses also showed that in upon stretch, Ad-LacZ fl/fl Vcl cells showed FAK phosphorylation responses similar to those previously reported for neonatal rat cardiac ventricular myocytes (Senyo et al., 2007) (Figure 5).

Heterozygous vinculin knockouts show no differences in focal adhesion kinase activation as compared to controls

FAK phosphorylation activity in response to an anisotropic mechanical perturbation has shown differences in western blotting in the absence of vinculin in compared to wildtype cells, but localized responses to directional perturbation has not been elucidated. To further our understanding on how protein location may affect mechanotransduction responses, we incorporated a FAK FRET biosensor into heterozygous vinculin knockout neonatal murine cardiac ventricular myocytes. Heterozygous vinculin knockout mice have been previously reported to have a 58% reduction of vinculin (Zemljic-Harpf et al., 2004). Mating a heterozygous vinculin knockout (+/- Vcl KO) mouse with a wildtype mouse, neonatal pups were obtained, genotyped, and the hearts were isolated. Cells were lysed and used for western blotting with anti-vinculin and GAPDH antibodies. Densitometric analyses showed a 53% reduction of vinculin in +/- Vcl KO NMVMs (N = 5) as compared to controls (N = 5) (Figure 3).

NMVMs from both +/- Vcl KO and wildtype mice were transfected with a FAK FRET biosensor and their responses in FAK activation was compared using 100nM endothelin-1 stimulation. Results showed that both +/- Vcl KO and wildtype cells show increases in focal adhesion kinase phosphorylation activity in response to endothelin-1 (Figure 3b) and there was no statistical difference between the groups in how the FAK FRET biosensor reported the FAK activity (Figure 3c).

Anisotropic responses of focal adhesion kinase to force application are disrupted in

vinculin deficient neonatal murine cardiac ventricular myocytes

Neonatal murine cardiac ventricular myocytes which were wildtype or heterozygous vinculin knockouts were plated and probed for FAK FRET responses to mechanical forces applied by laser tweezers. Focal adhesion kinase phosphorylation as reported by the FAK FRET biosensor decreased in heterozygous vinculin knockouts as compared to controls when force was applied in the short axis of the cell in the transverse direction (Figure 4a). For forces applied in the longitudinal axis of the cell, focal adhesion kinase phosphorylation as reported by the FAK FRET biosensor increased as compared to wildtype controls (Figure 4b).

8.4 Discussion and Conclusions

The major finding of the present study is that vinculin is a novel mediator for FAK dependent anisotropic mechanotransduction in neonatal murine cardiac ventricular myocytes. Through the use of Cre adenovirus treatment of cardiac specific floxed vinculin neonatal murine ventricular myocytes, it was shown that vinculin can be reduced and this cell system allows further studies of vinculin's role in a cardiac myocyte through vinculin depletion studies.

Changes in focal adhesion kinase activity of cultured of neonatal murine cardiac ventricular myocytes in elastic membrane stretchers after stretch showed results similar to those previously reported in literature by Senyo et al., 2007. These results suggest that this culture and stretch system can be used to observe changes of genetically manipulated neonatal murine cardiac ventricular myocytes in response to anisotropic stretch. Using this system, our data suggest that focal adhesion kinase activity is altered in vinculin deficient neonatal murine cardiac ventricular myocytes in response to anisotropic stretch. This finding suggests that vinculin may play a role in mediating FAK dependent mechanotransduction responses.

A dramatic finding in the present study was that anisotropic responses of focal adhesion kinase to directional dependent force application are disrupted in vinculin defi-

cient neonatal murine cardiac ventricular myocytes. The differences observed in the vinculin deficient cells were attributed to the loss of vinculin and not due to the manner in which the cells handled the FAK FRET reporter as determined by the endothelin-1 studies. Our results suggest that vinculin's localization in the costamere complexes in well defined spacing along the longitudinal axis of the cell contribute to how FAK dependent mechanotransduction responses are altered in vinculin deficient cells. The precise role of how vinculin's localization to the costamere site contributes to alterations of FAK dependent mechanotransduction responses will require further study. Based on these findings, it is proposed that vinculin is a mediator for anisotropic responses of FAK-P in cardiac mechanotransduction. Possible explanations for the anisotropic mechanotransduction responses are that a decrease in vinculin may lead to a decrease in available protein involved in mechanotransduction, resulting in a decrease in FAK-P when forces are applied in the transverse axis of the cell (Fluck et al., 2002). Alternatively, a decrease in vinculin may lead to an increase in FAK-P when forces are applied along the longitudinal axis of the cell because an absence in vinculin can lead to an overall decrease in stiffness at the costamere site. With decreased stiffness caused by vinculin reduction, the cells will have altered force transmission, in which the pleating of the membranes and outward-directed festoons (Pardo et al., 1983; Block et al., 2003) will be altered and the cell will be subjected to more force and stretch than normal, which could contribute to an overall rise in FAK-P. Further study of changes in cardiac myocyte ultrastructure in vinculin depleted cells as compared to wildtype controls in response to directionally applied forces is required.

8.5 Acknowledgements

We would like to thank the members of the Cellular Biophotonics Lab, Cardiac Mechanics Research Group, and the Ross Lab for their assistance. We would like to acknowledge Yingxiao Wang for providing the original FAK FRET reporter. This study has been supported by an American Heart Association Pre-doctoral Fellowship

(to A.L.H.), the University of California, San Diego, Cardiovascular Science Scholarship (to A.L.H.), National Institutes of Health, National Heart Lung and Blood Institute 5P01HL46345 (K.U.K., to A.D.M. and R.S.R. (Project 3)), the National Science Foundation (BES-0506252; to A.D.M), and a grant from the Air Force Office of Scientific Research (F9620-00-1-0371; to M.W.B).

Chapter 8 is being prepared for publication titled ”Vinculin mediates anisotropic mechanotransduction response of focal adhesion kinase in neonatal murine cardiac ventricular myocytes” by Amy L. Hsieh, Tiffany W. Hsu, Alice Zemljic-Harpf, Robert S. Ross, Michael W. Berns, Andrew D. McCulloch for submission. The dissertation author is the primary investigator of this paper.

8.6 Figures

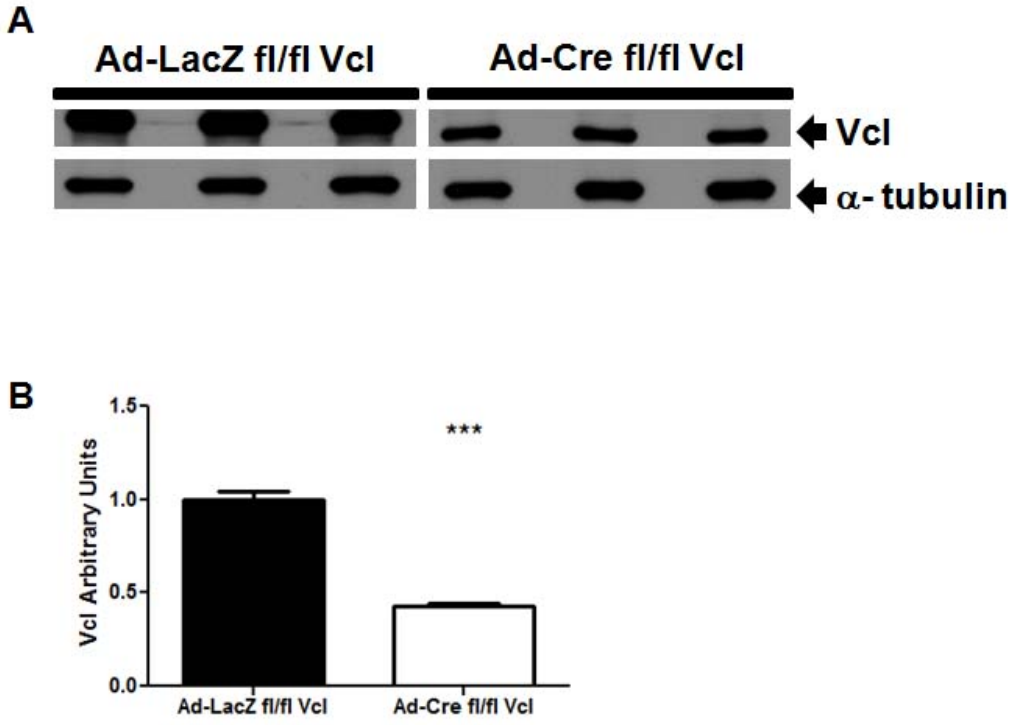

Figure 8.1: Western blot for adenoviral treated floxed vinculin neonatal murine cardiac ventricular myocytes. A) Floxed cells were treated with 5 MOI adenoviral LacZ (Ad-LacZ) or 5 MOI adenoviral Cre (Ad-Cre). Vinculin expression was normalized to α-tubulin expression. B) Densitometric analyses showed a 57% reduction of vinculin in the Ad-Cre fl/fl Vcl cells as compared to Ad-LacZ fl/fl Vcl cells 72 hours after treatment with adenovirus. *** $P < 0.005$

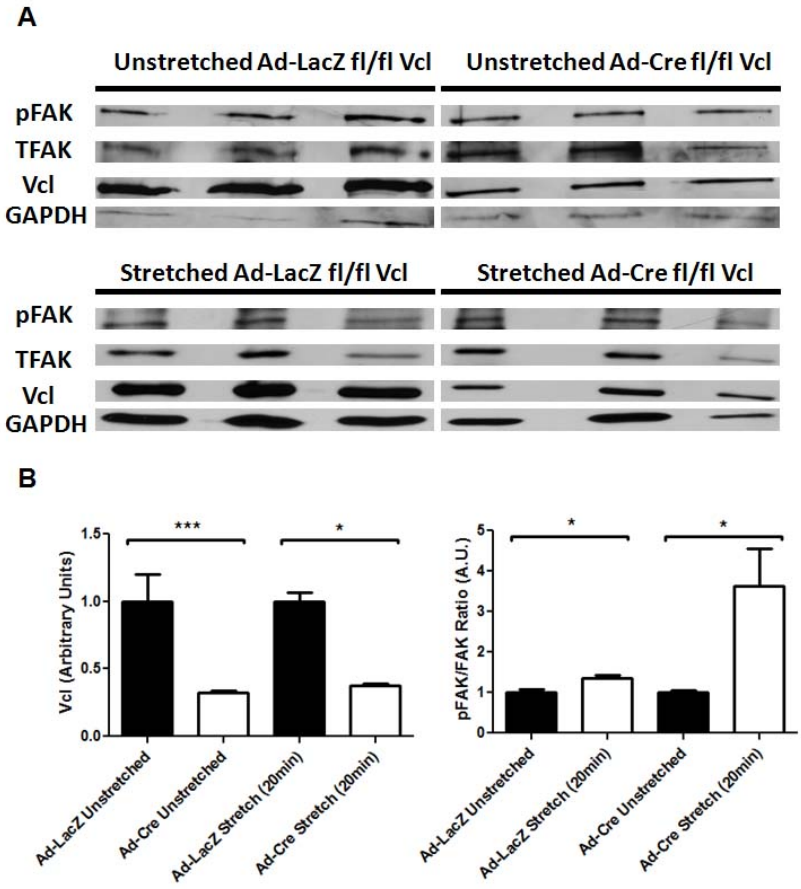

Figure 8.2: A) Western blot for adenoviral treated floxed vinculin neonatal murine cardiac ventricular myocytes under unstretched and 20 minutes stretched conditions. Floxed cells were treated with 5 MOI adenoviral LacZ (Ad-LacZ) or 5 MOI adenoviral Cre (Ad-Cre). Focal adhesion kinase phosphorylation at the tyrosine 397 site (pFAK), total focal adhesion kinase (TFAK), and vinculin (Vcl) expression were normalized to glyceraldehyde 3-phosphate dehydrogenase (GAPDH) expression. B) Densitometric analyses showed a 68% reduction of vinculin in the Ad-Cre fl/fl Vcl cells as compared to Ad-LacZ fl/fl Vcl cells 72 hours after treatment with adenovirus in unstretched conditions and reduced 63% in stretched conditions (*** $P < 0.005$, * $P < 0.05$, N = 3 in all groups). pFAK/FAK ratio of unstretched and stretched conditions for both Ad-LacZ fl/fl Vcl cells and Ad-Cre fl/fl Vcl cells showed that pFAK/FAK ratio increased after 20 minutes of stretch (* $P < 0.05$, N = 3 in all groups). In Ad-LacZ fl/fl Vcl cells, pFAK/FAK ratio increased 35% and in Ad-Cre fl/fl Vcl cells, pFAK/FAK ratio increased 263% with stretch.

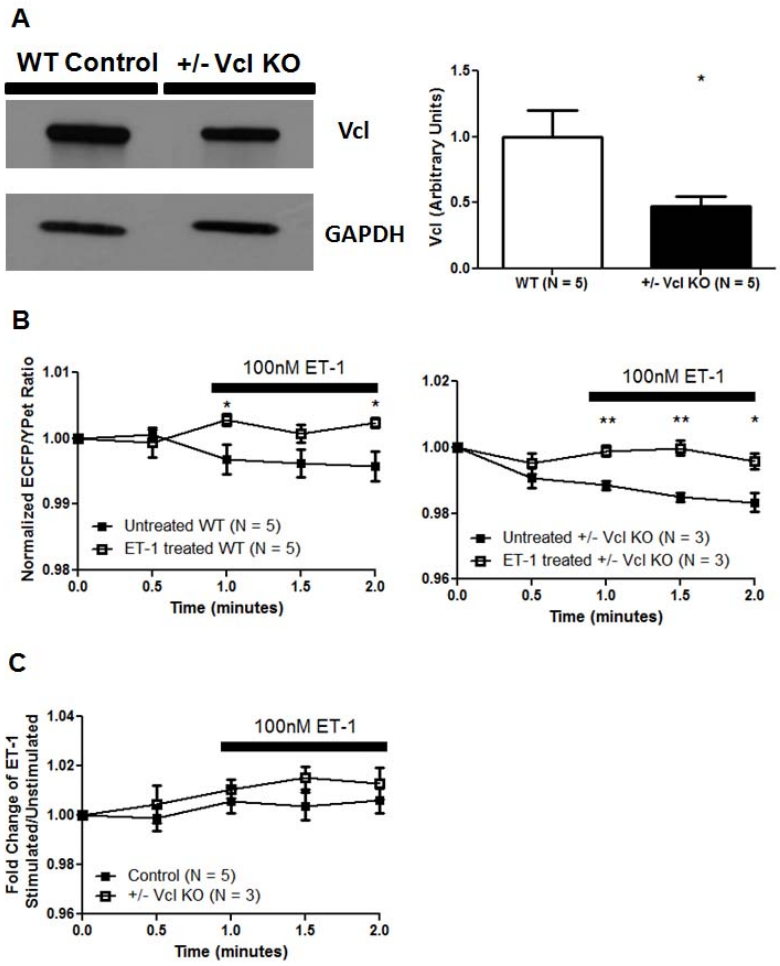

Figure 8.3: A) Western blot for isolated neonatal murine cardiac ventricular myocytes from wildtype (WT) and heterozygous vinculin knockout mice (+/- Vcl KO) (left). Vinculin expression was normalized to GAPDH expression. (right) Densitometric analyses showed a 53% reduction in vinculin between the heterozygous vinculin knockout mice and their wildtype littermates (* $P < 0.05$). B) Normalized ECFP/YPet Ratio time course for wildtype cells (left) and heterozygous vinculin knockout (+/- Vcl KO) (right) untreated and treated with 100nM endothelin-1. Results show that both the wildtype and heterozygous vinculin knockouts report FAK-P via the FAK FRET reporter upon stimulation with endothelin-1 (* $P < 0.05$, ** $P < 0.01$). C) Fold change of endothelin-1 stimulation in comparison to unstimulated cells of the normalized ECFP/YPet ratio in wildtype control (N = 5) and heterozygous vinculin knockout cells (N = 3). Results show no differences in the differing cell types' ability to report changes in FAK phosphorylation.

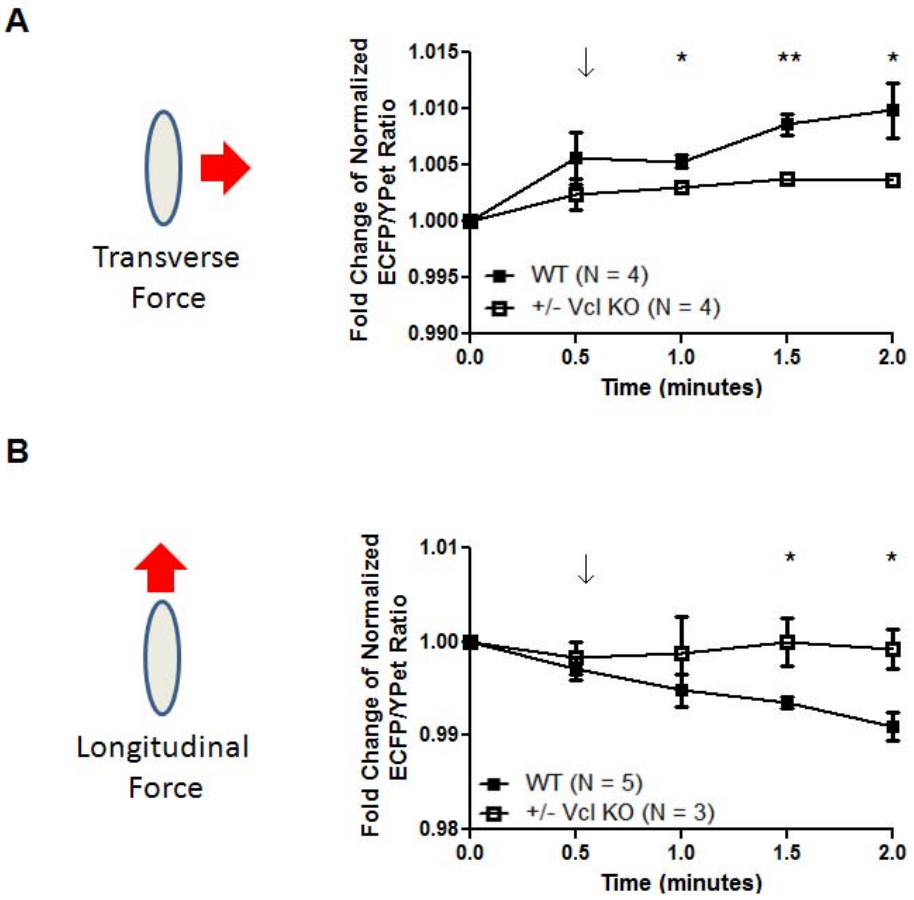

Figure 8.4: Anisotropic responses of FAK-P in response to directionalized force application. A) Normalized ECFP/YPet ratio of force applied area on a cell and unstimulated site of a cell during transverse force, short axis force stimulation using laser tweezers in both wildtype and heterozygous vinculin knockout cells. Arrow (↓) indicates the beginning of static force application. Results show a decrease in FAK-P in knockout cells as compared to wildtype controls (* $P < 0.05$, ** $P < 0.01$). B) Normalized ECFP/YPet ratio of force applied area on a cell and unstimulated site of a cell during longitudinal force stimulation using laser tweezers in both wildtype and heterozygous vinculin knockout cells. Arrow (↓) indicates the beginning of static force application. Results show an increase in FAK-P in knockout cells as compared to wildtype controls (* $P < 0.05$).

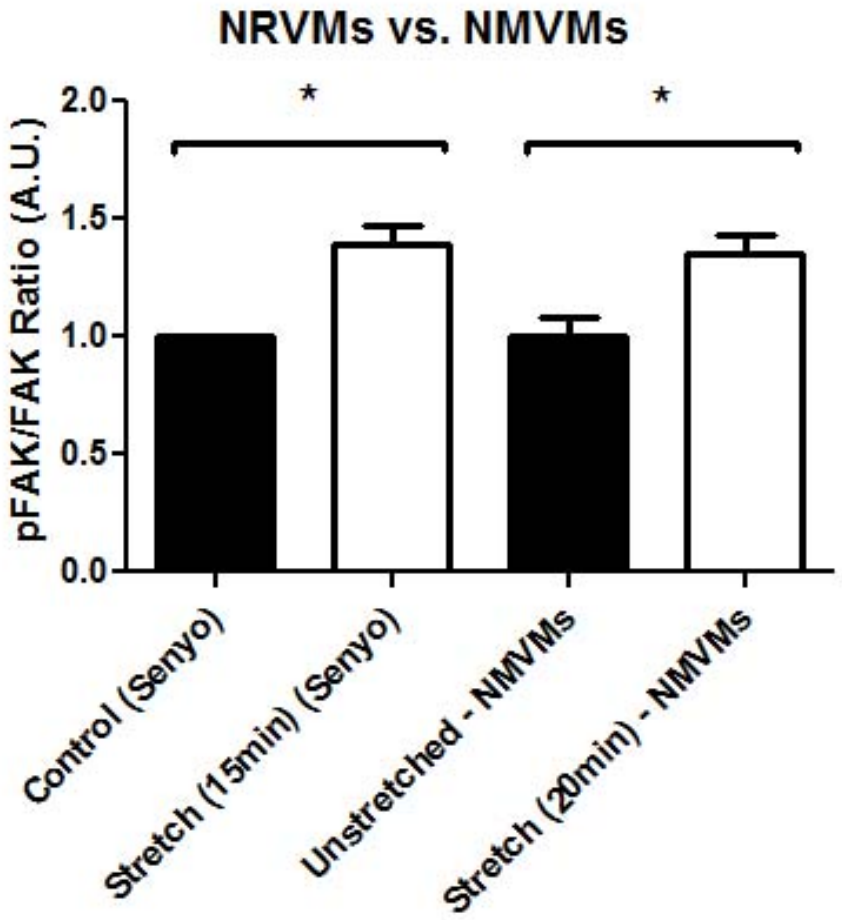

Figure 8.5: Focal adhesion kinase phosphorylation (pFAK) and total focal adhesion kinase (FAK) ratio comparison for unstretched and stretched neonatal rat ventricular cardiac myocytes (NRVMs) and neonatal murine ventricular cardiac myocytes (NMVMs). Results show densitometric analyses of western blots of pFAK/FAK ratio. From left to right: unstretched control previously reported in Senyo et al., 2007, 15 minute uniaxial 10% stretch of NRVMs previously reported in Senyo et al., 2007, unstretched NMVMs, 10% transverse, 5% longitudinal 20 minute stretch of NMVMs. Results presented show stretch results normalized to their unstretched controls. Results show that NMVMs can be stimulated by stretch using the 10% transverse, 5% longitudinal elastic membrane stretchers and reflect pFAK/FAK ratio changes as previously reported in NRVMs (Senyo et al., 2007).

8.7 References

[1] Botvinick, E.L., Berns, M.W. (2005). Internet-based robotic laser scissors and tweezers microscopy. Microsc Res Tech. 68(2):65-74.

[2] Botvinick, E. L., & Wang, Y. (2007). Laser tweezers in the study of mechanobiology in live cells. Methods Cell Biol., 82, 497-523.

[3] Brancaccio, M., Hirsch, E., Notte, A., Selvetella, G., Lembo, G., & Tarone, G. (2006). Integrin signalling: The tug-of-war in heart hypertrophy. Cardiovasc Res, 70(3), 422-433.

[4] Bloch, R. J., & Gonzalez-Serratos, H. (2003). Lateral force transmission across costameres in skeletal muscle. Exerc. Sport Sci Rev., 31(2), 73-78.

[5] Camelliti, P., Gallagher, J. O., Kohl, P., & McCulloch, A. D. (2006). Micropatterned cell cultures on elastic membranes as an in vitro model of myocardium. Nat Protoc., 1(3), 1379-1391.

[6] Danowski, B.A., Imanaka-Yoshida, K., Sanger, J.M., and Sanger, J.W. (1992). Costameres are sites of force transmission to the substratum in adult rat cardiomyocytes. J Cell Biol. 118, 1411-1420.

[7] Flck, M., Ziemiecki, A., Billeter, R., & Mntener, M. (2002). Fibre-type specific concentration of focal adhesion kinase at the sarcolemma: Influence of fibre innervation and regeneration. The Journal of Experimental Biology, 205, 2337-2348.

[8] Humphries, J., Wang, P., Streuli, C., Geiger, B., Humphries, M., & Ballestrem, C. (2007). Vinculin controls focal adhesion formation by direct interactions with talin and actin. J Cell Biol, 179, 1043-1057.

[9] Ingber, D.E. (2006). Cellular mechanotransduction: putting all the pieces together again. FASEB J. 20, 811-827.

[10] Keller, R.S., Shai, S.Y., Babbitt, C.J., et al. (2001). Disruption of Integrin Function in the Murine Myocardium Leads to Perinatal Lethality, Fibrosis, and Abnormal Cardiac Performance. Am J Pathol., 158:1079-1090.

[11] Lapidos, K.A., Kakkar, R., McNally, E.M. (2004). The dystrophin glycoprotein complex: signaling strength and integrity for the sarcolemma. Circ Res. 94,1023-1031.

[12] Legate, K. R., M., E., Kudlacek, O., & Fssler, R. (2006). ILK, PINCH and parvin: The tIPP of integrin signalling. Nat Rev Mol Cell Biol., 7, 20-31.

[13] Mansour, H., de Tombe, P.P., Samarel, A.M., et al. (2004) Restoration of resting sarcomere length after uniaxial static strain is regulated by protein kinase Cepsilon and focal adhesion kinase. Circ Res. 94, 642-649.

[14] Pardo, J. V., Siliciano, J. D., & Craig, S. W. (1983). A vinculin-containing cortical lattice in skeletal muscle: Transverse lattice elements ("costameres") mark sites of attachment between myofibrils and sarcolemma. Proc. Natl. Acad. Sci., 80, 1008-1012.

[15] Ross, R.S., Pham, C., Shai, S.Y., et al. (1998). Beta1 integrins participate in the hypertrophic response of rat ventricular myocytes. Circ Res., 82, 1160-1172.

[16] Samarel, A.M. (2005). Costameres, focal adhesions, and cardiomyocyte mechanotransduction. Am. J. Physiol Heart Circ. Physiol., 289, H2291-H2301.

[17] Senyo, S., Koshman, Y., & Russell, B. (2007). Stimulus interval, rate and direction differentially regulate phosphorylation for mechanotransduction in neonatal cardiac myocytes. FEBS Lett., 581, 4241-4247.

[18] Shai, S.Y., Harpf, A.E., Babbitt, C.J., et al. (2002). Cardiac myocyte-specific excision of the beta1 integrin gene results in myocardial fibrosis and cardiac failure. Circ Res., 90, 458-464.

[19] Sieg, D.J., Hauck, C.R., Ilic, D., Klingbeil, C.K., Schaefer, E., Damsky, C.H., Schlaepfer, D.D. (2000). FAK integrates growth-factor and integrin signals to promote cell migration. Nat Cell Biol., 2, 249-256.

[20] Valencik, M.L., Keller, R.S., Loftus, J.C., et al. (2002). A lethal perinatal cardiac phenotype resulting from altered integrin function in cardiomyocytes. J Card Fail., 8, 262-272.

[21] Valencik, M.L., Zhang, D., Punske, B., et al. (2006). Integrin activation in the heart: a link between electrical and contractile dysfunction? Circ Res., 99, 1403-1410.

[22] Wang, Y., Botvinick, E., Zhao, Y., Berns, M., Usami, S., Tsien, R., et al. (2005). Visualizing the mechanical activation of src. Nature, 434, 1040-1045.

[23] Wiesner, S., Legate, K.R., Fassler, R. (2005). Integrin-actin interactions. Cell Mol Life Sci., 62, 1081-1099.

[24] Zemljic-Harpf, A., Miller, J., Henderson, S., Wright, A., Manso, A., Elsherif, L., et al. (2007). Cardiac-myocyte-specific excision of the vinculin gene disrupts cellular junctions, causing sudden death or dilated cardiomyopathy. Mol Cell Biol, 27, 7522-7537.

[25] Zemljic-Harpf, A., Ponrartana, S., Avalos, R., Jordan, M., Roos, K., Dalton, N., et al. (2004). Heterozygous inactivation of the vinculin gene predisposes to stress-induced cardiomyopathy. Am J Pathol, 165, 1033-1044.

Chapter 9

Summary and conclusions

9.1 Summary

The purpose of this dissertation was to (1) develop a method to study cardiac mechanotransduction and (2) to use this method to investigate the role of vinculin in cardiac mechanotransduction. Chapter 2 discusses the theory of optical trapping and multiphoton fluorescence microscopy and discussion of its application to study cardiac mechanotransduction. Chapter 3 discusses the hardware, software, and optical design used for studying cardiac mechanotransduction.

Chapter 4 discusses the effects of optical trapping and multiphoton fluorescence microscopy on cardiac mechanotransduction. Neonatal rat ventricular cardiac myocytes (NRVMs) were the first cell type used due to its availability in the lab. Studies with NRVMs show that the FAK FRET biosensor can be activated when forces are applied to a ligand coated bead adhered to the cell. Studies also revealed that the inherent beating of the cells would interfere with a static force application. As such two classes of inhibitors were used, 2, 3-butanedione monoxime (BDM) and blebbistatin. With the availability of genetically manipulated murine models, studies were switched to use neonatal mouse ventricular cardiac myocytes (NMVMs). Studies showed that BDM could not be used to study cardiac mechanotransduction in NMVMs because it caused detachment of cells

from their substrate, and that the application of blebbistatin did not alter the dynamics of the FAK FRET reporter over a short time period. Tuning of wavelengths to achieve two photon excitation revealed that 780nm was a compatible wavelength for activation of the ECFP in our FAK FRET reporter. Additionally, it was shown that the thermal heating effects of the laser tweezers limited the power of the laser beam to 300mW and an application period less than 5 minutes. These parameters were used in subsequent laser tweezers experiments to study cardiac mechanotransduction.

Chapter 5 discusses the development of an adenovirus containing a FAK FRET reporter. This virus was used in neonatal murine cardiac ventricular myocyte and in adult cardiac ventricular myocyte and provides a means to study cardiac mechanotransduction in a variety of cell types. Chapter 6 discusses the combination of laser tweezers and multifocal multiphoton fluorescence resonance energy transfer microscopy system to study cardiac mechanotransduction. The effects of force application on a ligand-coated bead on wildtype neonatal murine cardiac ventricular myocytes are measured. Results indicate that FAK FRET responses are localized to the site of force application and not distally. Results also show that forces applied in the transverse direction, perpendicular to the longitudinal axis lead to increases in FAK phosphorylation as reported by FAK FRET whereas forces applied to the longitudinal axis of the cell lead to decreases in FAK phosphorylation. These results reveal that types of load on a single cell, may trigger upregulation or downregulation of hypertrophy.

Chapter 7 discusses the development and characterization of a tamoxifen inducible cardiac specific vinculin knockout mouse. This model is a temporally controlled cardiac specific vinculin knockout model activated by the administration of tamoxifen. The dosage for tamoxifen administration was determined to be 40 micrograms of tamoxifen/gram of body weight. Vinculin knockdown in cardiac myocytes was noted two weeks after injection. Echocardiograms indicate decrease in cardiac function 12 weeks after injection as reported by percent fractional shortening. Additionally, vinculin deletion led to decrease in stiffness in the fiber direction as determined by papillary muscle testing. Upon tamoxifen administration, vinculin deletion in the tamoxifen

inducible cardiac myocyte specific vinculin knockout mouse led to dilated cardiomyopathy. Lastly, the development of the double reporter tamoxifen inducible cardiac myocyte specific vinculin knockout mouse provides a means to study the effects of vinculin in intact isolated adult murine cardiac myocyte.

Chapter 8 discusses the role of vinculin in isolated neonatal murine cardiac ventricular myocytes. Cardiac specific floxed vinculin neonatal murine ventricular myocytes were used and upon addition of an adenoviral Cre, results showed a reduction of vinculin. In culturing these cells in elastic membrane stretchers, a 20 minute stretch was imposed on the cells, resulting in changes in focal adhesion kinase activity as compared to the unstretched state of the vinculin reduced cells. Lastly, anisotropic responses of focal adhesion kinase to directional dependent force application using laser tweezers are disrupted in isolated vinculin deficient neonatal murine cardiac ventricular myocytes. These results reveal the role of the microanatomy of the costamere in determining mechanotransduction events and alterations in hypertrophic signaling.

In this dissertation, I discussed a novel method for studying cardiac mechanotransduction using laser tweezers and multiphoton fluorescence microscopy to study the role of vinculin in mechanotransduction. Using this system, it was revealed that in wildtype cells, FAK-P responses were dependent on the orientation of the local force with respect to the cell geometry. This suggests that hypertrophic responses are modulated by the type of load applied as well as the orientation in which the load is applied. Additionally, through the use of vinculin knockdown neonatal murine cardiac ventricular myocytes, it was shown that directionally applied localized forces caused varying responses in hypertrophic signalling as compared to controls. These results suggest that the microanatomy of the costamere plays a role in altering mechanotransduction responses and alterations in hypertrophic signalling.

9.2 Model of vinculin's contribution to cardiomyopathy

Based on results obtained from wildtype cardiac mechanotransduction studies (Chapter 6), heterozygous vinculin knockout cardiac mechanotransduction studies (Chapter 8), papillary muscle stretching studies (Chuang et al., 2010), and current results from literature, a simple model describing how vinculin plays a role in the development of cardiomyopathy can be proposed.

Hypothesis for hypertrophy in normal cardiac myocytes

Results from wildtype cardiac mechanotransduction studies demonstrated that types of load on a single cell may trigger upregulation or downregulation of hypertrophy. When forces were applied along the short axis of the cell, FAK phosphorylation was increased at the site of force application, whereas, when forces were applied along the longitudinal axis of the cell, FAK phosphorylation decreased. Due to the cytoskeletal architecture of the cell, the costamere ultrastructure may provide a possible explanation for the anisotropic FAK responses observed.

Costameres are the site where mechanical information are transduced across the cell membrane and in our experiments, we probed the integrin complex located in the costamere. In a simplistic representation of the costamere, the integrin heterodimer spans the cell membrane. The talin head binds to the cytoplasmic domain of an integrin receptor, and the tail domain binds F-actin. Vinculin, also binds to a helix located in talin and in the tail region of vinculin, there exists a focal adhesion kinase binding domain.

In a previous study performed by del Rio et al., 2010, magnetic tweezers experiments and molecular steered dynamic simulations showed that when forces were applied to the head region and tail region of talin, it resulted in protein unfolding and opening up of vinculin binding sites in talin. These experiments and simulations are similar to those found in the short axis force application experiments of wildtype cells in my study (Figure 1).

A possible explanation for the increase in FAK phosphorylation is that when

forces are applied at the integrin by a fibronectin coated bead, forces transduced into the cell cause a force to pull at the head domain of talin. Additionally, due to the binding of the tail domain of talin to the F-actin network, a force in the opposite direction causes talin to unravel, revealing vinculin binding sites within talin. With the recruitment of vinculin, focal adhesion kinase binding sites become available and activation of FAK phosphorylation may occur.

In comparison, when forces applied along the longitudinal axis of the cell (Figure 2), the talin head and talin tail are sheared such that the helix in which the original vinculin binding site is found at rest becomes masked, vinculin no longer can bind, and the focal adhesion kinase binding site disappears. This provides a possible explanation as to why FAK phosphorylation decreases in response to longitudinal force application.

To understand how anisotropic responses of FAK phosphorylation may alter hypertrophy in normal and diseased cardiac myocytes, results obtained from current literature lend insight as to the regulation of hypertrophy in normal cardiac myocytes (Figure 3). In a study by DiMichele et al., 2006, deletion of focal adhesion kinase (FAK) decreased concentric hypertrophy. If downregulation of focal adhesion kinase phosphorylation led to a decrease in concentric hypertrophy, in turn, it is possible that focal adhesion kinase phosphorylation activation is necessary to initiate concentric hypertrophy. In comparison, in a study done by Peng et al., 2006, FAK was inactivated in cardiomyocytes and led to the development of eccentric hypertrophy.

In the optical trapping experiments of wildtype cells, when forces were applied to the transverse short axis direction, increase of FAK phosphorylation was noted. From results obtained from DiMichele et al., 2006, it is hypothesized that forces applied along the short axis of the cell mediates concentric hypertrophy through the activation FAK phosphorylation. Conversely, from results obtained from Peng et al., 2006, it is hypothesized that forces applied along the longitudinal axis of the cell mediates eccentric hypertrophy through the inactivation of FAK phosphorylation. Through the delicate balance of transverse and longitudinal directed forces, the cardiac myocyte is able to regulate its overall physiologic hypertrophy.

Hypothesis for hypertrophy in vinculin reduced cardiac myocytes

Results in optical trapping studies of heterozygous vinculin knockout described a possible role of the microanatomy of the costamere in determining mechanotransduction events and alterations in hypertrophic signaling. My studies revealed that anisotropic responses to mechanotransduction as reported by our FAK FRET biosensor are mediated by vinculin.

In extending the hypothesis for hypertrophy in normal cardiac myocytes to take into account changes that occur in vinculin reduced cardiac myocytes (Figure 4), experiments showed that vinculin reduction caused a decrease in FAK phosphorylation in response to forces applied in the short axis of the cell. This decrease in FAK phosphorylation may alter hypertrophic signaling to change the cardiac myocyte's predisposition from concentric hypertrophy to eccentric hypertrophy. Additionally, in vinculin reduced cardiac myocytes, FAK phosphorylation levels off in response to forces applied along the longitudinal axis of the cell. This equilibrium of FAK in the phosphorylated and dephosphorylated state may result in overall signaling being governed by forces applied in the short axis of the cell, resulting in eccentric hypertrophy of vinculin reduced cardiac myocytes.

Possible model for the role of vinculin in the development of dilated cardiomyopathy

In the conclusions mentioned in this thesis, the possible connection between vinculin's role in mechanotransduction and the development of dilated cardiomyopathy has begun to be formed.

Optical trapping experiments performed in this thesis involved quiescent cardiac myocytes, thus force application experiments are more correlated to a diastolic, passive filling state of the heart versus a contracting systolic state. The forces applied to the short axis of the cell are similar to stresses and strains involved in the cross-fiber axis of a heart, whereas forces applied to the longitudinal axis of the cells are similar to stresses and strains involved in the fiber direction of the heart. In a previous study by Omens et

al., 1991 of the passive inflation of a canine heart, passive deformation of the wall was noted to maximize the epicardial fiber strain and minimize endocardial fiber extension, and more cross-fiber strain was observed in the endocardium and the midwall than in the epicardial layer.

Although the optical trapping experiments were not performed using cells from the endocardial, midwall, and epicardial layers of the heart, based on results from Omens et al., 1991, it is hypothesized that epicardial cardiac myocytes are predisposed to eccentric hypertrophy because fiber strain is maximized during passive filling, whereas it is hypothesized that the endocardial and midwall cardiac myocytes are predisposed to concentric hypertrophy due to the observation of more cross-fiber strain than in the epicardial layer. By balancing concentric and eccentric hypertrophy, cardiac myocytes help to maintain a normal functioning heart.

When vinculin is reduced in cardiac myocytes, results from papillary muscle studies of cardiac specific vinculin knockout tissue was shown to be more compliant in the fiber direction than in wildtype tissue (Chuang et al., 2010). A more compliant tissue would result in increased fiber strains in vinculin knockout tissue as compared to wildtype tissue when the same amount of force is applied. These results may cause all cardiac myocytes to be predisposed to eccentric hypertrophy. Additionally, results from heterozygous vinculin knockout cardiac myocytes indicate that cardiac myocytes would be predisposed to eccentric hypertrophy due short axis force application. The predisposition of eccentric hypertrophy caused by softer cardiomyocytes and decreased FAK phosphorylation signaling could result in the absence of concentric hypertrophy normally found in the endocardial and midwall layer of the heart and resulting in eccentric hypertrophy throughout the heart. In literature, Carabello, 2002 noted that the failure of concentric hypertrophy to normalize the increase in systolic stress caused by eccentric hypertrophy could contribute to supernormal wall stress and afterload excess, thereby reducing ejection fraction. A reduction of ejection fraction in addition to the elongated cardiac myocytes caused by eccentric hypertrophy could contribute to the development of dilated cardiomyopathy and ultimately in heart failure.

9.3 Future directions

For this dissertation, studies were focused on neonatal murine cardiac ventricular myocytes, but in the future, studies can be extended to study embryonic and adult cells as well. Additionally, this system can be used to study how mutations in proteins can affect mechanotransduction.

Experiments also were limited to using fibronectin coated beads and a FAK FRET biosensor, but future directions include using other extracellular matrix protein coated beads and compatible biosensors including Src (Wang et al., 2005) and RhoA (Yoshizaki et al., 2003). Alternatively, bead coating concentrations can be varied to gain an understanding of the dynamic relationship between integrin engagement and changes in a FRET reporter. Additionally, experiments in this dissertation were focused on looking at vinculin's role in mechanotransduction and genetically manipulated vinculin knockout mice were used, but currently, there exist a variety of other genetically manipulated mouse models for cytoskeletal proteins that have been implicated in having a role in cardiomyopathies (Cox et al., 2008). By combining the information gained from the various genetically manipulated mouse models and different FRET reporters available, in the future, one may combine these experimental results to construct a computational modeling of cell signaling. Using computational models will provide another means to understand cardiac mechanotransduction, assess pharmacological interventions, and provide insight into the development of future therapeutics for treating cardiomyopathies.

Other future studies including engaging multiple beads and forces to a single cell using two laser tweezers, applying forces along the z-axis of the cell, altering force application from a static process to a dynamic process, altering the substrate stiffness such that it mimics different states such as basal stiffness of the myocardium or the stiffness found in an infracted heart. Additionally, this system can be combined with pacing, to understand how mechanotransduction pathways may be altered by factors such as calcium handling.

Currently this system is limited because of the introduction of blebbistatin to allow a constant static force to be applied, but by using electrodes to control the beat rate of the cell, constant force can be applied dynamically and the need for blebbistatin will be eliminated. Another limitation of this system is that the throughput of the system is limited by the ability to have a bead adhered to a single cell. One possible solution is to include in our current software the ability to trap a bead with a click of a button as described in Shi et al., 2008. This implementation will greatly increase the likelihood of bead being adhered to a cell as the user can trap a ligand coated bead and adhere it to a cell of choice. These types of implementations can help to optimize experiments and increase the throughput of these types of cardiac mechanotransduction studies.

9.4 Conclusions

In summary, the system described here provides an optically-based platform to study cardiac mechanotransduction. This platform has been used to demonstrate (1) that mechanotransduction responses of neonatal murine cardiac ventricular myocytes are directional dependent and (2) that vinculin is a mediator of the anisotropic responses of FAK-P in response to localized force application. In conclusion, this system is a powerful tool for furthering our understanding of cardiac mechanotransduction and in the future possibly a tool for screening pharmacological or biotherapeutic approaches for treating heart failure. In addition, our results reveal that directional dependent loads may alter hypertrophic signaling and that the microanatomy of the costamere plays a role in altering mechanotransduction responses which may contribute to the development of cardiomyopathy and ultimately, in heart failure.

9.5 Figures

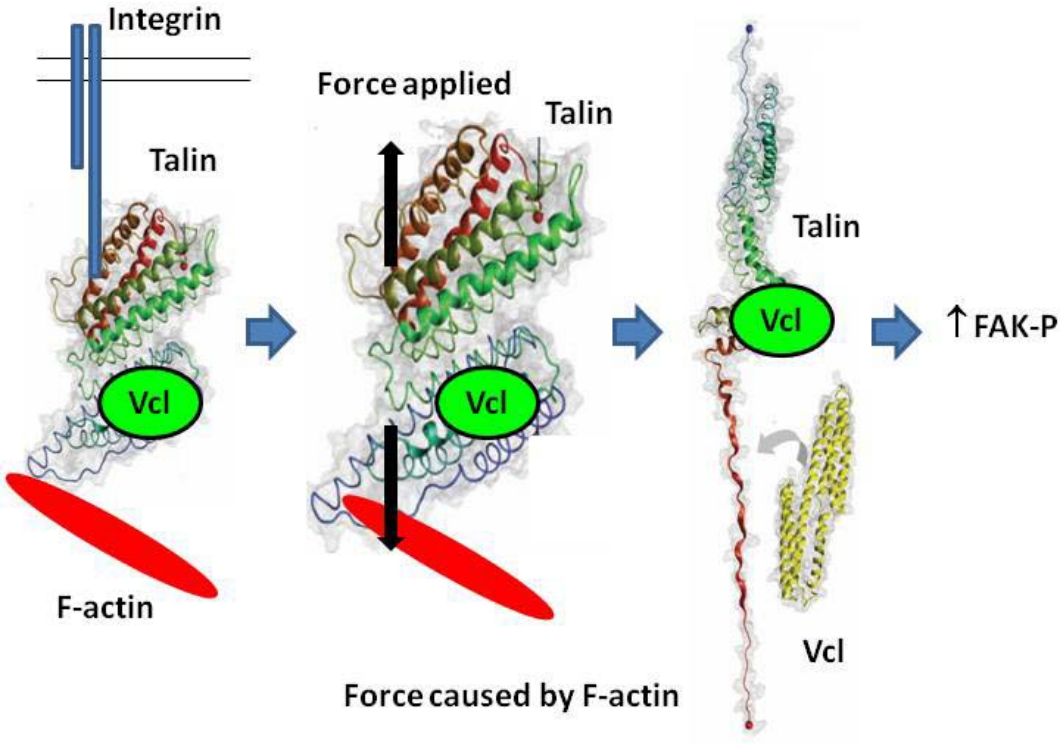

Figure 9.1: A simple representation of transverse force application at the integrin complex using laser tweezers. The integrin heterodimer spans the cellular membrane and the talin head binds the cytoplasmic portion of integrin, whereas the talin tail binds the F-actin network. Within talin, a vinculin binding site exists and vinculin binds. Using laser tweezers, forces applied at the integrin complex are transduced into the cell and a force is applied at the talin head. Due to the binding of the tail portion of talin to the F-actin network, a force in the opposite direction enables the unfolding of talin. This unfolding results in the opening of additional vinculin binding sites. Within vinculin, a focal adhesion kinase binding domain exists and as more vinculin binding sites are available, FAK activation may occur.

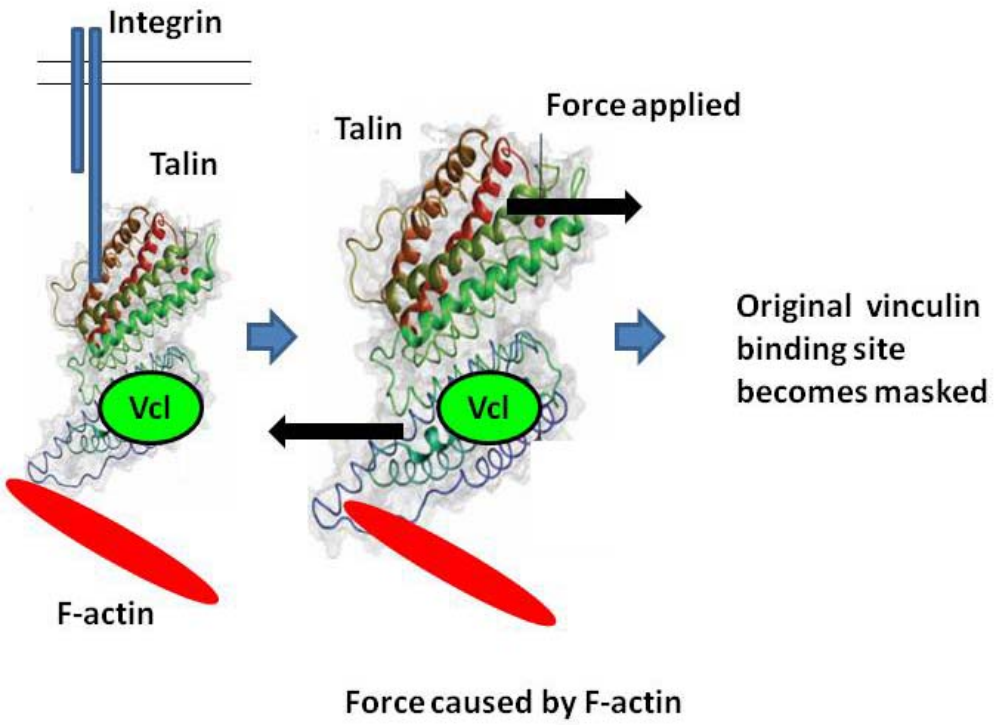

Figure 9.2: A simple representation of longitudinal force application at the integrin complex using laser tweezers.When longitudinal forces are applied at the integrin complex, the force is transduced into the cell causing the talin head and talin tail to shear against one another such that the original vinculin binding site in talin becomes masked. This may cause focal adhesion kinase binding site within vinculin to vanish such that FAK phosphorylation decreases.

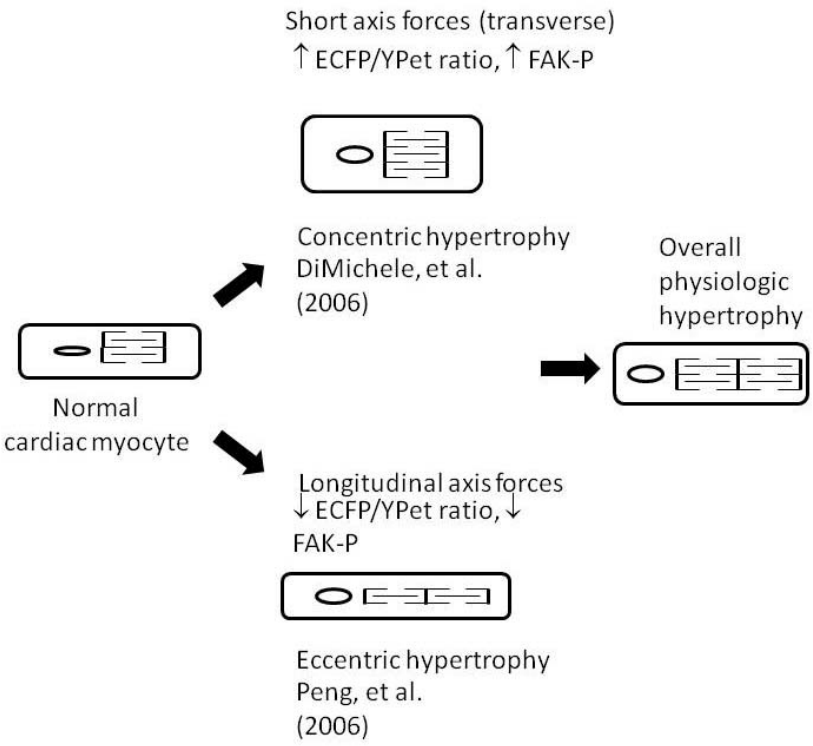

Figure 9.3: Hypothesis for hypertrophy in normal cardiac myocytes. It is hypothesized that when a normal cardiac myocyte sees forces applied in the short axis of the cell, it leads to the activation of FAK, which has been noted in literature by DiMichele et al., 2006 to play a role in concentric hypertrophy. In comparison, when a normal cardiac myocyte is challenged with forces applied in the longitudinal axis of the cell, FAK phosphorylation decreases, and inactivation of FAK has been previously noted by Peng et al., 2006 to predispose the heart to eccentric hypertrophy. Overall, the delicate balance of concentric and eccentric hypertrophy allows the cardiac myocyte to maintain physiologic hypertrophy necessary to maintain cardiac function.

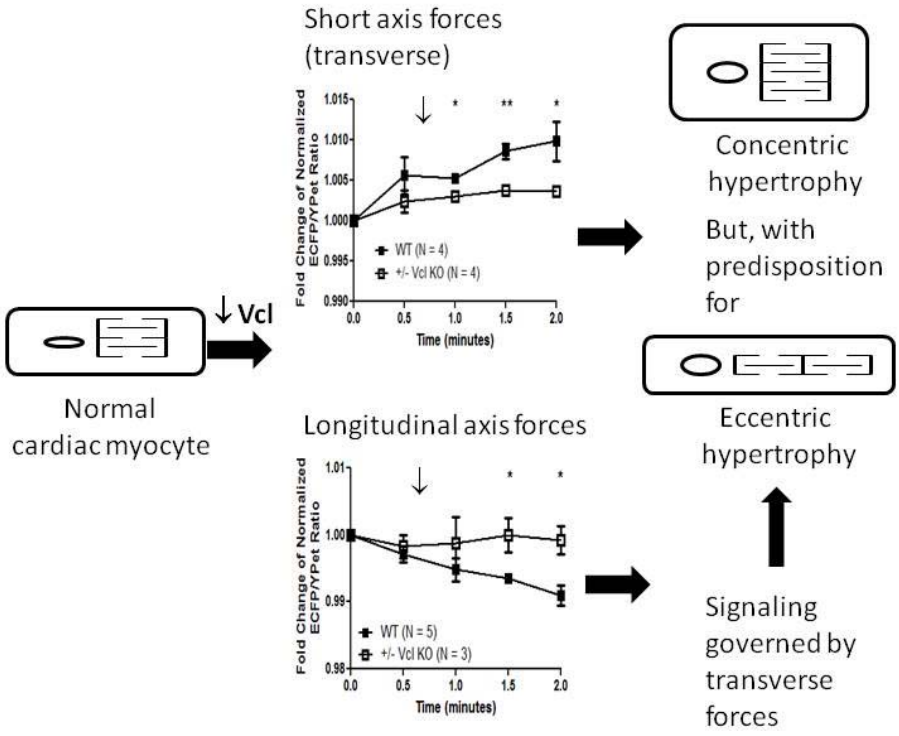

Figure 9.4: Hypothesis for hypertrophy in vinculin reduced cardiac myocytes. Vinculin reduction causes a decrease in FAK phosphorylation in response to forces applied in the short axis of the cell. This decrease in FAK phosphorylation alters the cardiac myocyte hypertrophic signaling from concentric hypertrophy to eccentric hypertrophy. Vinculin reduction also causes a leveling off of FAK activity in which the phosphorylated and dephosphorylated states reach equilibrium. This in turn may cause mechanotransduction responses in the cardiac myocyte to be governed by the transverse short axis forces, resulting in an overall predisposition of cardiac myocytes for eccentric hypertrophy.

9.6 References

[1] Carabello, B. A. (2002). Concentric versus eccentric remodeling. Journal of Cardiac Failure, 8(6, Part 2), S258-S263.

[2] Chuang, J. S. (2010). The role of costameric proteins in cardiac force transmission and signaling. (Doctoral dissertation). Retrieved from ProQuest Dissertations and Theses Database. (AAT 3390089)

[3] Cox, L., Umans, L., Cornelis, F., et al. (2008). A broken heart: a stretch too far: an overview of mouse models with mutations in stretch-sensor components. Int J Cardiol., 131, 33-44.

[4] del Rio, A., Perez-Jimenez, R., Liu, R., Roca-Cusachs, P., Fernandez, J. M., & Sheetz, M. P. (2009). Stretching single talin rod molecules activates vinculin binding. Science, 323(5914), 638-641.

[5] DiMichele, L. A., Doherty, J. T., Rojas, M., Beggs, H. E., Reichardt, L. F., Mack, C. P., et al. (2006). Myocyte-restricted focal adhesion kinase deletion attenuates pressure overload-induced hypertrophy. Circulation Research, 99(6), 636-645.

[6] Omens, J. H., May, K. D., & McCulloch, A. D. (1991). Transmural distribution of three-dimensional strain in the isolated arrested canine left ventricle. AJP - Heart and Circulatory Physiology, 261(3), H918-928.

[7] Peng, X., Kraus, M. S., Wei, H., Shen, T. L., Pariaut, R., Alcaraz, A., et al. (2006). Inactivation of focal adhesion kinase in cardiomyocytes promotes eccentric cardiac hypertrophy and fibrosis in mice. J Clin Invest., 116(1), 217-227.

[8] Shi, L. Z., Nascimento, J. M., Chandsawangbhuwana, C., Botvinick, E. L., & Berns, M. W. (2008). An automatic system to study sperm motility and energetics. Biomed Microdevices., 10(4), 573-583.

[9] Wang, Y., Botvinick, E., Zhao, Y., Berns, M., Usami, S., Tsien, R., et al. (2005). Visualizing the mechanical activation of src. Nature, 434, 1040-1045.

[10] Yoshizaki, H., Ohba, Y., Kurokawa, K., Itoh, R. E., Nakamura, T., Mochizuki, N., et al. (2003). Activity of rho-family GTPases during cell division as visualized with FRET-based probes. J Cell Biol., 162(2), 223-232.

Appendix A

Imspector user manual

A.0.1 Preface

ImSpector is a software developed by La Vision BioTec used for data acquisition and evaluation. Here we will describe the basics for using this program for our experiments. Instructions are written for operation and are modified from the La Vision BioTec Software Manual for ImSpector Image Acquisition and Analysis.

A.0.2 Safety Notes:

Laser Safety

Because ImSpector uses a 710-990nm tunable Ti:sapphire laser, it is necessary to always wear safety goggles when operating the laser. These goggles have a shade of red or green tint which blocks out these wavelengths from contact with your eyes.

Biological Sample Safety

When handling all types of cells, it is advised that you wear gloves. Although the lab generally does not use any cells that are known to cause cancer or any other illnesses, taking the precaution to wear gloves when handling cells is always the best practice.

A.0.3 Hardware Specifications:

Axiovert 200M microscope; Hamamatsu camera; Spectra Physics 710-990nm tunable Ti:sapphire laser; Computer: Dell Windows 7

A.0.4 Panel Overview

The ImSpector system is comprised of 4 panels.

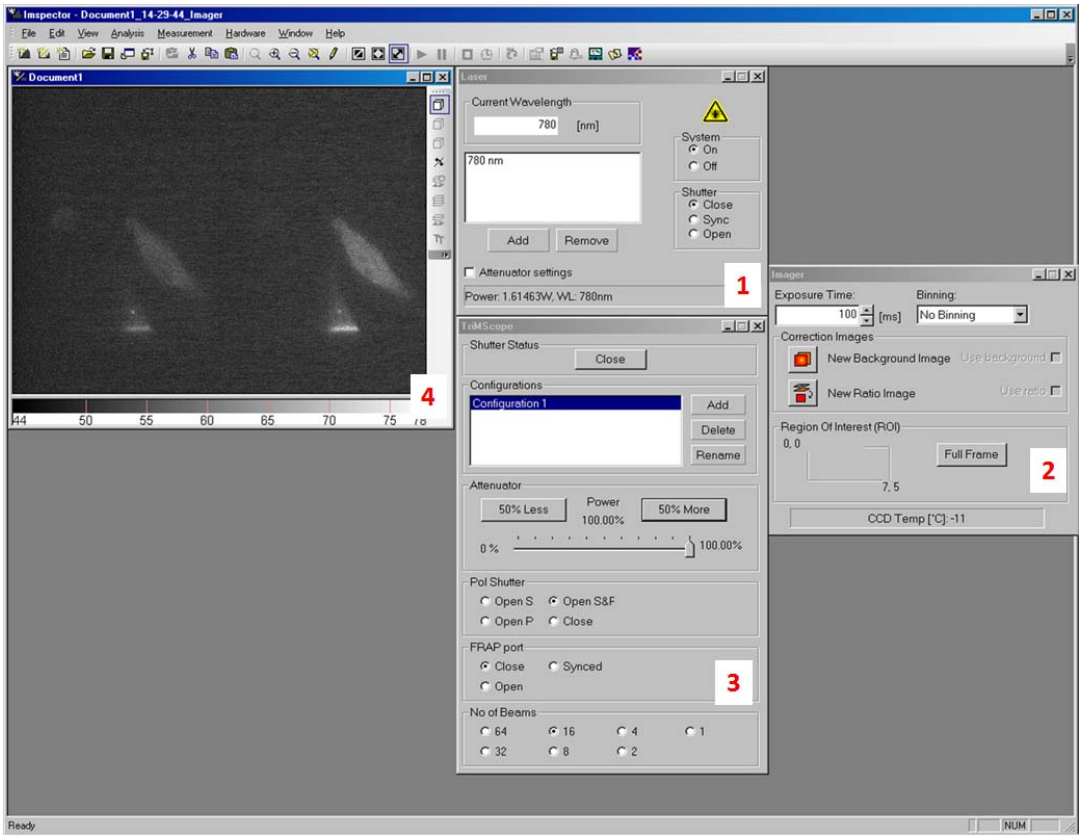

Figure A.1: System with individual panels 1, 2, 3, and 4, numbered in red.

A.1 Use of ImSpector

A.1.1 How to turn on the system

Microscope:

To turn on the Axiovert microscope, press the green switch located on the right side of the microscope. When the green light is on and the microscope has stopped making mechanical noises, the microscope is ready. The microscope MUST BE ON before the ImSpector program can run.

Camera:

To turn on the a cooled digital 12 bit SensiCam CCD Camera, press the on switch located on the back of the SensiCam CCD Camera.

Laser:

To turn on the laser, turn the key on the laser power unit located under the optical bench setup. Turn the power on and set the laser power accordingly.

ImSpector Program:

To turn on ImSpector, open the project explorer window for ImSpector.

A.1.2 Image Acquisition

In order to take images, make sure the cells are loaded and are in focus through the eyepiece of the microscope. Move the switch located on the front of the microscope from the eyepiece to the camera port so that image can be seen in ImSpector.

For fluorescence imaging, two photon excitation using a Ti:sapphire laser is used. To access the laser panel, go to view laser information. The following panel should appear:

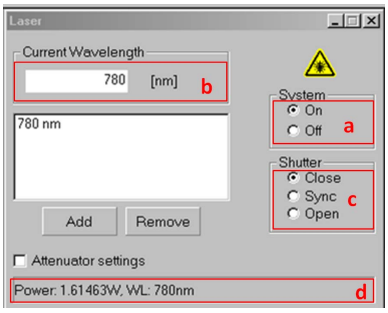

Figure A.2: Panel 1 with sub-labels a, b, c, d in red.

Begin by turning on the system (panel1.a). Then adjust the wavelength desired (panel1.b) and check that the system is powered and set at the right wavelength (panel1.d).

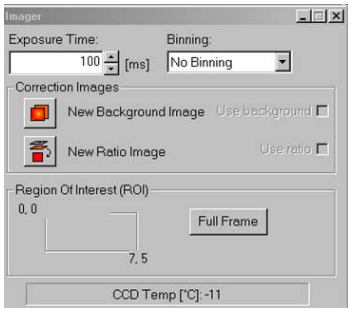

Figure A.3: Panel 2

Set the time for acquisition by changing the exposure time settings in panel 2. If binning is required, binning can be adjusted using the pull down menu.

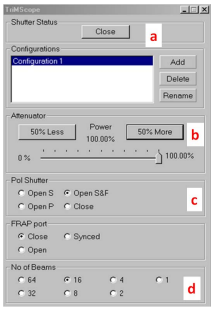

Figure A.4: Panel 3 with sub-labels a, b, c, d in red.

The power of the laser can be adjusted by changing the attenuator settings (panel-

3.b), the active polarizers (panel3.c), and the number of beamlets used can adjust for the amount of power in each beamlet (panel3.d).

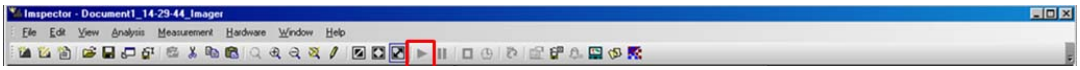

Figure A.5: Main control panel.

To begin image acquisition at the current settings for the set exposure time, set the laser to ”sync” button (panel1.c), and hit the play button found on the main control panel (Figure A.5). After the image is measured, it will be displayed in the image acquisition window (panel 4) as shown below (Figure A.6).

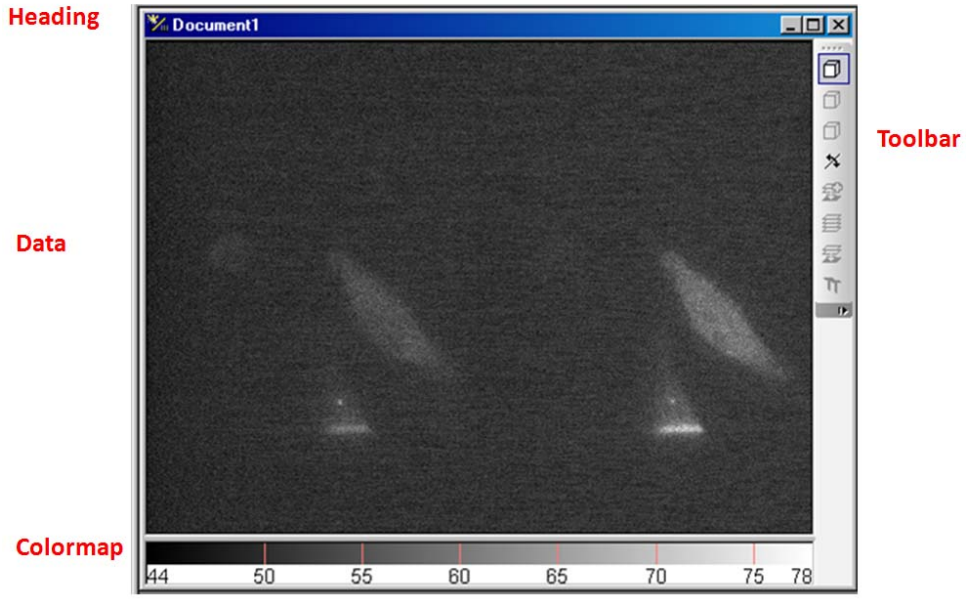

Figure A.6: Image acquisition window.

A.1.3 Save image

Images in ImSpector can be saved in multiple formats. The data files can be saved as ImSpector Data Files (*.spv) and measurements can be saved as ImSpector

Measurements (*.msr). Files can also exported into file types such as *.tiff or *.jpeg. *.tiff files are usually higher in resolution and therefore take up more hard drive space.

A.1.4 Laser Control

Measuring laser power:

To measure the laser power, the power meter is needed. Turn on the power meter first and set the wavelength to your desired wavelength (i.e. 780 nm) and press the attenuation button, labeled ATTN. Now on the microscope, switch the objective so that an open filter cube slot is available. Place the measuring device from the power meter on the objective hole to measure the power. For this system, two shutters must be opened. Set each shutter to the open position (panel1.c and panel 3.a). For the largest power supplied by the laser, set the polarizers for both S and P (panel3.c).

A.2 References

[1] La Vision BioTec Software Manual for ImSpector Image Acquisition and Analysis

Appendix B

Robolase III user manual

B.0.1 Preface

Robolase III is a labview program designed and operated by the Biophotonics lab at UCSD. The Biophotonics lab is led by Dr. Michael Berns and operated by Dr. Zhixia (Linda) Shi. Robolase III is an innovative research program that allows the user to use laser tweezers to manipulate cells. These cells can be followed in real-time and have pictures taken to record the responses of the cells.

B.0.2 Safety Notes:

Laser Safety

Because Robolase III uses a 1064 nm laser, it is necessary to always wear safety goggles when operating the laser. These goggles have a shade of red or green tint which blocks out the infrared laser beam from contact with your eyes.

Biological Sample Safety

When handling all types of cells, it is advised that you wear gloves. Although the lab generally does not use any cells that are known to cause cancer or any other illnesses, taking the precaution to wear gloves when handling cells is always the best practice.

B.0.3 Hardware Specifications:

Axiovert 200M microscope; Hamamatsu camera; Spectra Physics 1064nm laser; Alienware Computer: Intel Core 2 Duo 2.67 GHz, 2 GB Ram, Windows XP

B.0.4 Panel Overview

The Robolase III system is comprised of 4 panels.

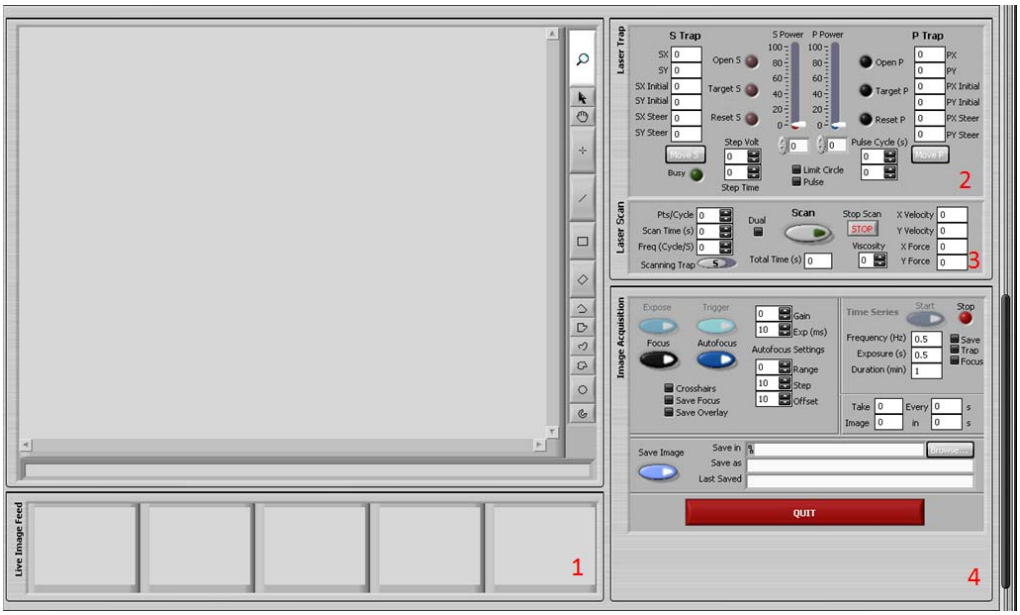

Figure B.1: System with individual panels 1, 2, 3, and 4, numbered in red.

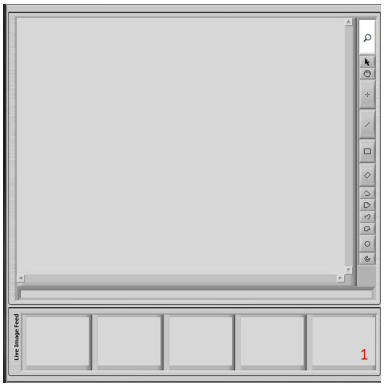

Figure B.2: Panel 1 is for image acquisition and image acquisition history

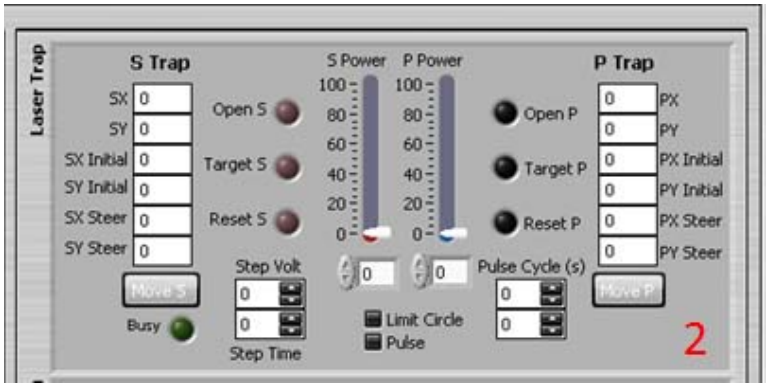

Figure B.3: Panel 2 is for static control of laser tweezers

Figure B.4: Panel 3 is for dynamic control of laser tweezers

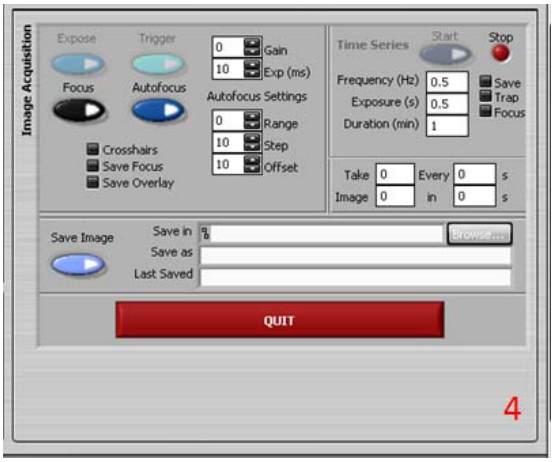

Figure B.5: Panel 4 is for control of image acquisition

B.1 Use of Robolase III

B.1.1 How to turn on the system

Microscope:

To turn on the Axiovert microscope, press the green switch located on the right side of the microscope. When the green light is on and the microscope has stopped making mechanical noises, the microscope is ready. The microscope MUST BE ON before the LabVIEW Robolase program can run.

Camera:

To turn on the Hamamatsu camera, press the on switch located on the Hamamatsu controller and turn on the on switch of the temperature controller of the camera.

Laser:

To turn on the laser, turn the key on the laser power unit located on the optical bench setup. Turn the power on and set the laser power accordingly.

Labview Program:

To turn on Labview, open the project explorer window for labview, and find the file labeled Robolase IV Alien.vi. Open this and it will bring you to the Front Diagram. Now to turn on Robolase, you must click the start arrow button located in the top left panel of labview.

B.1.2 Cells that can be used

Petri dishes

The Petri dish the most common type of specimen holder used for cells that will be manipulated with bead and laser tweezers. The stage compatible for Petri dishes has a large circular hole in center and can hold 35mm diameter glass bottom dishes. The stage compatible for these dishes is also temperature controlled by a stage temperature controller. The settings for the temperature control are located on the stage temperature controller.

B.1.3 Protocol: Mounting the stage and Specimen Holder

Cleaning the Objective

A clean objective is very important when imaging cells. Before mounting the sample, the objective must be cleaned by taking a strip of lens paper about an inch wide, placing a drop of lens cleaner near the center, and wiping the objective with the wet lens paper in one direction. Then, take another strip of lens paper and wipe the objective dry once again in only one direction. Once the objective is dry, place no more than a drop of objective oil (brown Zeiss-labeled bottle) on the lens of the objective.

After an experiment is over, wipe off the oil on the objective with a new piece of lens paper. Then, clean the objective as before first with a strip of lens paper with lens cleaner, then drying with another piece of lens paper.

Finding the right stage:

Depending on which type of cells you are going to use, find the corresponding stage that will fit the cells. The various stages are found in the top drawer directly to the left of the Robolase III computer. In order to put the stage on the microscope correctly, place the top corners of the stage in first, and then press down on the bottom two corners to correctly place the stage on the microscope.

B.1.4 Imaging cells properly

Focusing

Begin by ensuring that the correct annular phase ring for the corresponding objective is in place. To bring a sample into focus, move the focus knob up and down to find the right focal plane for the cells. After placing the specimen holder in the stage, move the objective (with oil) up using the coarse adjustment knob (the large, outer knob). Slowly bring the objective up to the specimen holder until the drop of oil on the objective touches the bottom of the specimen holder (the drop should spread as it looks between two surfaces). Be careful not to move the objective too high against the specimen holder, which may break the objective lens. If in doubt, use the fine adjustment knob.

Once the oil has touched the specimen holder, look through the eyepiece and use

the fine adjustment knob to bring the cells into focus. If the microscope starts beeping while you focus, then you moved the objective as high as possible. If you have trouble finding the cells, please ask for assistance.

Kohler Illumination

Kohler illumination allows the user to adjust the condenser such that there is uniform light reaching the focal plane. To perform Kohler illumination, use the two large black knobs slightly below the halogen lamp that move the condenser up and down, the silver lever right under where light comes out that controls the size of the aperture, and two small silver knobs below the filters that move the condenser laterally. First, move the silver lever all the way to the back (towards the right) so that very little light can come through the condenser. Looking through the eyepiece, you should see a tiny hexagon through which you can see the sample. Move the condenser up and down until the edges of the hexagon are as sharp as possible. Then, adjust the two silver knobs so that the hexagon is in the middle of the field of view. Once in the middle, pull the silver filter back towards you until all sides of the hexagon lie just outside the field of view and the edges of the hexagon is no longer visible. Note that the hexagon gets larger as you pull it towards you and to the left.

When to do Kohler Illumination

Kohler illumination needs to be done whenever the focal plane changes (i.e. whenever you move the focus knob). For small changes in focus, it is not as essential, but when finding a new field of view or using a new sample, Kohler illumination must be done. All samples are not homogeneous on within their holder (rose chamber, Petri dish, etc.), so image quality may decrease as you move around, requiring Kohler illumination to be done once again.

B.1.5 Image Acquisition

In order to take images, make sure the cells are loaded and are in focus through the eyepiece of the microscope. Move the switch located on the front of the microscope from the eyepiece to the camera port so that image can be seen in Robolase.

This section will mainly utilize the features on the Image Acquisition tab on Panel 4.

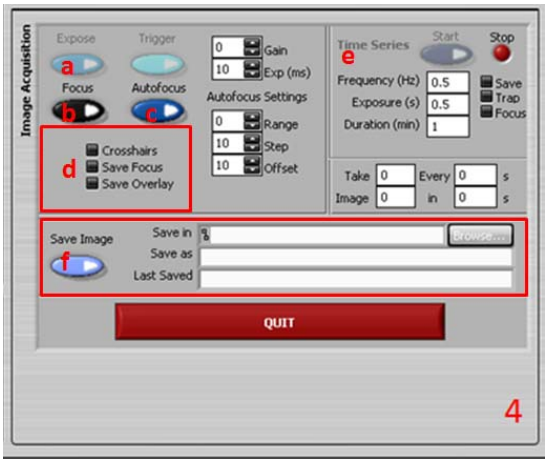

Figure B.6: Panel 4 Image Acquisition features labeled a, b, c, d, e, f.

Use the Focus (panel4.b) button to utilize the focus knob on the microscope to put cells in focus. Note that without pressing focus, the image on Robolase will not change in real time.

Use the Expose (panel4.a) button to snap the image so that it can be seen on Robolase.

Use the Autofocus (panel4.c) button to let the computer use an algorithm to focus in on the best image possible. It is always better to manually focus, as the auto focus may not focus on the proper cells.

Use the Save Image (panel4.f) button to save the image seen on Robolase. This button will save the image into a folder specified in panel4.f. The text boxes denote where and how an image will be saved. The top box labeled, Root directory, tells you where the

image will be saved. Last saved tells you where the last image was saved. Save as allows you to label the image appropriately.

The boxes in panel4.d allow you to change some of the image settings. Check marks in the boxes denote that the function is currently being used. Click on the box to create or delete a check mark. This will allow you to save modified images.

Time series (panel 4.e) allows a series of pictures to be taken. The interval between pictures (frequency) and the amount of time the time series lasts (duration) can be set. Or, every frame acquired by the camera can be saved by checking the ”Save” box. The ”Focus” checkbox allows one to view a continuous acquisition (real-time video) of the field of view between saved images

This function also allows for a timed series of trap on/off sequences by checking ”Trap.” The exposure setting determines how long the shutter of the trap is open. The on/off sequence is synchronized with the sequence of images that are acquired.

B.1.6 Autofocus

Autofocus utilizes a widely-used algorithm employed by Marcellinus S. Harsono in the Robolase systems that looks at a set a focal planes, calculates the best ”focused” image, then automatically oves the objective to the corresponding focal plane. The settings for the autofocus section can be found in the ”Autofocus Settings” section in Panel 4. A higher range means that the autofocus will go through more focal planes equidistant above and below the current plane. Because autofocus calculates the best possible image out of this set, if the sample is very out of focus the resulting image may not be appropriately focused. Also, because the ”best” image is according to a mathematical algorithm, the result may not always be the most focused according to subjective human eyes. Thus, always make sure that the image seen is the correct and proper image and do not rely completely on autofocus to obtain the image quality you

prefer.

B.1.7 Save image

To save an image, press the button labeled Save Image. The image will be saved in a folder specified by the Root Directory. Note that if the focus button is pressed, The Save Image button will need to be held longer so that it can take an image.

File name and location

Robolase automatically saves files in a folder designated by default. The images are currently saved in the folder ”C:/RobolaseIIIData”, and then are sorted by date. In order to change the location of the save location, change the root directory box in panel 4.f to the desired location. To save the image under a certain file name, enter in the desired name in the box labeled Save as. Each image will save under that name, and will have a different image number, which is automatically labeled by Robolase. To see the recently saved image, the box labeled Last Saved will tell you the directory and file name of the last saved image.

B.1.8 Type of image

Type:

Images in Robolase can be saved in two formats, .tiff, and .jpg. Tiff files are usually higher in resolution and therefore take up more hard drive space. Tiff images are saved immediately, but if jpeg images are preferred, one simple can click overlay (panel 4.d) and a jpeg folder of images will be generated.

Overlay or no overlay:

To save the image and the position of the laser trap, check the save the image with the overlay (panel 4.d). There is also the option to have no overlay, which does not show the laser tweezers position. The best option is to save under both which does both overlay and no overlay. Note that .tiff files cannot be saved with an overlay.

B.1.9 Laser Control

Measuring laser power:

To measure the laser power, the power meter is needed. Turn on the power meter first and set the wavelength to 1064 nm and press the attenuation button, labeled ATTN. Now on the microscope, switch the objective so that an open filter cube slot is available. Place the measuring device from the power meter on the objective hole to measure the power. Now, turn open the shutter which is the open S button on panel 2 and measure the power.

Laser Tweezers

For use of the laser tweezers, one the main shutter control is opened at the base of the laser, the laser tweezers can be then controlled from Robolase via the Open S button on panel 2.

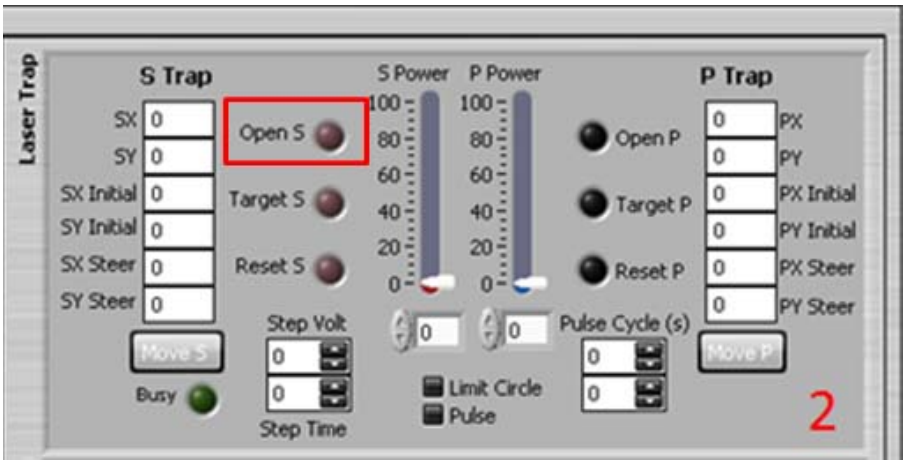

Figure B.7: Panel 2 Image denoting the Open S tab control of the laser tweezers

For more advanced use of the laser tweezers. One can set up a laser scan. Laser scan allows one to set the duty cycle of the laser tweezers in the on and off state. This allows for dynamic application of forces. To set up a scan, the user must draw a line using ROI tools on the image. The algorithm then calculates an array of points on which to target the trap and then lets the trap move back and forth on the line for a specified

time (Scan Time). Pts/cycle determines how many steps the trap moves in one cycle and is taken into account when calculating the array of points while Freq determines how many cycles occur per second.

Figure B.8: Panel 3 Image showing control of the laser tweezers using laser scan

B.1.10 Logmein control

Robolase was designed to allow for remote user use. The Biophotonics lab currently uses the LogMeIn service to remotely access the computer controlling Robolase. All of the functions in Robolase can be accessed via LogMeIn and is very helpful when conducting experiments overnight. The tab in Panel 4 is a messaging device designed to allow for messages to be sent from a remote user to a local user.

Appendix C

Dual view calibration user manual

C.0.11 Preface

Robolase is a labview program designed and operated by the Biophotonics lab at UCSD. The Biophotonics lab is led by Dr. Michael Berns and operated by Dr. Zhixia (Linda) Shi. Robolase is an innovative research program that allows the user to use laser tweezers to manipulate cells. These cells can be followed in real-time and have pictures taken to record the responses of the cells.

C.0.12 Dual View Calibration Overview

For Dual View calibration using Robolase, the sensicam_ratio_calibration.vi will be used.

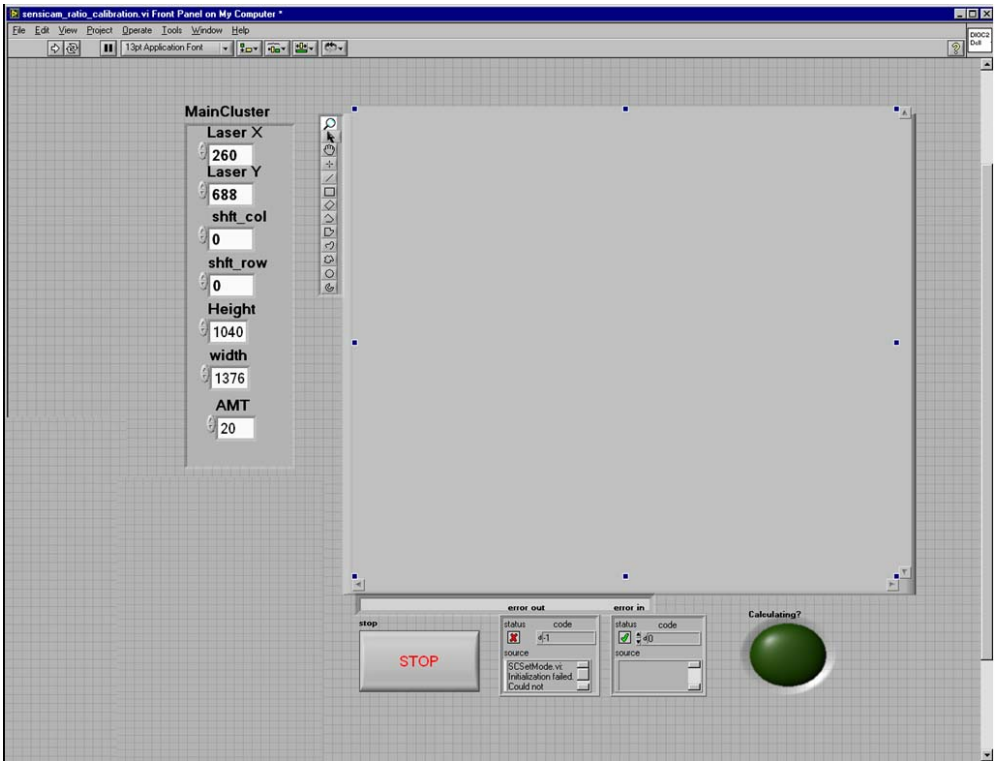

Figure C.1: sensicam_ratio_calibration.vi panel

In this appendix, we will focus on Dual View calibration using the sensicam_ratio_calibration.vi.

C.1 Dual View calibration

C.1.1 Turn on the system

Microscope:

To turn on the Axiovert microscope, press the green switch located on the right side of the microscope. When the green light is on and the microscope has stopped making mechanical noises, the microscope is ready. The microscope MUST BE ON before the LabVIEW Robolase program can run.

Camera:

To turn on the Sensicam camera, press the on switch located on the back of the camera.

Labview Program:

To turn on Labview, open the project explorer window for labview, and find the file labeled sensicam_ratio_calibration.vi. Open this and it will bring you to the Front Diagram. Now click the start arrow button located in the top left panel of labview.

C.1.2 Setting up the Dual View System

Set the filter cube in place and slide the slider port to the Dual View mode. Then use a micrometer or gridded slide and capture the image using sensicam_ratio_calibration.

Adjust the Dual View tube using the R/L or U/D knobs until the program registers a zero shift in column (shft_col) and a zero shift in row (shft_row). The logic of the program will calculate any shifts in the left hand and right hand of the split images and prompt the user to make fine tune adjustments of the Dual View tube until zero shifts are achieved.

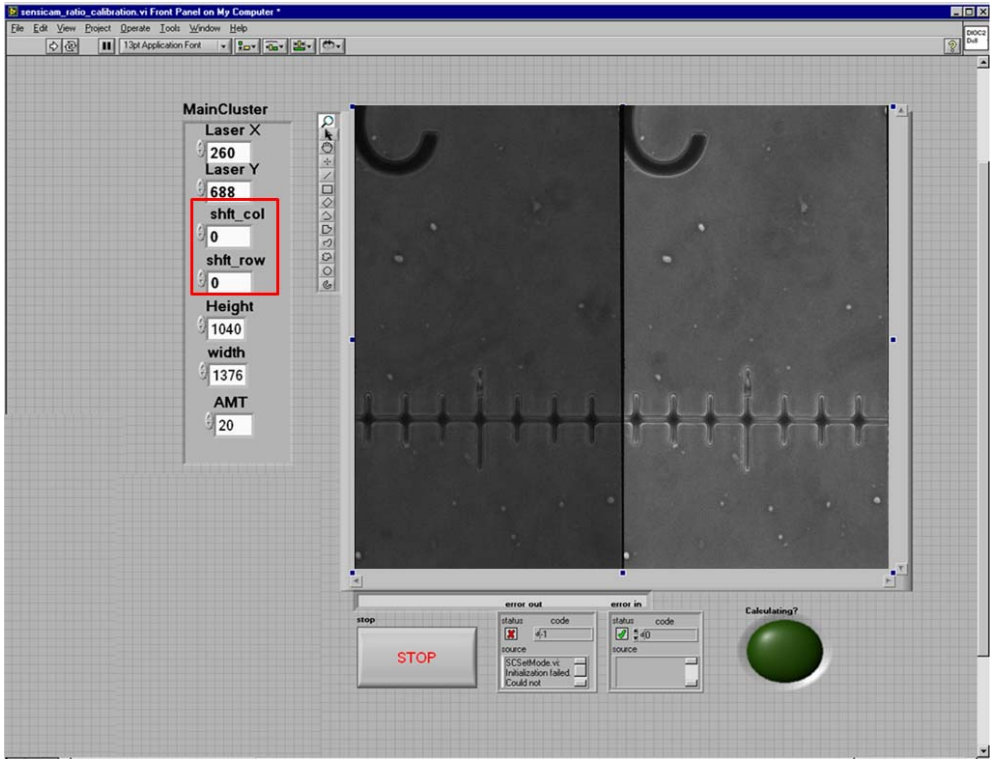

Figure C.2: sensicam_ratio_calibration.vi showing zero shift in column and row for the imaged micrometer

Appendix D

Laser tweezer force calibration user manual

D.0.3 Preface

Robolase is a labview program designed and operated by the Biophotonics lab at UCSD. The Biophotonics lab is led by Dr. Michael Berns and operated by Dr. Zhixia (Linda) Shi. Robolase is an innovative research program that allows the user to use laser tweezers to manipulate cells. These cells can be followed in real-time and have pictures taken to record the responses of the cells.

D.0.4 Safety Notes

Laser Safety

Because Robolase III uses a 1064 nm laser, it is necessary to always wear safety goggles when operating the laser. These goggles have a shade of red or green tint which blocks out the infrared laser beam from contact with your eyes.

Biological Sample Safety

When handling all types of cells, it is advised that you wear gloves. Although the lab generally does not use any cells that are known to cause cancer or any other

illnesses, taking the precaution to wear gloves when handling cells is always the best practice.

D.0.5 Force Calibration Overview

For force calibration on the Robolase IIII system, two computers utilizing Robolase III.vi and Robolase IV Alien.vi will be implemented. RobolaseIII.vi is comprised of 4 panels.

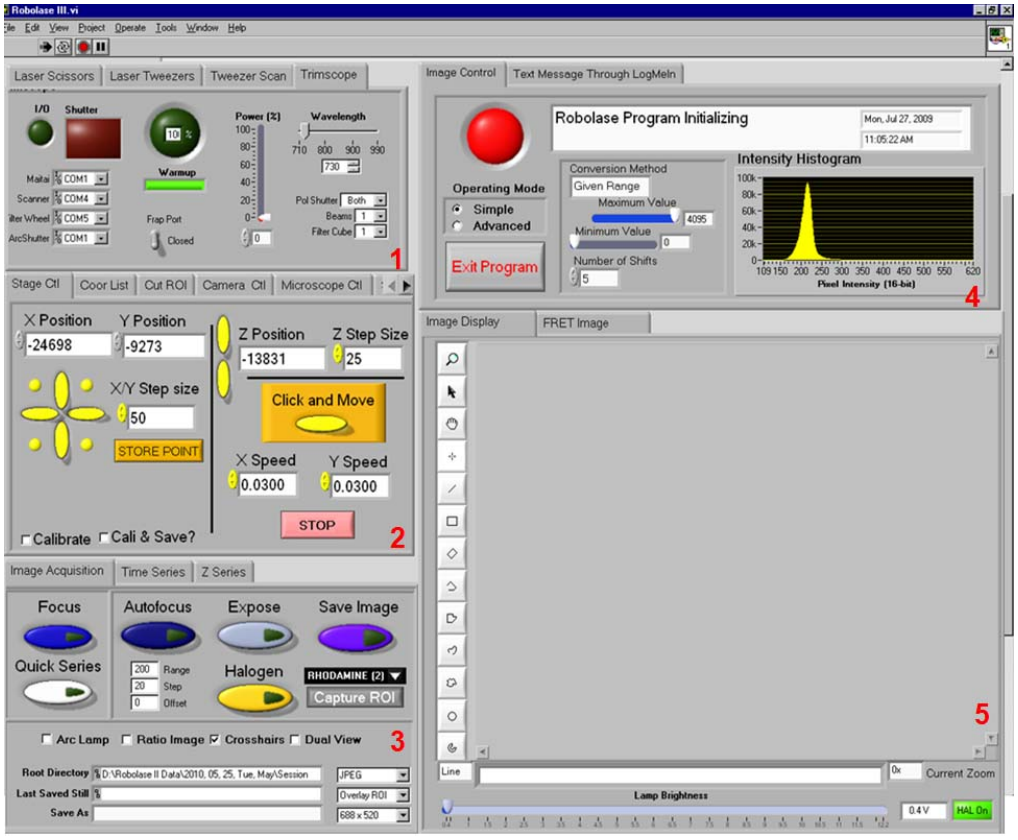

Figure D.1: RobolaseIII.vi System with individual panels 1, 2, 3, 4, and 5, numbered in red.

In this appendix, we will focus on force calibration using the RobolaseIII.vi, for more information about using the other capabilities of Robolase III, please contact Dr. Berns and Dr. Zhixia (Linda) Shi at the Cellular Biophotonics Laboratory (http://-robolase.ucsd.edu).

D.1 Force calibration using Robolase

D.1.1 Turn on the systems

Microscope:

To turn on the Axiovert microscope, press the green switch located on the right side of the microscope. When the green light is on and the microscope has stopped making mechanical noises, the microscope is ready. The microscope MUST BE ON before the LabVIEW Robolase program can run.

Camera:

To turn on the Hamamatsu camera, press the on switch located on the Hamamatsu controller and turn on the on switch of the temperature controller of the camera.

Laser:

To turn on the laser, turn the key on the laser power unit located on the optical bench setup. Turn the power on and set the laser power accordingly.

Labview Program:

To turn on Labview, open the project explorer window for labview, and find the file labeled Robolase IV Alien.vi and RobolaseIII.vi. Open this and it will bring you to the Front Diagram. Now click the start arrow button located in the top left panel of labview.

D.1.2 Beads

Prepare a 35 mm glass bottom dish filled with water and beads of the desired diameter.

D.1.3 Imaging the beads

Clean the objective and place oil on the objective lens, mount the petri dish stage holder, and set the dish containing the beads until the beads become in focus.

D.1.4 Trapping the beads

Using Robolase IV Alien.vi, turn on the trap (for more details see Appendix B). Record the position by creating a box showing the center of the trap, click the save overlay button, and save image.

D.1.5 Moving the stage, imaging the beads, and calibration of the forces of the trap

To calibrate the forces of the trap, Stokes flow approximation will be used to determine the force of the trap (for more details, see Chapter 2). To move the stage, use RobolaseIII.vi and click calibrate (1) (see Figures below). To adjust the velocity of the stage, adjust the x or y speed (2) and click on the x position (3) or y position (4) on the stage controller pad to move the stage.

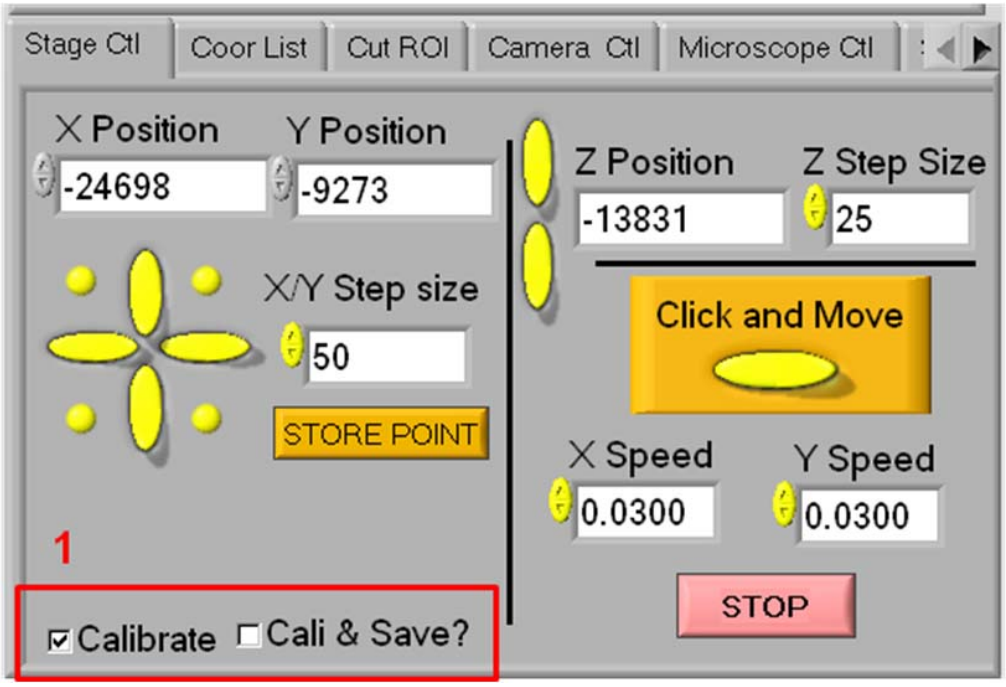

Figure D.2: Click Calibrate to enable calibration process

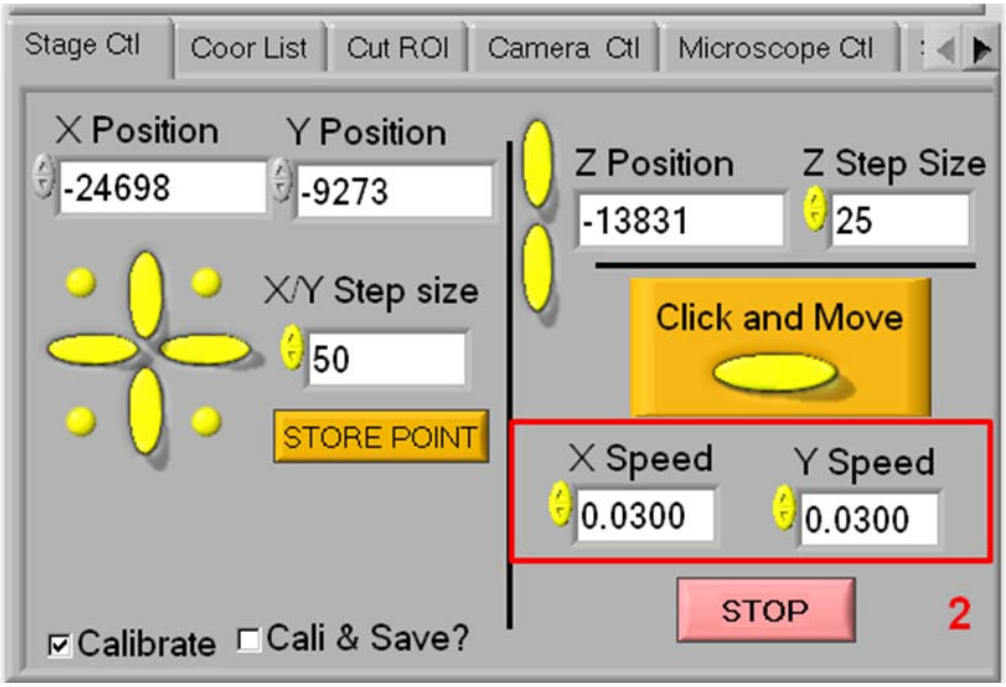

Figure D.3: Adjust either X speed or Y speed to move the stage a known velocity (mm/s).

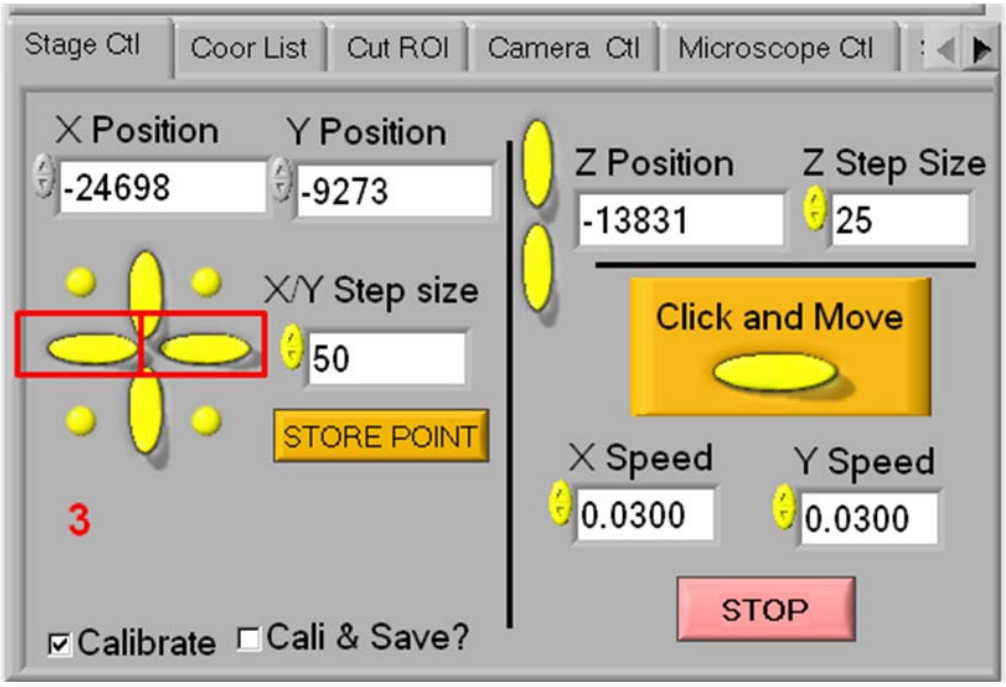

Figure D.4: Click the x position, either left or right, to move the stage left or right.

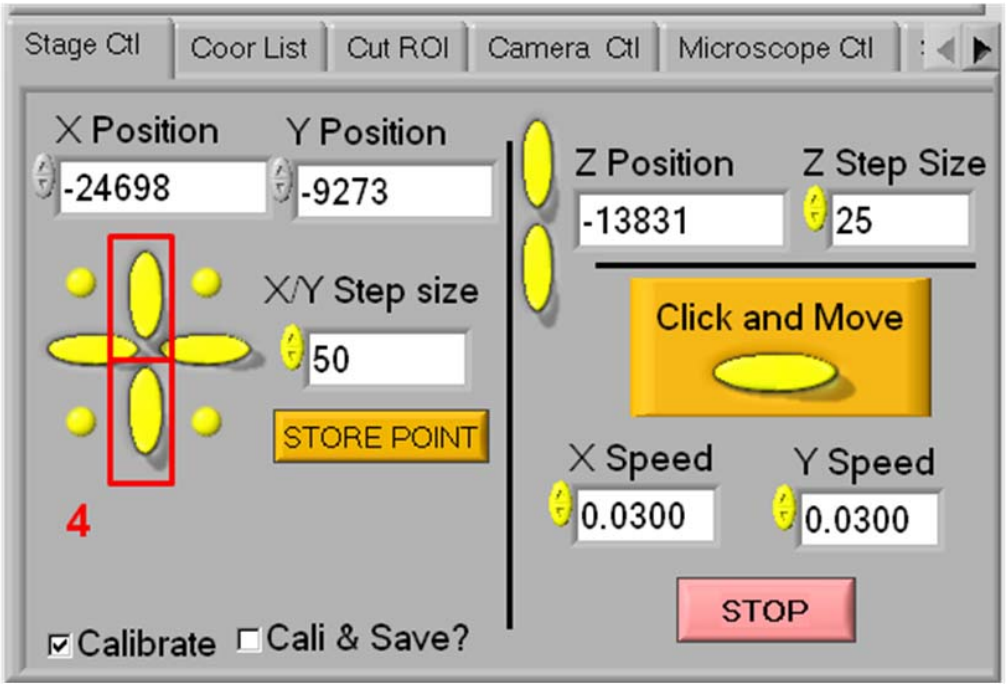

Figure D.5: Click the y position, either up or down to move the stage in the y axis.

While the stage is moving, use Robolase IV Alien.vi to capture the position of the bead when the stage is moving.

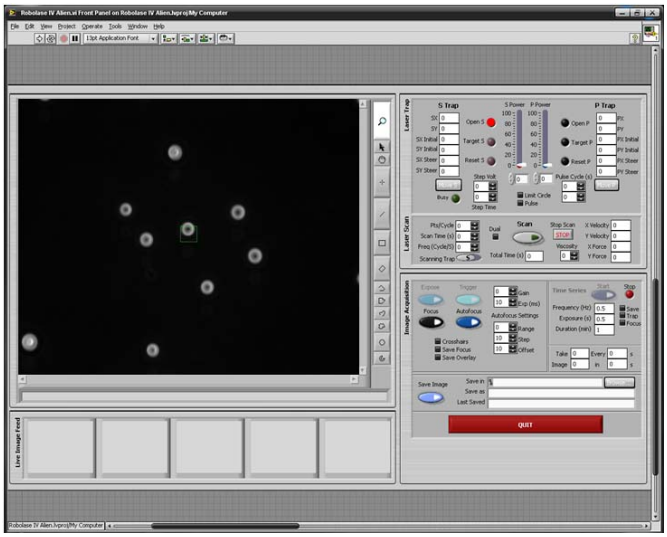

Figure D.6: Image of stably trapped bead being moved with a known velocity. Green box denotes the position of the trap.

Once an image is captured, stop the movement of the stage using Robolase III.vi

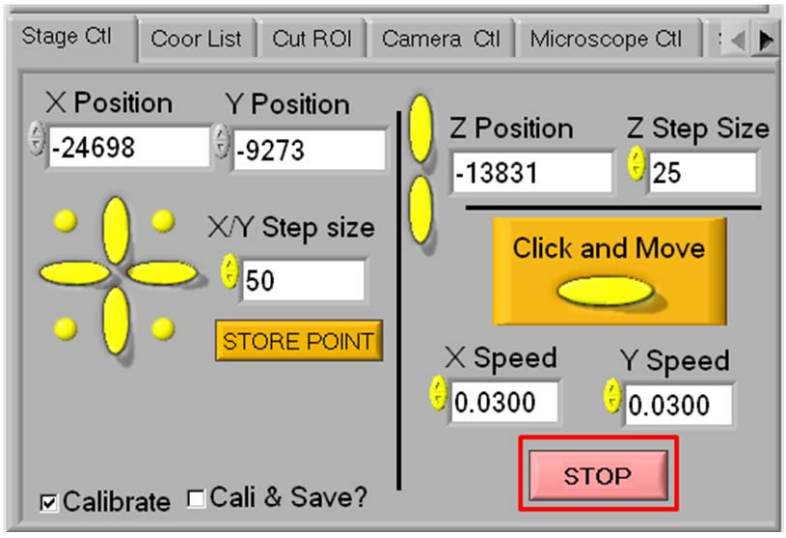

Figure D.7: Click stop to halt the movement of the stage.

Change the velocity of the x speed or y speed and repeat taking images, until the bead can no longer be stably trapped.

Using an image editor, calculate the distance between the center of the trap and the center of the bead in pixels.

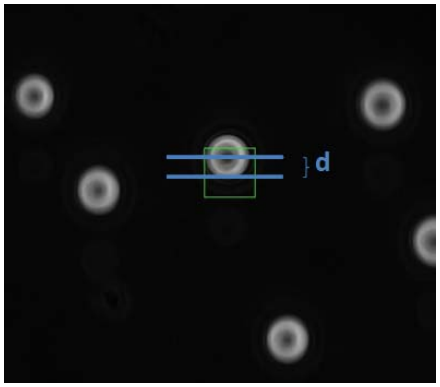

Figure D.8: Picture showing the position of the center of the trap and the center of the bead. The distance, d, is defined as the distance between the center of the trap and the center of the bead at the set velocity and trapping power.

Using this method, create a force calibration curve of force calculated from Stokes flow approximation versus distance between the center of the trap and the center of the bead.

These results may then be used to determine the forces applied on a cell based on the distance between the center of the bead and the center of the trap.

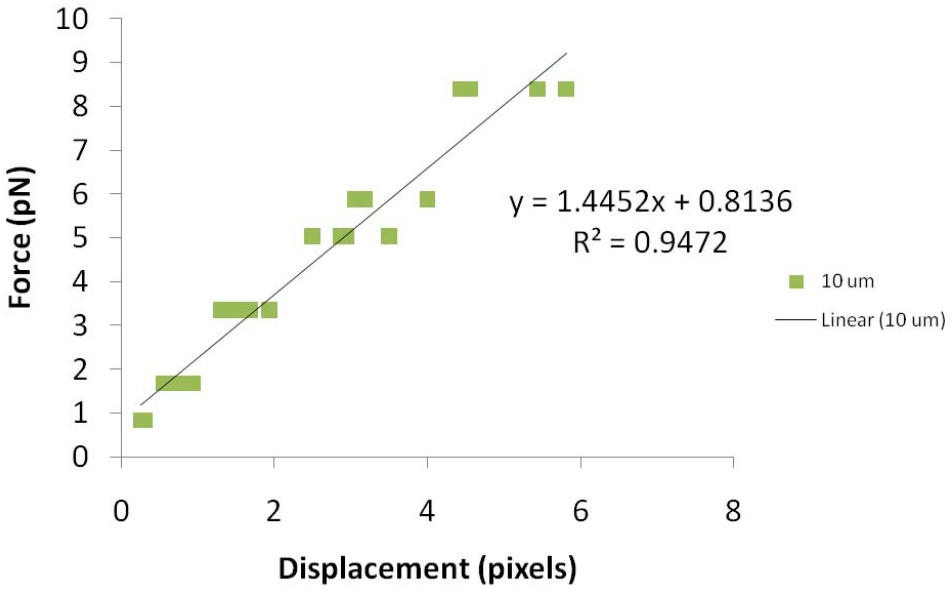

Figure D.9: Force calibration curve generated from Stokes flow approximation calibration for laser tweezers

Appendix E

The Use of Fluorescence Correlation Spectroscopy to Determine Ligand Concentration per unit Area of a Polystyrene Bead used in Mechanotransduction Experiments

E.1 Introduction

In studying mechanotransduction, some studies use ligand coated beads that are adhered to cells and then optical traps or magnetic traps have been used to apply force to the cell (Huang et al., 2004). The use of these systems has furthered the understanding of cell stiffness and signaling cascades involved in mechanotransduction. To further our understanding of mechanotransduction, it is important to understand the relationship between the ligands that are on the bead and how they interact with the receptors on the cell surface, and subsequently how the interplay between the two affects mechanotransduction.

Currently, radioactive labeling of proteins provides a means to quantifying the number of ligands on a bead surface, however, limitations of radioactive labeling include: safety conditions for performing experiments, radioactive waste, and short half-lives of the labeled compounds (Li et al. 2008). Another method for determining the concentration of ligand per unit area on a bead is the use of fluorescence correlation spectroscopy. Fluorescence correlation spectroscopy (Bulseco and Wolf, et al. 2007) has been used to measure the diffusion times of macromolecules, the concentration of fluorescently labeled molecules, and the kinetics of chemical reactions. In this study, we describe the use of fluorescence correlation spectroscopy to determine the concentration of ligand molecules on a coated bead surface.

E.2 Methods

Ligand. For this study, we used a commercial, fluorescently labeled collagen type IV (Invitrogen C13185) dissolved to 1mg/mL in PBS.

Lowry assay. Dilutions of the fluorescently labeled collagen type IV stock were made and a standard curve was established using bovine serum albumin. The concentration of fluorescently labeled collagen type IV stock solution was measured using a Lowry assay (Biorad # 500-015, 500-0114, 500-0115).

Coating beads. One micron microspheres (Duke Scientific # 4009A) were coated using the following method: beads were centrifuged, the supernatant was removed, the beads were washed three times with cold PBS and incubated with 50ug/mL Collagen Type IV- Oregon Conjugate in PBS at room temperature. The sample was centrifuged and the bead were collected, incubated with 10mg/mL bovine serum albumin in PBS at room temperature for 1 hour, washed three times with cold PBS and stored in PBS at 4°C.

Fluorescence Correlation Spectroscopy (FCS). Samples containing: a) 1um beads alone, b) labeled protein alone, c) 1um beads coated with the labeled protein were prepared. Samples were sent to Sensor Technologies LLC (Shrewsbury, MA) for analysis using FCS. FCS data was collected for collagen alone, and for the coated beads. The total number of particles for each (Figure 1) and the total intensity for each was measured (Figure 2) and the average brightness of each particle (counts per particle, cpp) was determined. The average number of labeled collagen molecules per bead was determined by dividing the brightness of the one micron beads by the brightness of the Oregon Green labeled collagen.

E.3 Results

The average counts per particle for the Oregon Green labeled type IV collagen was 87 ± 5. The average counts per particle of the Oregon Green labeled type IV collagen coated one micron beads was 810 ± 60. The average number of Oregon Green labeled type IV collagen was 9.3 ± 0.9.

E.4 Discussion

In this experiment, we show that fluorescence correlation spectroscopy can be used to determine the number of collagen units on a one micron diameter bead. Using a fluorescently labeled collagen, the average number of collagen units on the one micron diameter bead was determined to be 9.3 ± 0.9. Our results support the use of FCS to determine the number of ligands on a one micron coated bead. These results also provide information that may be used in a mathematical model to further our understanding of mechanotransduction and cell signaling.

Future studies include fluorescent labeling of a variety of other proteins used to further our understanding of mechanotransduction and testing a variety of bead coating concentrations and determining the subsequent concentration on the bead per unit area.

Additionally, using these experiments on smaller beads and extrapolating concentrations of protein on larger beads will further our understanding of mechanotransduction by providing a means to study ligand-receptor interactions. A variety of different ligand types can also be used to coat microspheres and subsequently used in optical trapping or magnetic trapping experiments.

E.5 Acknowledgements

We would like to acknowledge Carla Coltharp and David Wolf of Sensor Technologies, LLC (Shrewsbury, MA) for their work involved in this experiment.

E.6 Figures

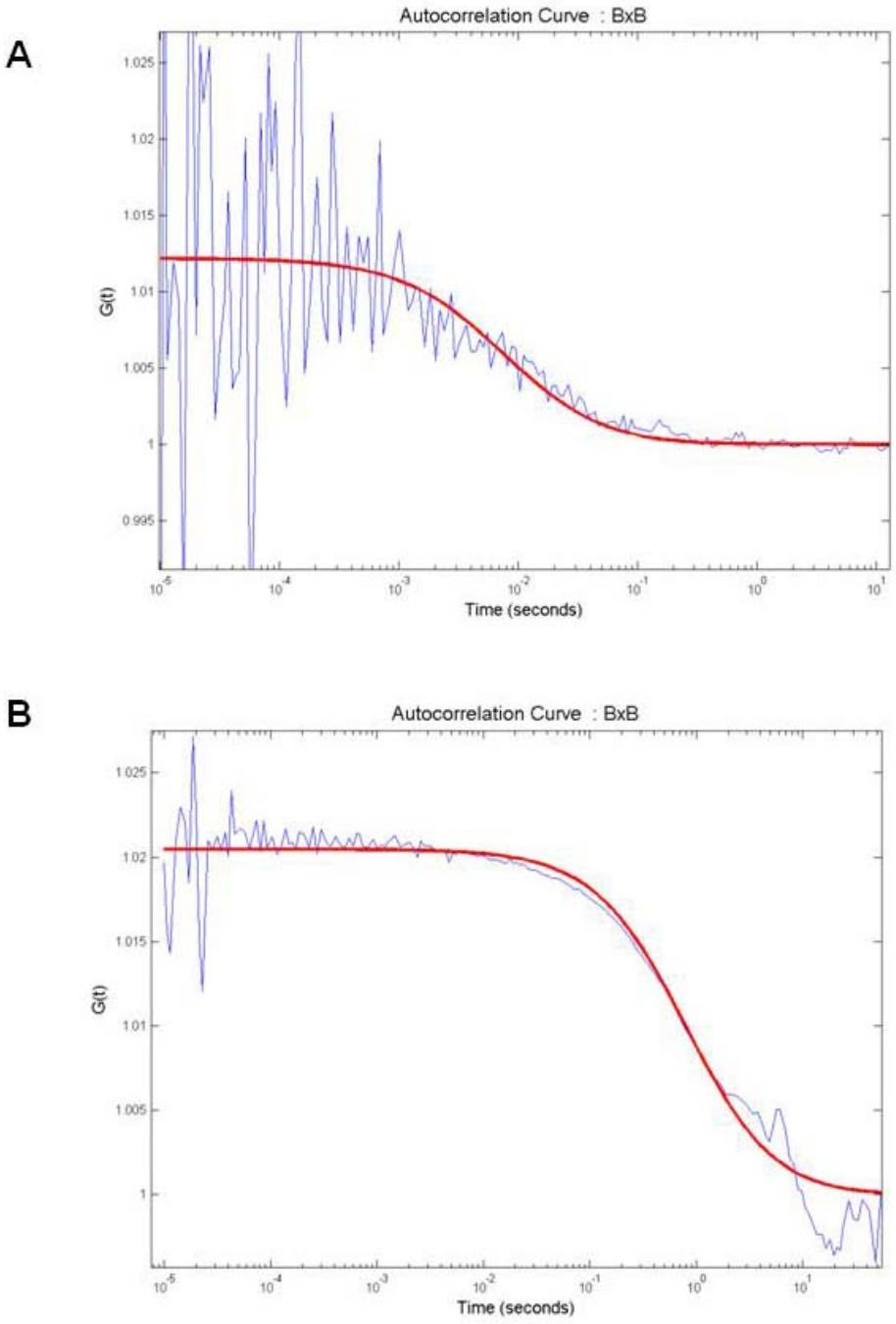

Figure E.1: Sample FCS data for determining number of a) Collagen particles, and b) 1 micron bead particles. Data courtesy of Carla Coltharp.

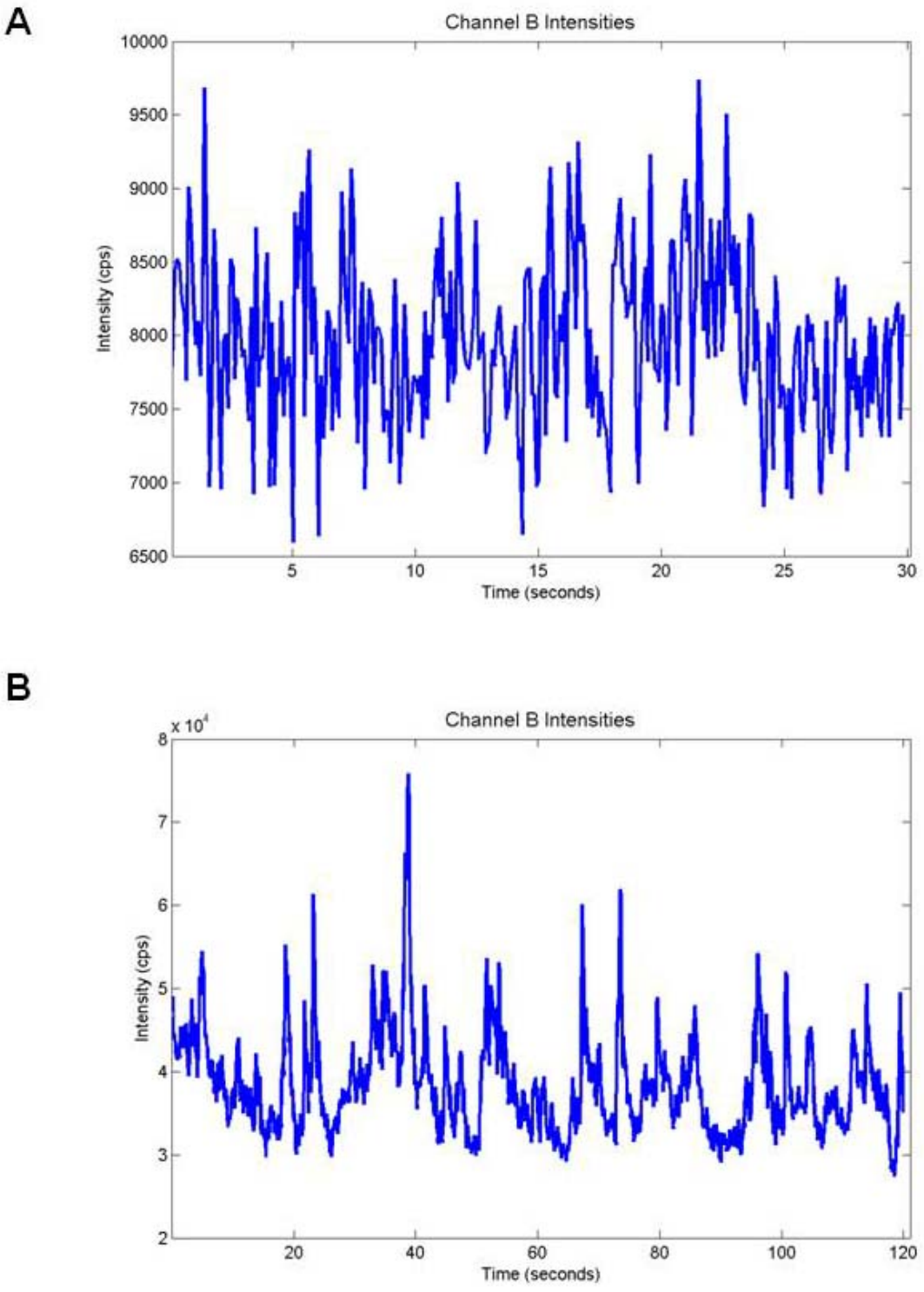

Figure E.2: Sample FCS data for determining intensity values of a) Collagen particles, and b) 1 micron bead particles. Data courtesy of Carla Coltharp.

E.7 References

[1] Huang, H., Kamm, R., & Lee, R. (2004). Cell mechanics and mechanotransduction: Pathways, probes, and physiology. Am J Physiol Cell Physiol, 287, C1-C11.

[2] Li, Y., Xie, W., & Fang, G. (2008). Fluorescence detection techniques for protein kinase assay. Anal Bioanal Chem, 390(8), 2049-2057.

[3] Bulseco, D., & Wolf, D. (2007). Fluorescence correlation spectroscopy: Molecular complexing in solution and in living cells. Methods Cell Biol., 81, 525-559.

Appendix F

Modeling the Anisotropy of Stress and Strain in an Individual Cardiac Myocyte

F.1 Introduction

The heart is a multicellular organ consisting of cardiac myocytes interconnected to each other and to the extracellular matrix. The intercalated disc located at the bipolar ends of the myocyte provide both structural and electrical integrity. Desmosomes and adherens junctions serve to strengthen the linkage of contractile cells and gap junctions provide action potentials a means for conductance. Myocyte stability is also maintained by structures similar to the hoops of a wooden barrel which are aligned perpendicular to its later surface, called costameres (Samarel, 2005). Costameres are the site that link the sarcomere, through the cytoskeleton, to the extracellular matrix. Over the years many of the proteins located in the intercalated disc and costameric junction have been linked to the basis for cardiomyopathies.

Costameres have been recognized as critical mechanosensors which could modulate contractile function. Through the use of genetically manipulated mice and vari-

ous studies from the cellular, tissue, and whole heart level, our understanding of how costameres function in the cardiac myocyte has been enhanced, but many of the current techniques to investigate how mechanics are altered at the costamere are limited. Such studies include soft lithography methods for applying controlled anisotropic multi-axial strain to cultured cardiomyocytes in vitro (Camelliti et al., 2005; Gopalan et al., 2003) and measurement of force and sarcomere length changes in isolated papillary muscles (Lorenzen-Schmidt et al., 2005; Stuyvers et al., 2002). Although these methods have provided different degrees of experimental control, it is difficult to understand how small changes at cellular junctions may affect stress and strain distribution within a single individual cardiomyocyte. As such, we aim to use computational models to investigate how a cardiac myocyte's stress and strain distribution may be altered based on substrate deformation such as in patterned membrane studies versus at a localized area such as studies involving laser tweezers or magnetic tweezers.

F.2 Methods

Finite element model. Simulations for a single cardiac myocyte were generated in Continuity 6.3, a finite element package (www.continuity.ucsd.edu).

Biomechanics model. The biomechanics model is run using displacement boundary conditions.

For the substrate displacement model, we assumed that the cell is perfectly adhered to the substrate and the displacement field was imposed on the flat bottom surface. The magnitude of nodal displacement was proportional to distance from the center. The maximum displacement was set at 1% of total length of each axis.

For modeling the deformation caused by a ligand coated bead and an optical trap, the single node displacement model was created. It assumes that optical trap experiments cause deformation to occur only at one node. The displacement was set at 10% of distance to adjacent node, resulting in 0.37% of total longitudinal cell length.

Model Parameters. Model parameters were set accordingly for this model: stiffness coefficient (longitudinal = 1.0kPa, tranverse = 1.5kPa), viscous coefficient (longitudinal = 0.20 kPa $*$ s, transverse = 0.25 kPa $*$ s), the bulk modulus was 100kPa, and the time steps were set at 0.01s for 10 steps of displacement, 100 steps of relaxation. Model parameters were then varied to look at the effects of stiffness and viscous components.

Analysis of model results. Nodal residuals representing the force required to impose the set displacement boundary conditions with respect to time were saved and residual values were then imported into MATLAB to analyze the time dependent response of the cell at selected nodes.

F.3 Results

Mesh for a single cardiac myocyte

A half-elliptical geometric mesh with a 10:1 longitudinal: transverse axis length ratio (Parker 2007) was created in prolate spheroidal coordinates (Figure 1). The mesh was then refined and converted to Cartesian coordinates before performing deformations. The final mesh consists of 891 nodes and 512 elements.

Time dependent results

Both substrate deformation and point deformation models, were run with a varying time dependence as indicated in the methods section (Figure 2). In both cases, a sharp decrease in and then gradual re-development of stress before relaxation is observed. Additionally, the stress does not level off over time, but becomes increasingly negative.

Time dependent results with varying stiffnesses

For anisotropy stretch of a cell with an elasticity coefficient of 0.2 kPa $*$ s and

stiffness coefficient of 2 kPa (Figure 3a), the force keeps built up over time and has very little relaxation toward the end of 1 second time interval. For single-node stretch, an elasticity of 0.2 kPa $*$ s and stiffness of 2 kPa were tested and the relaxation part also lacked the stiffness property.

With increase of stiffness to 3 kPa and same elasticity of 0.2 kPa $*$ s, anisotropy stretch was conducted. Only the displacement of 0.1 second could obtain from test. The relaxation of the model was failed to resolve. In single-node stretch, similar results were obtained for 2 kPa $*$ s elasticity and 7 kPa stiffness and 1 kPa $*$ s elasticity and 5 kPa stiffness that the relaxation could not resolved.

Physiological values of elasticity and stiffness

Applying physiological values of 2 kPa $*$ s elasticity (Bausch et al., 1998) and 30 kPa stiffness (Lieber et al., 2004) on the model, the result show that only the displacement part could obtain (Figure 3b). The model has limited elasticity of 0.2 kPa $*$ s and stiffness of 3 kPa to obtain full process of displacement and relaxation. Coefficients that are greater than those values would only yield with displacement and the relaxation process would failed to solve.

F.4 Discussion and Conclusions

The objective of this study was to use Continuity 6.3 to model the stress and strain in a single cardiac myocyte in response to stretch by substrate deformation and stretch using an optical trap, occurring on substrates of varying stiffness, to demonstrate the effects of substrate rigidity on cell stress and deformation.

Generation of a mesh

A mesh for a single cardiac myocyte was generated in Continuity 6.3. Prolate spheroidal coordinates were chosen because of our interest in costameres. (Figure 4)

Combining active tension model with a constitutive model

Because cardiac myocytes have active tension capabilities, a standard linear (Kelvin) viscoelastic model with no updated variables or time-dependent variables could only represent a cell's passive tension capabilities. However, by combining an active tension model in which time-dependent variables or updated variables can be incorporated, this allows the model of the cardiac myocyte to provide information regarding active tension in the cell. By incorporating the active tension model with a constitutive model, we are able to represent the contributions of elasticity from structural components in the cell such as the actin-myosin network and the cytoskeletal network.

Incorporating anisotropy into the model

To probe the anisotropy of stress and strain in a single cardiac myocyte, we implemented the standard linear solid separately along each primary axis at each node in the mesh. The reasoning behind such implementation was because the heart is a three dimensional organ and the cells of the heart have a natural polarity in which there is a longitudinal axis and a short axis. Probing of the anisotropic relationship in a cardiac myocyte using a computational model, may help to explain results obtained from in vitro studies such as those performed with anisotropic stretchers (Senyo et al., 2007) or optical trapping experiments.

Time dependent results

The unstable behavior of these models (Figure 3) can most likely be attributed to the alterations that were made to the material parameters (stiffness) to achieve convergence. With stiffness reduced by such a large degree, the model behavior is dominated by the liquid-like components of the viscoelastic model. This causes the model to continue to deform indefinitely after the displacement has been fully imposed at t=0.1s (similar to the infinite creep that is observed when using the Maxwell model), and over time the spreading of the cell becomes significant enough to require a force be generated in the opposite direction to hold the fixed nodes in place.

Although these results are only preliminary, more work will be required to achieve model convergence using parameters that more accurately reflect physiological values. This will allow the quantification of stress output based on realistic parameters. Future directions for this project include varying substrate stiffness and the magnitude of stretch in each of the various models, varying the mesh to represent absences in costamere complexes (Figure 4), performing atomic force microscopy studies in cells to gain understanding of stiffnesses at sites of costamere complexes and non-costamere complexes. Additionally, future directions include measuring stiffness in various genetically manipulate murine knockout mice and compare how stress and strain distribution varies between the knockout animals and wildtypes. In conclusion, by modeling how the individual cardiomyocytes respond to mechanical perturbation varies based on the properties of its environment, a better understanding of cardiac tissue as a whole can be achieved.

F.5 Acknowledgements

I'd like to acknowledge Samantha Clark and Ming-Hui (Dee) Chen for all the work that they put into creating, testing, and understanding this computational model. I'd also like to acknowledge the National Science Foundation and the Bioengineering Research Experience for Undergraduates at UCSD for funding the work done by Samantha Clark.

F.6 Figures

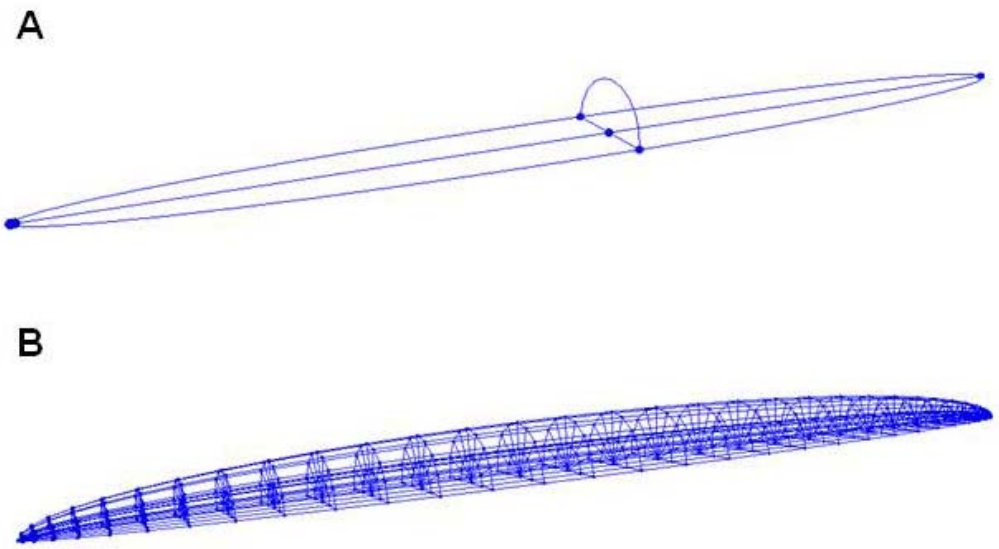

Figure F.1: Mesh for a single cardiac myocyte. A) A half-elliptical geometric mesh with a 10:1 longitudinal: transverse axis length ratio (Parker 2007) was created in prolate spheroidal coordinates, B) Final mesh after refinement and conversion to Cartesian coordinates.

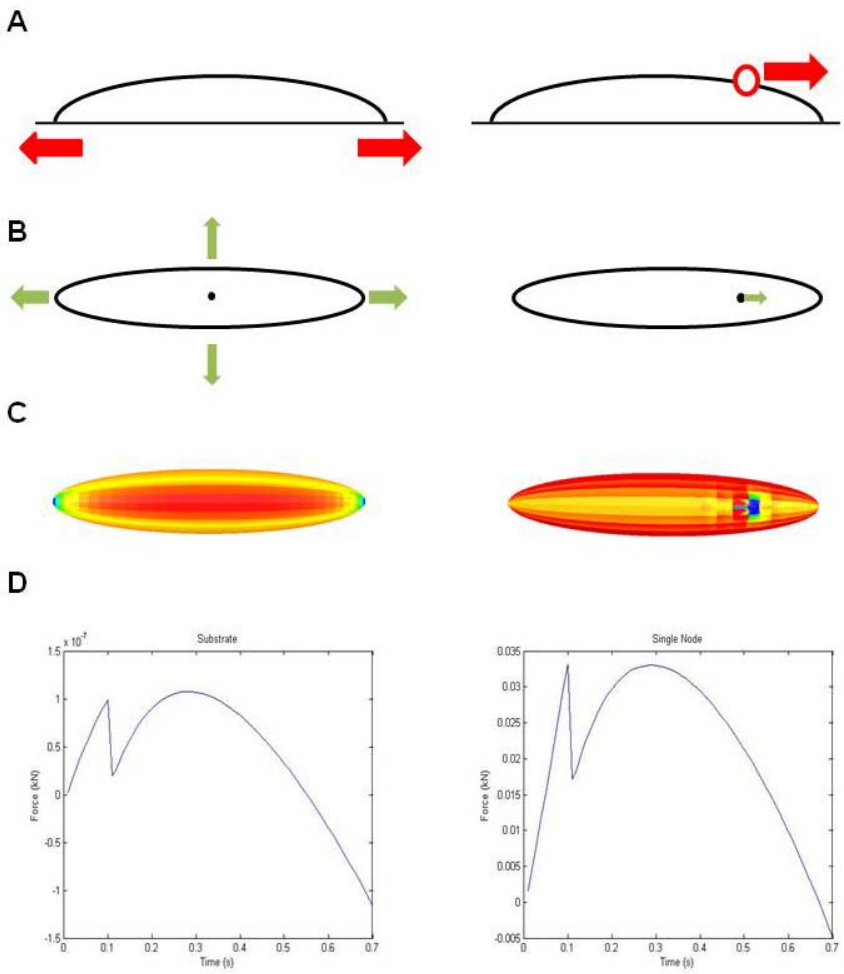

Figure F.2: Biomechanics of applying stretching via a substrate stretch (left) or an optical trap force application stretch (right). A) Cartoon of stretching from the side view of a cell. B) Cartoon of stretching from the top view of a cell. C) Example of stress for a single cardiac myocyte subjected to stretch. (left) P2 stress on the outer cell surface, (right) P1 stress on the outer cell surface. D) Example output of time dependent response of substrate stretch model (left) and single node stretch model (right). (left) Results represent the stress in the center of the bottom surface of the cell in the positive x1 direction in response to substrate displacement, and (right) depicts the stress on the displaced node in the direction of displacement.

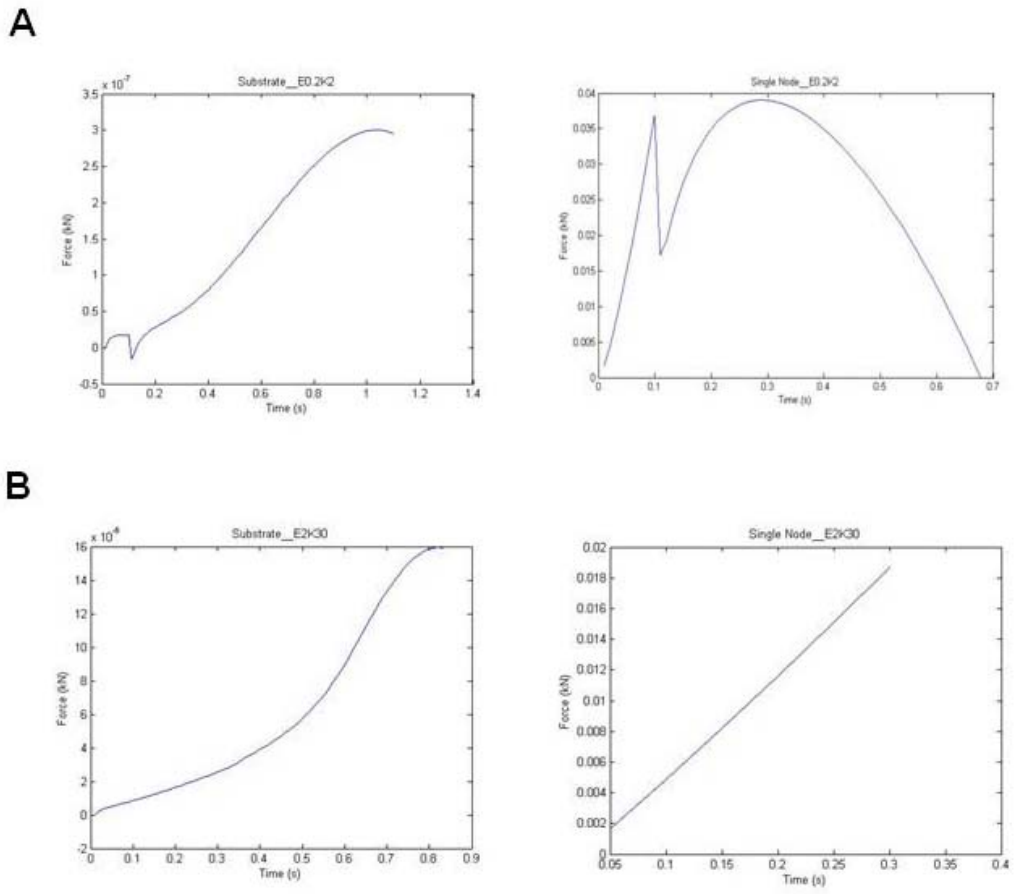

Figure F.3: Examples of output. A) (left) Results for anisotropic substrate stretch with elasticity of 0.2 kPa $*$ s and stiffness of 2 kPa. (right) Results for single-node stretch with elasticity of 0.2 kPa $*$ s and stiffness of 2 kPa. B) Results for anisotropic substrate stretch (left) and single-node stretch (right) with elasticity of 2 kPa $*$ s and stiffness of 30 kPa.

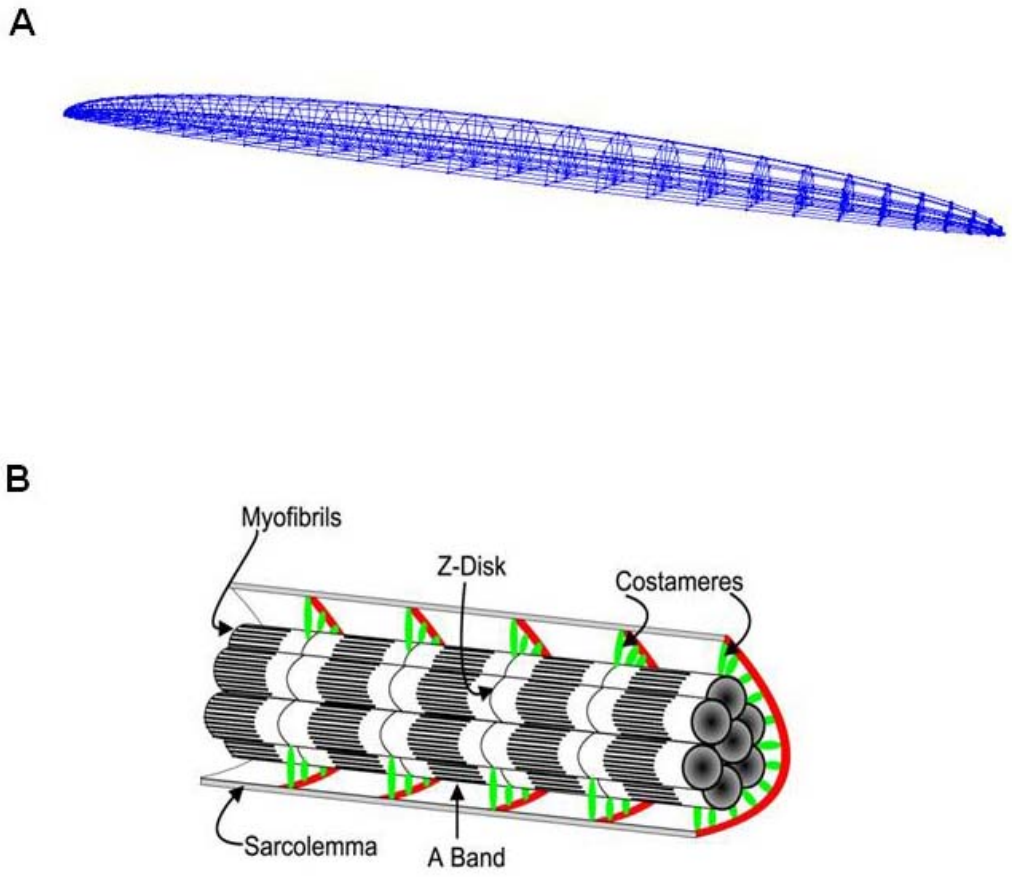

Figure F.4: A) Final mesh for a single cardiac myocyte after refinement and conversion to Cartesian coordinates. B) Cartoon of a cardiac myocyte showing costamere locations with respect to the cell and how it compares to that of our model (A). Cartoon from Ervasti, 2003.

F.7 References

[1] Bausch, A.R., Ziemann, F., Boulbitch, A.A., Jacobson, K., Sackmann, E. Local measurements of viscoelastic parameters of adherent cell surfaces by magnetic bead microrheometry. Biophysical Journal, v75: 2038-2049. 1998.

[2] Camelliti, P., McCulloch, A. D., and Kohl, P. (2005). Microstructured cocultures of cardiac myocytes and fibroblasts: a two-dimensional in vitro model of cardiac tissue. Microsc Microanal 11, 249-259.

[3] Ervasti, J. (2003). Costameres: the Achilles' Heel of Herculean Muscle. J Biol Chem 278, 13591-13594.

[4] Gopalan, S. M., Flaim, C., Bhatia, S. N., Hoshijima, M., Knoell, R., Chien, K. R., Omens, J. H., and McCulloch, A. D. (2003). Anisotropic stretch-induced hypertrophy in neonatal ventricular myocytes micropatterned on deformable elastomers. Biotechnol Bioeng 81, 578-587.

[5] Lieber, S.C., Aubry, N., Pain, J., Diaz, G., Kim, S.J., Vatner, S.F. Aging increases stiffness of cardiac myocytes measured by atomic force microscopy nanoindentation. American Journal of Physiology: Heart and Circulatory Physiology, 287: 645-651. 2004.

[6] Lorenzen-Schmidt, I., Stuyvers, B. D., ter Keurs, H. E., Date, M. O., Hoshijima, M., Chien, K. R., McCulloch, A. D., and Omens, J. H. (2005). Young MLP deficient mice show diastolic dysfunction before the onset of dilated cardiomyopathy. J Mol Cell Cardiol 39, 241-250.

[7] Parker, K.K., Ingber, D.E. Extracellular matrix, mechanotransduction, and structural hierarchies in heart tissue engineering. Philosophical Transactions of the Royal Society B, 362: 1267-1279. 2007.

[8] Samarel, A.M. (2005). Costameres, focal adhesions, and cardiomyocyte mechanotransduction. Am. J. Physiol Heart Circ. Physiol 289, H2291-H2301.

[9] Stuyvers, B. D., McCulloch, A. D., Guo, J., Duff, H. J., and ter Keurs, H. E. (2002). Effect of stimulation rate, sarcomere length and Ca(2+) on force generation by mouse cardiac muscle. J Physiol 544, 817-830.